# The ParA-like protein AgmE positively regulates cell division in *Myxococcus xanthus*

**D I S S E R T A T I O N**

zur Erlangung des Doktorgrades der Naturwissenschaften
(Dr. rer. nat.)

dem
Fachbereich Biologie
der Philipps-Universität Marburg
vorgelegt von

**Kryssia AGUILUZ FABIAN**

aus San Salvador, EL SALVADOR

Marburg/Lahn im April 2009

Die Untersuchungen zur vorliegenden Arbeit wurden von März 2007 bis März 2009 am Max-Planck-Institut für terrestrische Mikrobiologie unter der Leitung von Prof. Dr. MD Lotte Sogaard-Andersen durchgeführt.

Die Untersuchungen in der Zeit von Oktober 2005 bis Februar 2007 unter der Leitung von PD. Reiner Hedderich werden in dieser Arbeit nicht erwähnt und beschrieben. Die Ergebnisse aus diesen Experimenten werden demnächst in der folgenden Veröffentlichung zusammengefasst:

Kahnt, J., Aguiluz, K., Koch, J., Hoppet, M. and Hedderich, R. Proteomic Profiling of the *Myxococcus xanthus* outer membrane and native outer membrane vesicles. *In preparation*.

Vom Fachbereich Biologie der Philipps-Universität Marburg als

Dissertation am
_____ angenommen.

Erstgutachter: Prof. Dr. MD Lotte Søgaard-Andersen

Zweitgutachter: Prof. Dr. Martin Thanbichler

Tag der mündlichen Prüfung: _____

# Table of contents

# Abstract

Correct positioning of the division plane is a prerequisite for the generation of daughter cells with a normal chromosome complement and with a correct size. So far, all bacterial systems, which contribute to correctly place the division plane, regulate formation of the FtsZ cytokinetic ring at mid-cell.

*Myxococcus xanthus* belongs to the δ-proteobacteria and divides by binary fission. However, the mechanisms that ensure proper cell division are not known. In contrast, *M. xanthus* has been studied in detail because of its complex life cycle and for its gliding motility. *M. xanthus* possesses two motility systems referred to as the social (S) and the adventurous (A)-motility systems. While analyzing the adventurous gliding motility E protein (AgmE), which is a member of the ParA/Soj family of ATPases, we discovered that an in-frame deletion of the *agmE* gene results in the formation of filamentous cells and chromosome-free mini-cells. We determined that an Δ*agmE* mutant is neither impaired in chromosome replication nor in chromosome segregation. Moreover, an Δ*agmE* mutant cells displayed fewer division sites and frequently these sites were not located to mid-cell. These data strongly suggest that AgmE has a central function in cell division and in placing the division plane at mid-cell. Consequently, FtsZ localization was investigated. In WT, FtsZ localizes in a speckled-pattern in small-sized cells, i.e. early in the cell cycle, whereas in larger cells, i.e. later in the cell cycle, FtsZ localizes at mid-cell. On the contrary, in an Δ*agmE* mutant FtsZ localizes in a speckled-pattern independently of cell length and cell cycle. We hypothesized that AgmE is required to properly localize FtsZ and could act either positively by directing FtsZ to mid-cell or by stabilizing the FtsZ cytokinetic ring or negatively by inhibiting FtsZ cytokinetic ring formation at the poles.

To distinguish between these hypotheses, AgmE localization was studied. AgmE was found to localize in three distinct patterns, which correlates with cell length, i.e. the cell cycle. In small-sized cells, AgmE localizes in a patchy pattern, as cell size increases AgmE localizes to a single focus slightly off mid-cell and when the cells have reached a specific cell length

AgmE localizes at mid-cell. Genetic data suggest that the cell cycle dependent localization of AgmE depends on ATPase activity. The localization of AgmE at mid-cell implies that AgmE acts positively on FtsZ localization or stabilizes the FtsZ cytokinetic ring. To distinguish between these models, co-localization studies were carried out. These analyses demonstrated that FtsZ and AgmE co-localize at mid-cell. Intriguingly, some cells displayed mid-cell localization of AgmE in the absence of mid-cell localization of FtsZ. Moreover, *in vitro* analyses showed that AgmE interact directly with FtsZ. On the basis of the localization of AgmE to mid-cell and the observation that AgmE localize to mid-cell before FtsZ, we propose that AgmE is a novel cell division regulator that acts positively to direct FtsZ to mid-cell.

A systematic analysis of the *M. xanthus* proteome revealed a unique combination of cell division regulators, i.e. *M. xanthus* encodes an orthologue of DivIVA and lacks orthologues of MinCDE, MipZ, SlmA and Noc. These observations suggest that cell division regulators are yet to be discovered in *M. xanthus.* In this study, we have shown that *M. xanthus* possesses the orphan ParA-like protein AgmE, which is involved in cell division. Importantly, AgmE is the first example of a protein shown to positively regulate FtsZ localization. Interestingly, an in-frame deletion of *divIVA* has no obvious effect on cell division and a DivIVA-mCherry protein localizes in a speckled pattern. Moreover, *MXAN0636*, the downstream gene of *agmE*, seems to be an additional component for the regulation of cell division in *M. xanthus.*

# Zusammenfassung

In Bakterien ist die korrekte Positionierung der Zellteilungsebene eine Voraussetzung für die Entstehung von Tochterzellen mit einer normalen Chromosomenanzahl und einer definierten Zelllänge. Alle bis jetzt bekannten bakteriellen Systeme, welche einen Einfluss auf die Lage der Zellteilungsebene haben, begrenzen die Ausbildung des zytokinetisches FtsZ-Ringes auf die Zellmitte.

*Myxococcus xanthus* gehört zu den δ-Proteobakterien und vermehrt sich mittels binärer Zellteilung. Die genauen Mechanismen, welche die korrekte Positionierung der Zellteilungsebene gewährleisten, sind jedoch nicht bekannt. Vielmehr ist *M. xanthus* bis jetzt stets wegen seines komplexen Lebenszykluses und seiner gleitenden Zellmotilität von wissenschaftlichem Interesse gewesen. *M. xanthus* verfügt über zwei Motilitätssysteme, das sogenannte *social* S- und das *adventurous* A-Motilitätssystem. Wahrend der Analyse des adventurous gliding motility protein E (AgmE), welches zu der ParA/Soj ATPase Familie gehört, stellte sich heraus, dass eine „*in frame*" Deletion des *agmE* Gens in der Bildung von filamentösen Zellen und chromosomenfreien Minizellen resultiert. Es konnte festgestellt werden, dass weder die Chromosomenreplikation noch die –segregation in Δ*agmE* Mutanten eingeschränkt ist. Ferner zeigen Zellen mit einer Δ*agmE* Mutation weniger Zellteilungen, die darüber hinaus meist nicht in der Zellmitte stattfinden. Diese Ergebnisse deuten stark darauf hin, dass AgmE eine zentrale Rolle während der Zellteilung und der Positionierung der Zellteilungsebene in der Mitte der Zelle einnimmt. Folglich wurde die Lokalisation von FtsZ untersucht. In Wildtypzellen lokalisiert FtsZ in kleineren Zellen, wie sie vorwiegend im frühen Stadium im Zellzyklus auftreten, mit einem punktartigen Muster, wohingegen FtsZ in größeren Zellen, d.h. zu einem späteren Zeitpunkt im Zellzyklus, in der Zellmitte lokalisiert. Im Gegensatz dazu zeigt FtsZ in Δ*agmE* Mutanten ein punktartiges Lokalisationsmuster unabhängig von der Zelllänge oder des Zellzykluses. Wir nehmen daher an, dass AgmE für die richtige Lokalisation von FtsZ benötigt wird. Demzufolge könnte AgmE sowohl einen positiven als auch einen negativen Einfluss auf FtsZ ausüben. Für die positive Regulation wäre das Dirigieren von FtsZ in die Zellmitte oder die Stabilisierung des zytokinetischen FtsZ-Ringes durch AgmE denkbar. Eine negative Regulation könnte durch das Verhindern der Bildung des

zytokinetischen FtsZ-Ringes an den Zellpolen ermöglicht werden. Um diese verschiedenen Annahmen zu verifizieren, wurde die Lokalisation von AgmE untersucht. AgmE zeigte drei typische Lokalisationsmuster, welche mit der Zelllänge und damit dem Zellzyklus korrelierten. In kleineren Zellen ist AgmE ungleichmäßig verteilt, mit zunehmender Zellgröße hingegen lokalisiert AgmE als ein einzelner Focus in der Nähe der Zellmitte. Sobald die Zellen eine bestimmte Zelllänge erreicht haben, lokalisiert AgmE in der Zellmitte. Genetische Daten weisen darauf hin, dass die zellzyklusabhängige Lokalisation von AgmE auf seine ATPase Aktivität zurückzuführen ist. Die Lokalisation von AgmE in der Zellmitte impliziert, dass AgmE entweder einen positiven Einfluss auf die FtsZ Lokalisation oder die Stabilisierung des zytokinetischen Rings hat. Um diese beiden Effekte voneinander abgrenzen zu können, wurden Kolokalisationsstudien durchgeführt. Diese Untersuchungen zeigten, dass FtsZ und AgmE in der Zellmitte kolokalisieren. Interessanterweise zeigten einige Zellen eine Lokalisation von AgmE in der Zellmitte trotz Abwesenheit von einer FtsZ Lokalisation in der Zellmitte. Darüber hinaus zeigten zusätzliche Experimente, dass AgmE direkt mit FtsZ *in vitro* interagiert. Auf Grundlage des Lokalisationsmusters von AgmE und der Beobachtung, dass AgmE kurz vor der Ankunft von FtsZ in der Zellmitte lokalisiert, stellen wir die Behauptung auf, dass AgmE ein neuer Zellteilungsregulator ist, welcher einen positiven Einfluss auf FtsZ hat, indem er FtsZ zur Zellmitte dirigiert.

Eine systematische Analyse des *M. xanthus* Proteoms zeigte eine einzigartige Kombination an Zellteilungsregulatoren. *M. xanthus* besitzt zwar ein Ortholog zu DivIVA, weist aber keine Orthologien zu MinCDE, MipZ, SlmA oder Noc auf. Diese Tatsache deutet darauf hin, dass *M. xanthus* weitere bis *dato* noch unbekannte Zellteilungsregulatoren aufweisen könnte.

In dieser Arbeit konnte erstmals gezeigt werden, dass *M. xanthus* ein einzelnes ParA-ähnliches Protein AgmE besitzt, das auf genomischer Ebene nicht mit *parB* in einem Operon kodiert wird, und eine bedeutende Rolle in der Zellteilung spielt. Es ist hierbei hervorzuheben, dass AgmE das erste Protein ist, welches einen positiven Einfluss auf die FtsZ Lokalisation ausübt. Interessanterweise hat eine „*in frame*" Deletion im *divIVA* Gen keinen ersichtlichen Einfluss auf die Zellteilung und eine DivIVA-mCherry Proteinfusion lokalisiert in einem punktartiges Muster. Darüber hinaus scheint das stromabwärts von *agmE* gelegene Gen, *MXAN0636*, eine zusätzliche Komponente in der Regulierung der Zellteilung in *M. xanthus* zu sein.

# Abbreviations

| | |
|---|---|
| ADP/ATP | Adenosine di-/ Adenosine triphosphate |
| bp | Base pairs |
| cDNA | Single stranded complementary DNA |
| CTT | Casitone Tris medium |
| DAPI | 6-diamidino-2-phenylindole |
| DTT | Dithiothreitol |
| EDTA | Ethylendiamine tetra-acetic acid |
| GDP/GTP | Guanosine di-/ Guanosine triphosphate |
| GFP | Green fluorescence protein |
| h | Hours |
| HEPES | 4-(2-hydroxyethyl)-1-piperazineethanesulfonic acid |
| IPTG | Isopropyl β-D-1-thiogalactopyranoside |
| kb | Kilo base pairs |
| LB | Luria-Bertani medium |
| mCherry | Fluorescence protein derivative of mDsRed |
| min | Minutes |
| Ni-NTA | Nickel-nitriloacetic acid |
| OD | Optical density |
| PMSF | Phenylmethylsulfonylfluoride |
| rpm | Rounds per minute |
| RT | Room temperature |
| SDS-PAGE | sodium dodecyl sulfate polyacrylamide gel electrophoresis |
| WT | Wild type |
| X-Gal | 5-bromo-4-chloro-3-indolyl-β-D-galactopyranoside |

# 1 Introduction

Preservation of the genetic integrity of an organism is fundamental for the continuation of the species. Duplication of cells occurs by replication and partitioning the genetic material followed by division. During evolution cells have developed mechanisms regulating correct positioning of the cell division site.

## 1.1 *Myxococcus xanthus*

*Myxococcus xanthus*, a gram-negative δ-proteobacterium, divides by binary fission. However, the mechanisms that ensure failthful partitioning of genetic material and correct positioning of the cell division site are not known. In contrast, *M. xanthus* has been studied in detail because of its social behavior and two life cycles: growth and development (Dworkin, 1996; Shimkets, 1990). In the presence of nutrients, rod-shaped vegetative cells form spreading colonies in which they grow and divide. In nutrient limitation conditions, cell growth ceases and the developmental program is triggered. 24 hours after the start of starvation, cells have aggregated to form multicellular structures called fruiting bodies (Figure 1-1A). As the developmental program proceeds the rod-shaped cells inside the fruiting bodies differentiate into spherical, non-motile dormant spores, which are resistant to various physical and chemical stresses (Figure 1-1B). Once nutrients become available, the spores germinate and vegetative life cycle resumes. The developmental life cycle is controlled by a number of intra- and extra-cellular signals and also depends on the ability of the cells to regulate their motility behavior (Hagen *et al.*, 1978; Kroos and Kaiser, 1987; Leonardy *et al.*, 2008).

*M. xanthus* cells move by gliding motility, which is a type of surface movement characterized by smooth motion of the cells in the direction of the long axis of a cell and in the absence of flagellum/a. *M. xanthus* possesses two motility engines referred to as the social (S) and the adventurous (A)-motility systems (Hodgkin and Kaiser, 1979). Mutations in both engines lead to non-motile cells whereas mutation in only one engine leads to motility by means of the remaining engine.

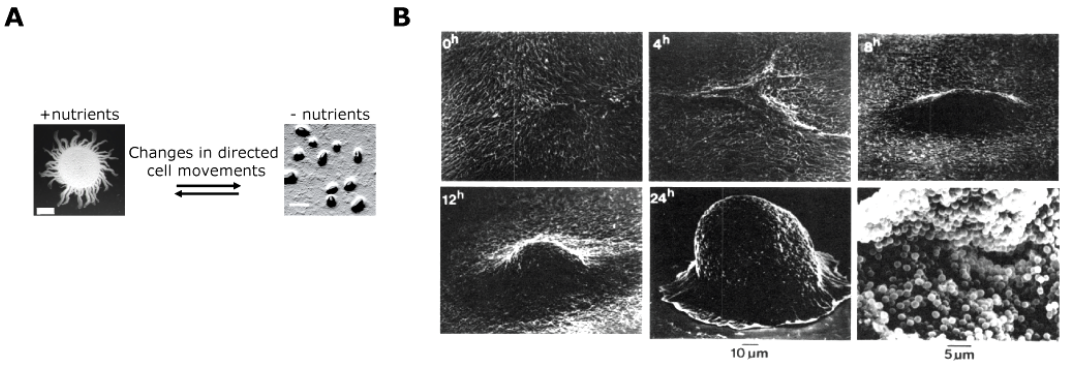


**Figure 1-1. Complex motility behaviors in the presence or absence of nutrients leading to the formation of spreading colonies or to the formation of fruiting bodies, respectively. A)** *M. xanthus* displays two types of directed cell movement. Left panel, in the presence of nutrients spreading colonies are formed. Scale bar 2 mm. Right panel, in nutrient limitation conditions, fruiting bodies are formed. Scale bar 0.2 mm. (Leonardy *et al.*, 2008) **B)** Scanning electron micrographs of *M. xanthus* cells during development. The first five photos display the formation of a fruiting body. The last photo shows the spherical spores present inside a fruiting body after 72 hours after the start of the developmental program (Shimkets, 1990)

The S-motility system depends on cell-cell contacts (Hodgkin and Kaiser, 1979) and force is generated by retraction of Type IV pili at the leading end of the cell (Mignot *et al.*, 2005; Sun *et al.*, 2000). During retractions, cells are pulled forward (Skerker and Berg, 2001).

The A-motility system allows cells to move as single cells (Hodgkin and Kaiser, 1979). In contrast to the S-motility system, it is not clear how force is generated for the A-motility system. There are currently two models to explain force generation. In the first model, slime extrusion from the lagging pole would generate force allowing the cells to be pushed forward (Wolgemuth *et al.*, 2002). This model is supported by the observation of nozzle-like structures embedded in the cell envelope at the cell poles (Wolgemuth *et al.*, 2002) and by the finding that many A-motility genes encode proteins involved in polymer synthesis and export (Youderian *et al.*, 2003; Yu and Kaiser, 2007). In the second model, A-motility is powered by focal adhesion complexes distributed along the cell body (Mignot *et al.*, 2007b). This model is supported by the observation that cells, moving only by means of the A-motility system, move with the same speed irrespective of cell length (Sun *et al.*, 1999). The drawback of these models is the lack of experimental evidence on how motive force is generated. The most studied A-motility proteins are the AglZ protein, a pseudo-response regulator and the RomR protein, a response regulator (Leonardy *et al.*, 2007; Mignot *et al.*, 2005). These two A-motility proteins have been shown

to localize to specific subcellular regions of the cell. The RomR protein localizes in a bipolar, asymmetric pattern with the large cluster at the lagging cell pole (Leonardy *et al.*, 2007), while the AglZ protein localizes with a large cluster at the leading pole and in focal adhesion complexes distributed along the cell body (Mignot *et al.*, 2007b). Both proteins are dynamically localized and the polar clusters relocate between the cell poles during cellular reversals (Figure 1-2). However, it is currently not known how RomR and AglZ achieve their localization patterns.

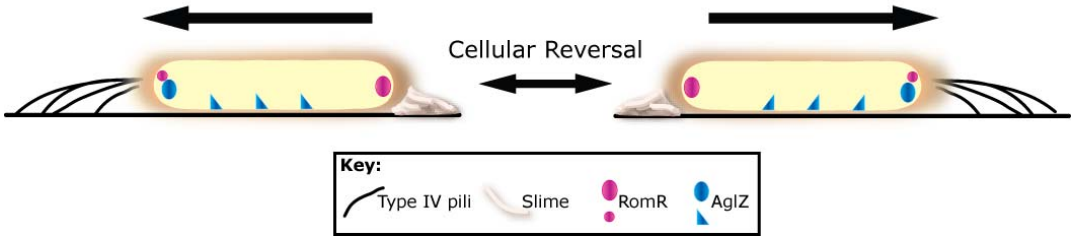


**Figure 1-2. Localization of Type IV pili and A-motility proteins RomR and AglZ.** Arrows indicates the direction of movement. Modified from (Leonardy *et al.*, 2008)

To understand how A-motility functions, it is clear that the force generating mechanism has to be identified and the mechanisms involved on protein localization elucidated.

Youderian *et al.* performed a transposon mutagenesis screen in order to identify genes involved in A-motility (Youderian *et al.*, 2003). This analysis identified 30 A-motility genes from which the adventurous gliding motility E (AgmE) was the most promising candidate as the A-motility motor or for being involved in protein localization. According to Youderian *et al.*, AgmE has homology with Soj/ParA-like proteins (Youderian *et al.*, 2003). ParA-like proteins are part of a cytoskeletal protein family with ATPase activity that has no clear eukaryotic counterparts. Moreover, ParA-like proteins are capable of polymerization and are involved in correct positioning of macromolecules i.e. plasmids, chromosomes and proteins in bacteria (Gitai, 2007). Therefore, AgmE could have a function in A-motility. However, this study provides evidence that AgmE is not directly involved in A-motility, but rather involved in regulation of cell division. Therefore, to understand the possible role of AgmE in cell division the mechanisms regulating this process will be discussed.

## 1.2 Assembly of the cell division machinery

### 1.2.1 Establishing the cell division site

Genetic approaches have led to the identification of a dozen of essential cell division proteins in *E. coli*. These proteins carry the *fts* designation because of the "filamentous temperature sensitive" phenotype displayed by the strains carrying the conditional lethal mutations (Hirota *et al.*, 1968). FtsZ is the first (known) component of cell division machinery to localize at the future division site. FtsZ assembles in a ring-like structure called the Z-ring (Bi and Lutkenhaus, 1991; Dajkovic and Lutkenhaus, 2006). The assembly of the Z-ring marks the position of the future division site and it is required to recruit other proteins to the cell division complex (Dajkovic and Lutkenhaus, 2006). FtsZ is present in almost all bacteria with a few exceptions (e.g *Chlamydiaceae* family, *Ureaplasmia urealyticum* and *Pirellula* sp. Strain 1) and is also present in some Archea (Figure 1-3, A) (Margolin, 2005; Vaughan *et al.*, 2004). FtsZ is often referred to as a universal and essential protein for cell division in bacteria and archae (Erickson, 1997).

FtsZ is a structural tubulin homologue (Figure 1-3B). Like tubulin, FtsZ polymerizes cooperatively into linear protofilaments in a GTP-dependent manner *in vitro* (Oliva *et al.*, 2004). Moreover, it has recently been reported that FtsZ by itself can generate force for constriction of the septum provided that it is tethered to the cytoplasmic membrane (Osawa *et al.*, 2008).

By immuno-fluorescence microscopy and FtsZ-GFP fusions, it has been shown that the mid-cell Z-ring localization in WT *E. coli* and *B. subtilis* is defined with a high degree of precision (Migocki *et al.*, 2002; Sun and Margolin, 2001). Furthermore, numerous studies have shown that the Z-ring undergoes three distinct phases throughout the cell cycle: first, FtsZ structures that oscillate in a helix-like pattern, second, the assembly of a stable FtsZ-ring at mid-cell, and third, constriction and disassembly during septation (Aarsman *et al.*, 2005; Peters *et al.*, 2007; Rueda *et al.*, 2003; Sun and Margolin, 1998; Thanedar and Margolin, 2004).

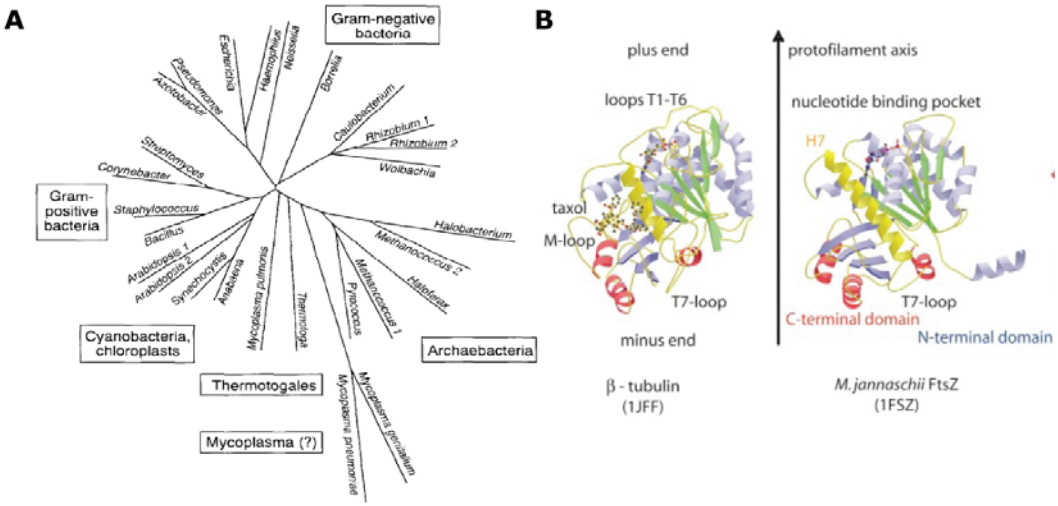


**Figure 1-3. FtsZ is a structural homologue of tubulin. A)** Phylogenetic tree of known FtsZ sequences. The conserved core sequences corresponding to the amino acids 10-316 of *E. coli* FtsZ were aligned using Clustal W algorithm and the tree was then calculated and drawn using the DrawTree algorighm of Phylip (Erickson, 1997). **B)** Crystal structure of FtsZ from *Methanococcus jannaschii* compared to β-tubulin (Löwe *et al.*, 2004).

### 1.2.2 Assembly of the cytokinesis machinery

In gram negative bacteria, the completion of cell division requires the coordinated constriction of the three layers of the cell envelope: the invagination of the inner membrane, the biosynthesis of septal peptidoglycan, and the invagination of the outer membrane. The formation of the cytokinesis machinery starts with the localization and formation of the FtsZ-ring that marks the future division site. Once the Z-ring is assembled at mid-cell, it recruits other cell division proteins required for cytokinesis such as FtsK, FtsQ, FtsL, FtsB, FtsW, FtsI (PBP3), FtsN, MurG, AmiC (Figure 1-4A), Tol-Pal complex and peptidoglycan synthetases and hydrolases in *E. coli* (den Blaauwen *et al.*, 2008; Derouaux *et al.*, 2008; Gerding *et al.*, 2007). While much is known about the individual proteins in terms of sequence, membrane topology, and their interdependency for localization (Figure 1-4B), the precise functions of most of these proteins remain unknown.

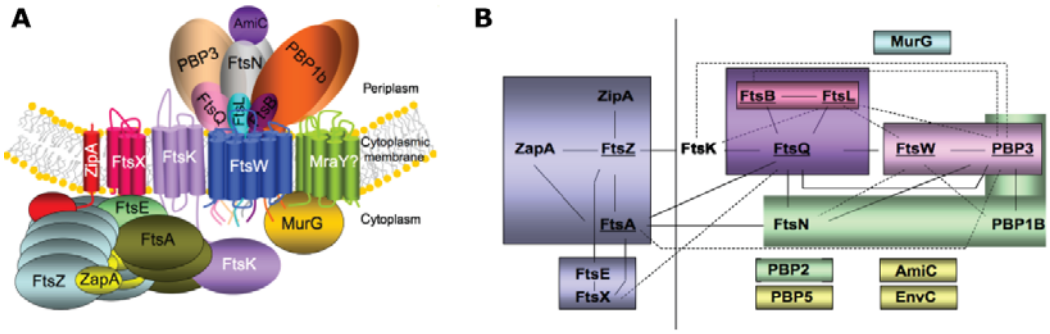


**Figure 1-4. Schematic representation of the divisome and its assembly in *E. coli*. A)** The subcellular localization of cell division proteins have been shown using GFP fusions and immuno-fluorescence **B)** Schematics representing the order of assembly of the components of the cell division machinery. Interactions shown by yeast-two-hybrid are depicted with the dashed lines and solid lines represent interactions proven by other methods (den Blaauwen *et al.*, 2008).

## 1.3 Regulation of the positioning of the cell division site

Correct positioning of the division site is a prerequisite for the generation of daughter cells with a normal chromosome complement and correct size. During evolution bacteria have developed mechanisms ensuring correct chromosome segregation and correct positioning of the cell division site.

### 1.3.1 DNA segregation

- Partitioning systems in plasmids

Plasmids have served as important models to understand chromosome segregation in bacteria. Correct segregation of low-copy-number plasmids into daughter cells relies on the function of partitioning (*par*) loci encoded by the plasmids themselves. The majority of *par* operons contain two genes: one that encodes a motor protein, which is typically an ATPase, and one that encodes a centromere-binding protein. In addition, near the *par* operon is a centromere-like site that is bound by the centromere-binding protein. All three components are required for plasmid segregation (Schumacher, 2008). Par systems are categorized into two groups based on the type of motor protein that is present in the *par* operon (Gerdes *et al.*, 2000).

The Type I is the most abundant of the *par* systems and contains motor proteins with the Walker-type ATPase motifs. The typical *par* locus consists of two genes, *parA* encoding the ATPase protein and *parB* encoding the

centromere-binding protein and the *parS* centromere-like site located upstream or downstream of the *par* locus (Figure 1-5A). Type I can be further subdivided in Type Ia in which the motor proteins are characteristically larger than Type Ib. Type Ia contains an N-terminus region, which is a putative helix-turn-helix (HTH) DNA-binding motif, whereas Type Ib do not contain this part. This DNA-binding motif allows Type Ia to autoregulate transcription of the respective *par* operon (Hayes and Barilla, 2006). The second type of *par* system, called Type II, contains ATPase proteins referred to as ParM (for motor) that belong to the actin/heat-shock protein 70 superfamily. The centromere-binding proteins in this system are named ParR. The genetic organization of the Type II *par* system resembles Type Ib (Figure 1-5A). Recently, a third putative class of *par* systems was discovered in which the motor protein is TubZ, a member of the tubulin/FtsZ GTPase superfamily of motor proteins, and the centromere-binding protein is TubR (Larsen *et al.*, 2007).

A model has been proposed of how Type I *par* systems function to drive plasmid segregation (Figure 1-5B) (Hayes and Barilla, 2006). In this model, the centromere-binding protein ParB binds the centromere site *parS* and upon dimerization recruits the motor protein ParA. ParA polymerizes in an ATP-dependent manner and this polymerization generates the force to pull or push the plasmids to the daughter cells. After cell division, the plasmids are accurately placed to the daughter cells and ParA depolymerizes. The crystal structures of several centromere-binding proteins have been solved and show that centromere-binding proteins use either HTH or ribbon-helix-helix (RBB) motifs to bind the centromere-like sites (Golovanov *et al.*, 2003; Schumacher *et al.*, 2007a; Schumacher *et al.*, 2007b). Furthermore, there is convincing evidence that several ParA proteins are able to polymerize in an ATP-dependent manner (Barilla *et al.*, 2005; Lim *et al.*, 2005). Inactivation of ParA ATPase activity by single amino acid substitutions abrogates plasmid segregation indicating that ATPase activity is crucial for the function of ParA in DNA segregation (Barilla *et al.*, 2005; Ebersbach and Gerdes, 2004; Libante *et al.*, 2001).

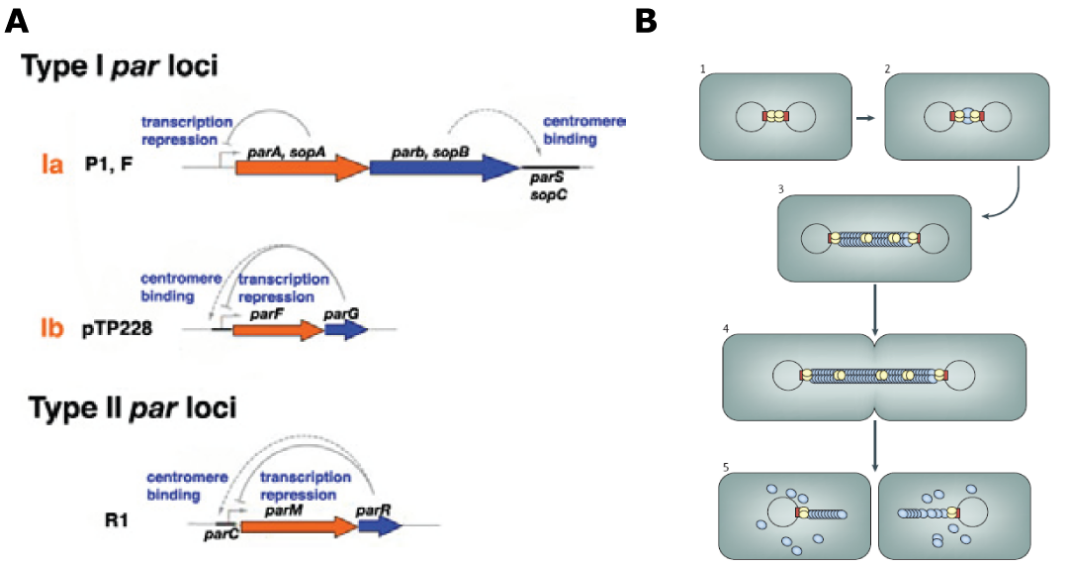


**Figure 1-5. Genetic organization of the two main families of *par* loci and model for ensuring segregation of plasmids encoding ParA proteins. A)** *par* loci shown are representatives from each class (type Ia, plasmids F and P1; type Ib, pTP228; and type II, plasmid R1). **Orange** arrows represent genes that encode motor proteins (ATPases) and blue arrows represent genes encoding centromere-binding proteins. Centromere sites are indicated by black bars and are labeled (e.g. *parS*, *sopC*, and *parC*). Arcs represent DNA-binding properties of the indicated gene products, continuous arcs show regulation of promoter activity by the indicated gene products and broken arcs represent formation of partition complexes. Modified from (Schumacher, 2008). **B)** Model for segregation of plasmids that encode ParA proteins. Following replication, plasmid pairs align at mid-cell through centromere-binding proteins (**yellow**) that are bound to the partition sites (**red**) (1). The ParA protein (**blue**) is recruited to the segrosome (2) and, in response to ATP binding, polymerizes bidirectionally between the segrosomes, pushing the plasmids in bipolar orientations (3). The centromere-binding protein modulates the organization of the ParA filaments (4). Following cell division, the plasmids have been accurately distributed to daughter cells, and the ParA polymers disassemble (5). Polymerization-mediated pushing of plasmids is illustrated, but bidirectional pulling of plasmids is also possible (Hayes and Barilla, 2006).

- Chromosomal partitioning systems

Partitioning systems have also been identified on chromosomes and these systems have been shown to be important for chromosome segregation. To date, all chromosomally encoded ParA proteins belong to the Type I *par* system. The best-studied examples of chromosomal *par* loci are from *Pseudomonas putida*, *Pseudomonas aeruginosa*, *Bacillus subtilis, Caulobacter crescentus* and *Vibrio cholerae* (Bartosik *et al.*, 2004; Lasocki *et al.*, 2007; Lin and Grossman, 1998; Mohl and Gober, 1997; Yamaichi *et al.*, 2007). Deletion of *parAB* in *P. aeruginosa* leads to the generation of 7% anucleate cells indicating that ParAB have a role in proper segregation of chromosomes (Lasocki *et al.*, 2007). In contrast, deletion of the *par* locus in *P. putida* has a chromosome segregation phenotype only in stationary growth phase, where up to 14% of cells are anucleated (Lewis *et al.*, 2002).

This phenotype shows parallels in *B. subtilis* and *S. coelicolor* in which deletion of *parAB* only causes minor segregation defects during vegetative growth but ParAB are important for chromosome segregation to the endospore in *B. subtilis* and during the differentiation of aerial hyphae into spores in *S. coelicolor* (Kim *et al.*, 2000; Sharpe and Errington, 1996). These minor segregation defects suggest that other mechanisms exist to ensure chromosome segregation in vegetative cells. It has been described in *B. subtilis* that the *smc* gene encoding the "structural maintenance of chromosomes" (SMC), a DNA-binding protein, contributes to chromosome compaction and organization (Hirano, 1998). Moreover, a Δ*smc*,Δ*soj* double mutant has dramatically perturbed nucleoid morphology, with irregular nucleoid size, anucleate and cut cells while most of the nucleoids in the Δ*smc* single mutant had regular size and spacing during vegetative growth. These results suggest that the partitioning role of Soj could be masked by the SMC protein and that both SMC and Soj participate in chromosome segregation (Lee and Grossman, 2006).

Contrary to what is described for *par* systems in *P. putida*, *B. subtilis* and *S. coelicolor*, the *par* systems in *C. crescentus* and for chromosome II of *V. cholerae* are essential for viability and chromosome segregation under normal cellular conditions. In the case of *C. crescentus* and for chromosome I in *V. cholerae* other factors may also be involved in chromosome segregation (Fogel and Waldor, 2006; Jensen and Shapiro, 1999; Mohl and Gober, 1997; Yamaichi *et al.*, 2007).

The chromosomal and plasmid encoded ParA proteins share several features:

1) ParA ATPase activity is important for their function. Inactivation of ATPase activity by single amino acid substitutions abrogates plasmid segregation (Barilla *et al.*, 2005; Ebersbach and Gerdes, 2004; Libante *et al.*, 2001). Moreover, Soj (ParA) mutant proteins from *B. subtilis* in which ATP binding or hydrolysis have been impaired have different localization patterns (Murray and Errington, 2008). In addition, it has been shown that mutations in the ATP binding motifs of ParA1 of chromosome I in *V. cholerae* abolish its dynamics (Fogel and Waldor, 2006).

2) Several ParA proteins are able to polymerize. The chromosomal ParA (Soj) from *Thermus thermophilus* as well as several plasmid-encoded ParA

proteins have been shown to be able to polymerize in an ATP-dependent manner *in vitro* (Barilla *et al.*, 2005; Ebersbach *et al.*, 2006; Leonard *et al.*, 2005; Lim *et al.*, 2005; Machon *et al.*, 2007).

3) The localization of ParA-like proteins is dynamic, but their localization patterns vary from organism to organism (Figure 1-6). ParA from the plasmid pB171 have been shown to oscillate is spiral-shaped structures over nucleoid regions (Ebersbach and Gerdes, 2004; Ebersbach *et al.*, 2006). Moreover, early in the cell cycle, ParA from *C. crescentus* and ParA1 from chromosome I of *V. cholearea* are localized in one cluster at the pole. Upon duplication of the origin of replication and migration towards the opposite cell pole, these ParA-like proteins are localized in two polar clusters (Fogel and Waldor, 2006; Mohl and Gober, 1997). Furthermore, the ParA orthologue (Soj) in *B. subtilis* has been shown to localize to the septum and in faint punctuate foci within the cytoplasm (Murray and Errington, 2008). However, whether these localization patterns change during the cell cycle is not known.

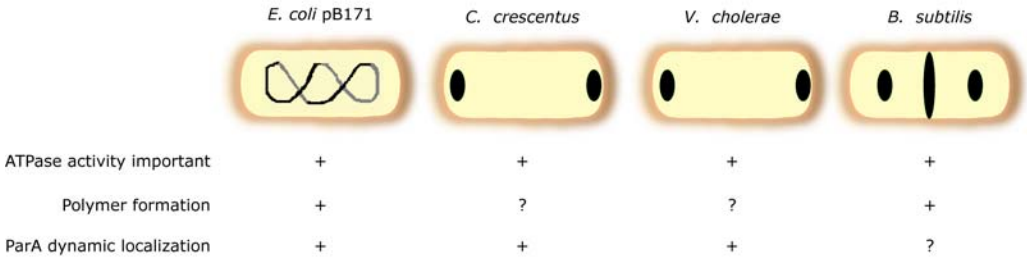


**Figure 1-6. Localization of plasmid and chromosomal encoded ParA proteins.** Localization of ParA of plasmid pB171 in *E. coli*, Soj in *B. subtilis*, ParA in *C. crescentus* and ParA1 of *V. cholerea.* ParA localization patterns are shown in black helical structures or in black ellipses. (+) means that the ATPase activity, polymer formation and dynamic localization has been shown experimentally and (?) that it is not known.

- Orphans ParA proteins involved in protein localization

One class of ParA-like proteins are orphans i.e. they are not located next to a *parB* gene. Two examples have been analyzed, and shown to have the ability to properly localize proteins. One example is the PpfA protein in *Rhodobacter sphaeroides*, which is involved in the correct localization of chemotaxis protein clusters to the ¼ and ¾ positions of the cell prior to cell division (Thompson *et al.*, 2006). The second example is the MipZ protein in *C. crescentus*. MipZ is required for the proper localization of the cell division protein FtsZ close to mid-cell (Thanbichler and Shapiro, 2006) (detailed description in section 1.3.2).

### 1.3.2 Spatial regulation of Z-ring assembly

Z-ring positioning is remarkably precise and the Z-ring persists for a considerable part of the cell cycle suggesting that mechanisms must exist ensuring the correct positioning of the Z-ring. In *B. subtilis* and *E. coli*, there are two well-known factors that influence the position of the Z-ring: nucleoid occlusion and the Min system. Both act negatively by preventing Z-ring assembly at inappropriate locations (e.g. over the nucleoids and poles). In contrast, *C. crescentus* lacks homologues of the Min system and nucleoid occlusion. The positioning of the Z-ring is negatively regulated by the orphan ParA-like protein MipZ.

- The nucleoid occlusion system

The observation that *E. coli* cells harboring mutations in DNA replication genes divide next to the centrally located nucleoid and not over it, led to the suggestion that the nucleoid influences the position of the septum. This phenomenon is called "nucleoid occlusion" (Mulder and Woldringh, 1989). A breakthrough in understanding how the nucleoid occlusion system works came with the discovery of two unrelated proteins affecting nucleoid occlusion, i.e. the unspecifically DNA-binding proteins SlmA in *E. coli* and Noc in *B. subtilis* (Bernhardt and de Boer, 2005; Wu and Errington, 2004) (Figure 1-7). Noc was accidentally discovered by the observation that when combined with a *minD* mutant, an *noc* (formely *yyaA*) deletion is practically lethal in *B. subtilis* (Wu and Errington, 2004). In *E. coli*, *slmA* was identified using a mutagenesis screen to select mutants that are synthetic lethal with a defective Min system (Bernhardt and de Boer, 2005). When *slmA* or *noc* are deleted in the absence of a functional Min system, Z-rings were observed to form over the nucleoid suggesting that nucleoid occlusion is absent in these mutants. Moreover, both proteins have been shown to localize over the nucleoid in their respective organisms. Furthermore, the overexpression of Noc or SlmA results in a complete cell division block. The above observations show that Noc and SlmA are involved in nucleoid occlusion by preventing Z-ring polymerization or accumulation in the vicinity of the nucleoid (Bernhardt and de Boer, 2005; Wu and Errington, 2004). It was shown that SlmA is able to interact directly with FtsZ *in vitro* indicating

that SlmA affects nucleoid occlusion by directly inhibiting FtsZ polymerization (Bernhardt and de Boer, 2005).

- The Min system

The Min system was discovered over 30 years ago when *min* mutants were isolated from *E. coli* and *B. subtilis* (Adler *et al.*, 1967; Reeve *et al.*, 1973). Mutations in *min* genes are viable; however the cells are able to divide not only at mid-cell but also at the poles giving rise to small DNA-free cells also referred as to mini-cells.

In *E. coli*, the *min* locus consists of three genes, *minC*, *minD* and *minE*, that map to a single operon (de Boer *et al.*, 1988). MinC is the actual inhibitor of polar cell division. MinC prevents the formation of a functional Z-ring by destabilizing FtsZ polymers (Dajkovic *et al.*, 2008; Hu *et al.*, 1999). MinC is localized to the poles via interaction with MinD, a membrane associated ATPase. MinD is member of the family of deviant Walker A ATPases. It was shown using GFP fusions and time-lapse microscopy that both MinC and MinD display a remarkable oscillatory behavior and oscillate between the cell poles with a period of 20-60 seconds (Hu *et al.*, 1999; Raskin and de Boer, 1999). MinCD oscillations require MinE, which is the topological factor that relieves division inhibition in the central region of the cell (Hu *et al.*, 1999; Raskin and de Boer, 1999) (Figure 1-7). It has been proposed that MinE first cause MinC to dissociate from MinD because MinE and MinC-binding sites overlap on the surface of MinD (Ma *et al.*, 2004). MinE then stimulates the ATPase activity of MinD and the release of MinD-ADP from the membrane (Hu *et al.*, 2002; Hu and Lutkenhaus, 2001; Lackner *et al.*, 2003). It has been shown that MinE also oscillates and forms a ring at the edge of MinD polar zone (Fu *et al.*, 2001). Therefore, MinD-ADP diffuses and nucleotide exchange allows MinD-ATP to rebind the membrane at the opposite pole because of the transient presence of MinE at the original site (Hu and Lutkenhaus, 2001). Average over time, the concentration of MinCD is the lowest at mid-cell. Therefore, the oscillatory pattern of MinCDE leads to inhibition of FtsZ polymerization at the poles leaving only the mid-cell available for Z-ring formation.

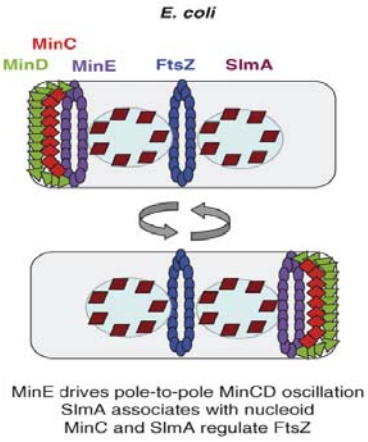


**Figure 1-7. Spatial regulation of Z-ring assembly in *E. coli*.** *E. coli* has two systems that regulate the localization of **FtsZ** at mid-cell. One is the nucleoid occlusion system defined by the unspecific DNA-binding protein **SlmA**. The other system is the oscillatory Min system which is composed by the inhibitor of FtsZ polymerization **MinC**, the membrane-associated ATPase **MinD** and the topological factor **MinE**. The remarkable oscillation of the Min system combined with the inhibitory action of SlmA allow the formation of the Z-ring only at mid-cell (Gitai, 2007).

*B. subtilis* also contains homologues of MinC and MinD, but lacks MinE and MinCD oscillations are not observed (Marston *et al.*, 1998). The function of MinE in the topological control of MinCD activity is provided by DivIVA, a coiled-coil protein that binds to the cell poles and later in the cell cycle to the septum (Edwards and Errington, 1997; Stahlberg *et al.*, 2004). DivIVA, through the adaptor protein MinJ, recruits MinCD to the poles, therefore inhibiting polar Z-ring formation (Patrick and Kearns, 2008). Later on in the cell cycle, these proteins localize at mid-cell so that they are already present when the new poles are completed (Marston and Errington, 1999). In this model, the *B. subtilis* Min system acts primarily to inhibit Z-ring formation at the poles. However, this view has recently been questioned (Bramkamp *et al.*, 2008; Gregory *et al.*, 2008) (Figure 1-8). While revisiting the role of the Min system in *B. subtilis*, Gregory *et al.* showed that MinC-GFP and MinD-GFP expressed from their native promoters are mainly localized at the septum and not at the poles as previously described (Marston and Errington, 1999). Moreover, they showed that the localization of MinC is dynamic, although in a different manner from *E. coli* MinC. MinC from *B. subtilis* relocalizes from the new pole to mid-cell immediately prior to division via membrane associated foci (Gregory *et al.*, 2008) (Figure 1-8). The observation that MinCD is mainly at the septum is supported by the localization of MinJ, the adaptor protein between MinD and DivIVA proteins, which is also mainly localized at the septum (Bramkamp *et al.*, 2008). Both studies propose a new mode of action for MinCD (Figure 1-8). In WT cells, FtsZ forms a ring at mid-cell and recruits the early division proteins FtsA, ErzA and ZapA (see section 1.3.3) and then the late cell division proteins

followed by DivIVA, and ultimately MinC and MinD (Figure 1-8, 1 to 4). After division is completed, MinC affinity for the pole is reduced and it moves away from the pole probably together with MinD. By doing so, MinC inhibits the formation of Z-ring at the pole, thereby allowing FtsZ to relocalize more efficiently to the new mid-cell (Figure 1-8, 6).

The characteristic phenotype of *min* mutants is filamentous cells and the production of mini-cells (Reeve *et al.*, 1973). This characteristic phenotype can be explained because the *minCD* mutant has a defect in the timing of cell division (Gregory *et al.*, 2008). While WT cells divide at regular intervals, *minCD* cells show highly variable interdivisional times. In the absence of MinC, FtsZ accumulates at the new poles and also mid-cell, therefore, splitting FtsZ between two sites leading to the elongation of the cells until both sites have accumulated enough FtsZ and other cell division proteins to support cell division. Consequently, the appearance of filamentous cells is due to the increased time it takes to accumulate FtsZ at sufficient concentration, and the production of mini-cells is due to the presence of FtsZ at the new poles. It has been shown that MinC is capable of inhibiting FtsZ bundling both *in vitro* and *in vivo* (Dajkovic *et al.*, 2008; de Boer *et al.*, 1992). Therefore, MinC inhibits FtsZ-ring assembly. However, it is not clear how MinC inhibitory function is kept inactive when present at the septum.

Despite the fact that some of the components of the Min system are conserved between *E. coli* and *B. subtilis* (MinC and MinD), it now seems that the mechanism by which the Min system regulates the positioning of the Z-ring differs in these organisms.

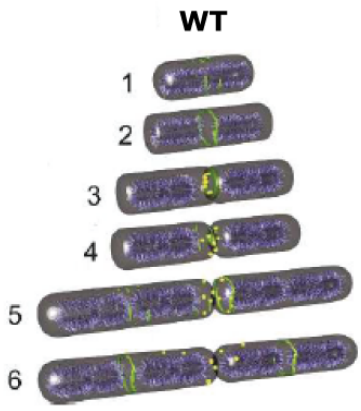


**Figure 1-8. Spatial regulation of Z-ring assembly in *B. subtilis*.** Model for mode of action of Min system in *B. subtilis*. (1 & 2) **Z-ring** is formed at mid-cell. (3 & 4) **MinC** is recruited late at mid-cell. (5) Once cell division is completed, **MinC** moves away from the poles and by doing so inhibits the **Z-ring** formation next the pole. (6) Therefore, **Z-ring** is able to be formed more efficiently at mid-cell (Gregory *et al.*, 2008).

- MipZ is involved in the temporal and spatial regulation of Z-ring assembly in *C. crescentus*

Unlike *E. coli* and *B. subtilis,* which divide to produce nearly identical cells, *C. crescentus* undergoes division near mid-cell to produce two different–size daughter cells with different fates (Ausmees and Jacobs-Wagner, 2003). This dimorphism is maintained by asymmetric cell division giving rise to two genetically identical but morphologically different daughter cells. One is a stalked cell that can immediately reenter the cell cycle and the other is the swarmer cell that has an obligate motile phase during which DNA replication and cell division are inhibited. The swarmer cells have to undergo cellular differentiation, which involves shedding the flagellum, retraction of the pili and growth of a stalk at the pole previously occupied by the flagellum and pili, to enter into the cell cycle. *C. crescentus* lacks homologues of the nucleoid occlusion and Min system. The spatial regulation of Z-ring assembly is achieved by the orphan ParA-like protein MipZ. Moreover, the MipZ protein is conserved in all α-proteobacteria that lack the MinCD homologues (Thanbichler and Shapiro, 2006).

The model for how MipZ spatially and temporally regulates the assembly of the Z-ring is shown in Figure 1-9. MipZ interacts directly with the partitioning ParB protein (Thanbichler and Shapiro, 2006). The ParB protein binds the centromere-like site *parS* that is located near the origin of replication (Mohl and Gober, 1997). This complex is located at the stalked pole of the cell. After initiation of DNA replication and duplication of the origin region, the MipZ-ParB complex reoccupies the newly synthesized origin region, which is rapidly moved towards the opposite cell pole. At the opposite pole, FtsZ is localized and upon arrival of the MipZ-ParB complex, FtsZ is destabilized and moves to mid-cell. It has been shown that MipZ and FtsZ interact directly and that MipZ stimulates FtsZ GTPase activity, thereby inducing conformational changes of the FtsZ polymers. Thus, FtsZ polymerization can only occur at mid-cell where the MipZ concentration is the lowest. MipZ is therefore involved in both the temporal and spatial regulation of Z-ring formation by preventing Z-ring formation close to the poles and the initiation of cell division before the start of chromosome segregation (Thanbichler and Shapiro, 2006).

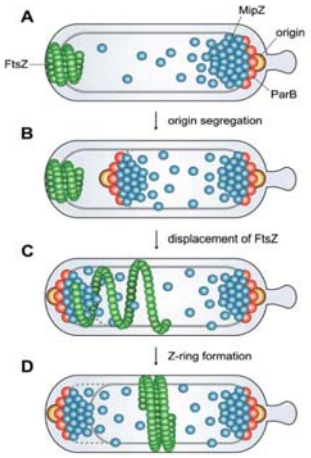


**Figure 1-9. MipZ is involved in temporal and spatial regulation of cytokinesis in *C. crescentus*: (A)** MipZ/ParB complex is associated with the chromosome at the stalked pole. **(B)** Upon replication, the newly synthesized chromosome migrates to opposite cell pole **(C)** where MipZ destabilizes FtsZ and **(D)** FtsZ moves to mid-cell where MipZ concentration is the lowest leading to the formation of the Z-ring/divisome (Thanbichler and Shapiro, 2006)

### 1.3.3 Stabilizing/destabilizing factors of Z-ring assembly

In addition to the negative regulators like the nucleoid occlusion, Min system and MipZ, several other proteins have been identified in bacteria that interact directly with FtsZ and function to regulate Z-ring assembly (Figure 1-10).

- Z-ring stabilizing factors

FtsA is the second most conserved cell division protein in bacteria after FtsZ. In *E. coli*, FtsA is an essential protein whereas in *B. subtilis ftsA* mutation leads to filamentation but it is not essential (Beall and Lutkenhaus, 1992; Jensen *et al.*, 2005). FtsA has sequence and structure similarity to actin (Bork *et al.*, 1992; van den Ent and Lowe, 2000). It has been shown that FtsA localizes at mid-cell and its localization is dependent on FtsZ (Hale and de Boer, 1999). Furthermore, FtsA interacts directly with FtsZ (Pichoff and Lutkenhaus, 2002). However, the exact role of FtsA in Z-ring assembly is not known. One possible role of FtsA is the anchoring of the Z-ring to the membrane which is important for cell division to occur. FtsA contains in its C-terminal an amphipathic helix motif that anchors FtsA and probably FtsZ to the membrane (Pichoff and Lutkenhaus, 2002, 2005). Another possible role is to support the formation and stabilization of Z-ring. In *E. coli*, two proteins might fulfill this role: FtsA and ZipA. Either protein can support the formation of the Z-ring (Pichoff and Lutkenhaus, 2002). ZipA also interacts with FtsZ. Several lines of evidence point to a stabilizing role of ZipA in Z-ring assembly because overexpression of ZipA suppresses the thermosensitivity of an FtsZ84 mutant and it seems that ZipA promotes the

formation of extensive bundles of FtsZ protofilaments *in vitro* (Hale *et al.*, 2000). In addition, ZipA is an integral membrane protein that may also assist FtsA in tethering FtsZ to the membrane (Hale *et al.*, 2000). However, while ZipA is essential for cell division in *E. coli* (Hale and de Boer, 1997), apparent stable Z-ring rings can be formed in its absence. This observation suggests that either ZipA or FtsA is sufficient for Z-rings to assemble, therefore, FtsA and ZipA might have overlapping roles in maintaining Z-ring integrity (Pichoff and Lutkenhaus, 2002). Besides, ZipA is not a highly conserved protein (Margolin, 2000). *B. subtilis* does not contain a ZipA homologue. However, it has recently been shown that SepF localizes at mid-cell in an FtsZ dependent manner and it is able to interact with FtsZ. Moreover, overexpression of SepF can complement the defect in Z-ring formation in a *ftsA* deletion mutant (Ishikawa *et al.*, 2006). This suggests that like ZipA in *E. coli*, SepF in *B. subtilis* may have an overlapping role with FtsA in supporting Z-ring assembly.

ZapA is another positive modulator of Z-ring assembly that interacts directly with FtsZ *in vitro* and co-localizes with FtsZ *in vivo* in *B. subtilis* (Gueiros-Filho and Losick, 2002). ZapA is not an essential protein but mutation of *zapA* in combination with *ezrA* leads to a synthetic block of cell division (Gueiros-Filho and Losick, 2002). ZapA is widely conserved in bacteria. The ZapA orthologue YgfE in *E. coli* shows a similar subcellular localization pattern as ZapA in *B. subtilis.* Moreover, ZapA as well YgfE has been shown to promote FtsZ polymerization *in vitro* (Gueiros-Filho and Losick, 2002; Small *et al.*, 2007).

ZapB is a coiled-coil protein that promotes assembly of Z-ring in *E. coli* (Ebersbach *et al.*, 2008). Deletion of *zapB* leads to delayed cell division and the formation of ectopic Z-ring whereas overexpression of ZapB resulted in aberrant cell division. The ZapB and FtsZ proteins co-localize and this co-localization is dependent on FtsZ. Furthermore, ZapB self-assembles into long filaments and bundles. Ebersbach *et al.*, have proposed that ZapB stimulates Z-ring assembly directly via its capacity to self-assemble.

- Z-ring destabilizing factors

In *E. coli*, SulA is expressed as part of the SOS response to DNA damage, which arrests cell division until the DNA is repaired. SulA binds directly to

FtsZ preventing FtsZ self-association. In addition, SulA inhibits the GTPase activity of FtsZ (Cordell *et al.*, 2003; Mukherjee *et al.*, 1998; Trusca *et al.*, 1998). SulA is not a highly conserved protein in bacteria and it seems that the suppression of Z-ring assembly during SOS response in *B. subtilis* is partially mediated by an unrelated protein YneA (Kawai *et al.*, 2003).

EzrA is another negative regulator of Z-ring assembly in *B. subtilis*. The loss of EzrA in the cell is not lethal, but results in the formation of multiples Z-rings, located at mid-cell as well as in polar positions (Levin *et al.*, 1999). It is thought that EzrA, which is bound to the cytoplasmic membrane, inhibits Z-ring assembly at incorrect positions (e.g. poles) and maintains the proper FtsZ assembly dynamics within the medial Z-ring. This model is supported by the direct interaction of EzrA with FtsZ in which EzrA inhibits FtsZ polymerization *in vitro*. Moreover, the overproduction of EzrA appears to inhibit the Z-ring assembly *in vivo* (Haeusser *et al.*, 2007; Haeusser *et al.*, 2004).

ClpX is the ATPase subunit responsible for specifically recognizing substrate proteins for proteolysis in the ClpXP protease complex (Ades, 2004). ClpX is a highly conserved protein which present in *B. subtilis* and *E. coli.* It has been shown that ClpX interacts directly with FtsZ in *B. subtilis* and *E. coli* (Flynn *et al.*, 2003; Weart *et al.*, 2005), and overexpression of ClpX inhibits Z-ring assembly only shown in *B. subtilis* (Weart *et al.*, 2005). However, the mechanism by which ClpX inhibits Z-ring assembly is poorly understood.

The fact that most of the Z-ring assembly regulators are neither essential nor highly conserved suggest that bacteria have evolved a robust FtsZ regulatory network that can support cell division even when one component is lost and that the specific components are modified to the needs of the individual species (Harry *et al.*, 2006).

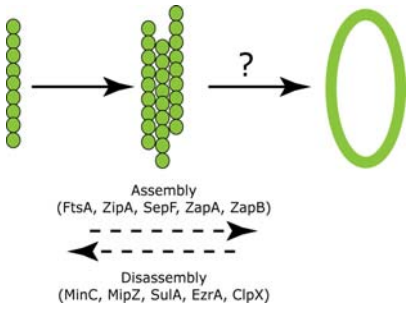


**Figure 1-10.** Formation of the Z-ring. FtsZ monomers (**green** circles) associate to form a linear protofilament. The protofilaments can associate laterally to form high-order assemblies. Then the Z-ring is assembled. The details of the Z-ring structure are not known. However, the Z-ring assembly requires stabilizing factors such as FtsA, ZipA, SepF, ZapA and ZapB as well as destabilizing factors like MinC, MipZ, SulA, EzrA and ClpX. The presence of destabilizing factors makes the Z-ring assembly reversible. Modified from Harry *et al.*, 2007.

### 1.3.4 Cell cycle timing

Several studies have shown that the Z-ring has three distinct phases during the cell cycle: first, FtsZ structures that oscillate in a helix-like pattern, second, the assembly of a stable FtsZ-ring at mid-cell, and third, constriction and disassembly during septation (Aarsman *et al.*, 2005; Peters *et al.*, 2007; Rueda *et al.*, 2003; Sun and Margolin, 1998; Thanedar and Margolin, 2004). As mentioned in the previous sections, the assembly of the Z-ring is highly regulated by spatial regulators and stabilizing/destabilizing factors. The persistence of the Z-ring before its contraction suggests that the contraction of the Z-ring is a regulated event. However, how this contraction is regulated is not known. Though, it might depend on the switch of cell wall synthesis from elongation mode to septal mode. This switch depends on FtsZ (Aaron *et al.*, 2007; de Pedro *et al.*, 1997).

## 1.4 Scope

Regulation of cell division has been largely studied in *E. coli*, *B. subtilis* and *C. crescentus*. However, nothing is known about how *M. xanthus* achieves the faithful partition of its genetic material and the correct positioning of the cell division site. While studying motility in *M. xanthus*, we came across the orphan ParA-like protein AgmE, which was suggested to be involved in A-motility. In this study, we show that AgmE is involved in cell division in *M. xanthus* and likely only indirectly affect motility. AgmE is the first protein described in *M. xanthus* as important for regulating cell division. Importantly, AgmE is the first example of a protein shown to positively regulate FtsZ localization. Thus, AgmE represents a fundamentally novel system for regulating the cell division site in a bacterial system.

# 2 Results

## 2.1 The Δ*agmE* mutant

Because AgmE was found in a screen designed to identify proteins involved in A-motility (Youderian *et al.*, 2003), and because of the features of ParA-like proteins, we hypothesized that AgmE could be involved in A-motility by generating mechanical force by polymerization. This would resemble actin treadmilling present at the leading edge of eukaryotic motile cells (Pollard and Borisy, 2003). Alternatively, AgmE could be involved in the correct localization of A-motility proteins.

### 2.1.1 AgmE is an orphan ParA-like protein

- Bioinformatics analysis on AgmE

ParA-like proteins belong to the class of ATPases with diverse functions and contain deviant Walker A ATP-binding motifs (Koonin, 1993). To confirm that AgmE belongs to the ParA family of proteins, bioinformatic analyses were carried out. To identify the known domains in AgmE, SMART and conserved domain searches were performed (Figure 2-1A & B). These analyses suggested that AgmE contains CbiA and ArsA domains. The CbiA family includes CobQ/ CobB /MinD /ParA proteins.

ArsA is an arsenite-translocating ATPase, which is part of a multi-unit pump that catalyses the extrusion of oxyanions (e.g. arsenite, arsenate) from the cell (Rosen, 1990). CobQ (cobyric acid synthase) and CobB (cobyrinic a,c-diamide synthetase) catalyse the amidation of cobalamin precursors (e.g. vitamin B12) (Blanche *et al.*, 1991). MinD is a membrane associated ATPase required for the correct placement of the division site in *E. coli* (de Boer *et al.*, 1991). ParA proteins are involved in plasmid and chromosome segregation (Hayes and Barilla, 2006) and also in the correct positioning of proteins (Thanbichler and Shapiro, 2006; Thompson *et al.*, 2006).

These proteins share the common feature of having specific variations of the Walker ATPase motifs, which are implicated in the binding and hydrolysis of ATP (Beyer, 1997).

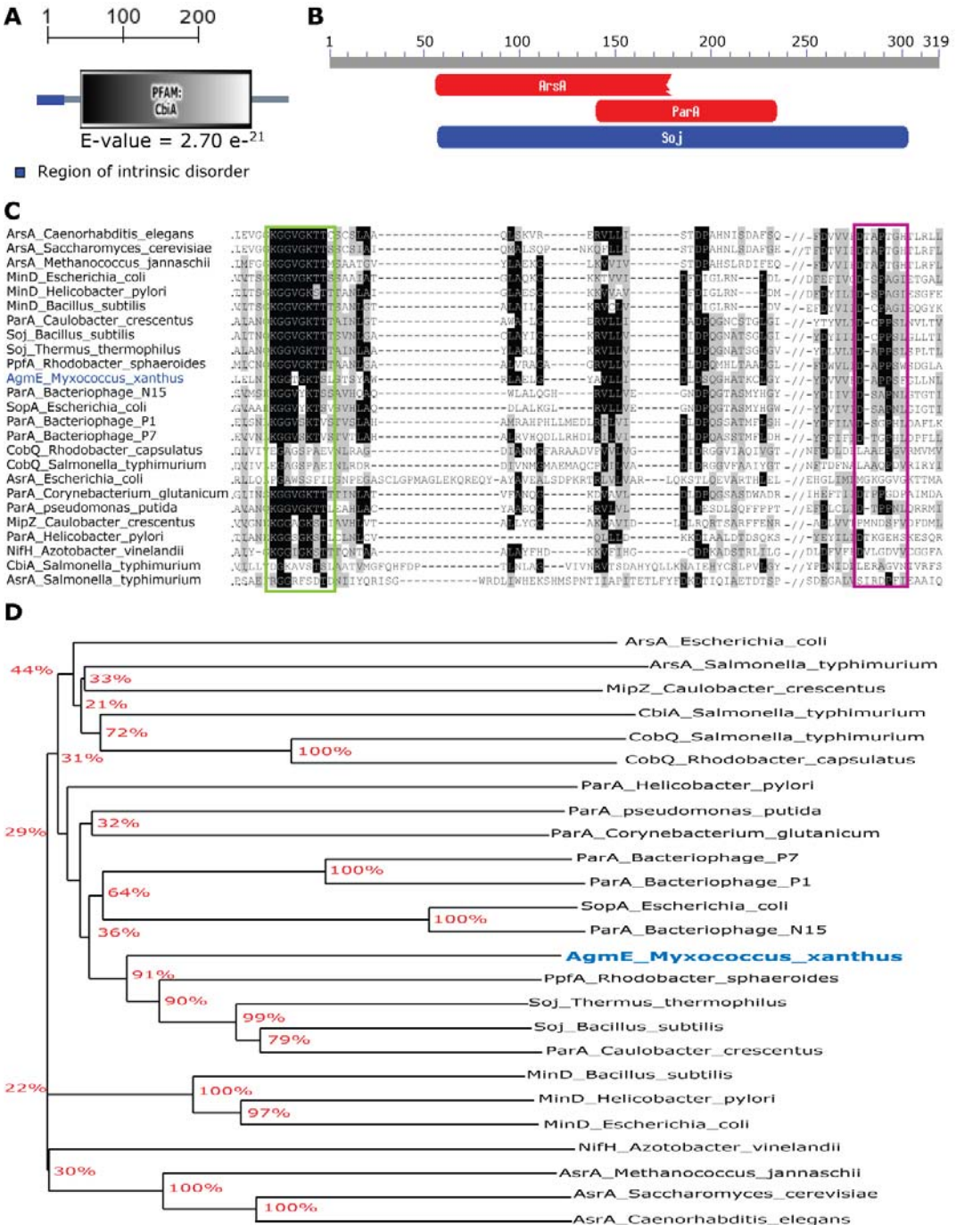


**Figure 2-1. Bioinformatics analysis of AgmE. A & B**) Domain architecture of AgmE according to SMART and Conserved Domain Searches from EMBL and NCBI, respectively. **C)** Partial sequence alignment of CbiA family and ArsA proteins (25 proteins) where AgmE is marked in blue. The alignment shows the Walker A motif (**green box**) and the ArsA signature sequence (**pink box**) **D)** Phylogenetic tree of CbiA family and ArsA proteins. Selected sequences were aligned using ClustalW (v. 1.81,(Thompson *et al.*, 1994)). The alignment was manually curated using Bioedit (v. 7.0.5.3, T.A. Hall) and subsequently used to generate a bootstrapped (1000 iterations) Neighbor Joining tree. The tree was visualized and annotated using TreeDyn (v. 198.3, Chevenet, F., *et al.*). The percentage (**%**) shows the probability of the proteins clustering together. Analyses were performed by Stuart Huntley.

These variations include a deviant Walker A box (consensus GxxGxGK [ST]) and a conserved aspartate at the beginning of the Walker B box (consensus [D]hhhhD) (Leipe *et al.*, 2002). To determine to which family AgmE belongs to, sequence alignments were generated (Figure 2-1C). The conservation of the Walker A motif was first examined (Figure 2-1C **green box**). The Walker A box is not conserved in the CobQ and CobB proteins, which means that AgmE is not likely to be a CobQ or CobB protein. The second feature examined was the presence of the signature sequence DTAPTGH, which is important for the function of ArsA proteins (Figure 2-1C **pink box**). AgmE does not possess this signature sequence suggesting that AgmE is not an ArsA protein. However, from this analysis, it can not be determined if AgmE belongs to the MinD or ParA family of proteins. In order to distinguish between these two possibilities, a phylogenetic tree was generated (Figure 2-1D). AgmE clusters together with ParA-like proteins and not with MinD proteins. On the basis of these analyses AgmE belongs to the ParA-like family of proteins.

- AgmE is an orphan ParA-like protein

The genetic organization of *agmE* is shown in Figure 2-2. *agmE* is flanked by two genes encoding for hypothetical proteins and there is no *parB* in the vicinity of *agmE*. MXAN0633, located two genes upstream of *agmE,* encodes a DNA binding protein, which contains a helix-turn-helix domain but does not show any sequence similarity to ParB proteins. Therefore AgmE is an orphan ParA-like protein.

It is important to notice that the *M. xanthus* genome possesses the typical *parA* and *parB* operon (MXAN7477-MXAN7476) and also two additional orphan ParA-like proteins (MXAN5815 and MXAN3920). The observations that AgmE is an orphan ParA-like protein and that *M. xanthus* possesses the typical *parAB* operon suggest that AgmE is involved in processes other than chromosome segregation.


**Figure 2-2. *agmE* genetic organization.** Arrows indicate open reading frames (ORFs) and the direction indicates the transcriptional direction. The proteins encoded by each gene are marked above the ORFs. The numbers in the gray circles indicates the distance between two genes.

### 2.1.2 *agmE* mutant has both A- and S-motility defects

To understand the function of AgmE in motility, an *agmE* in-frame deletion mutant was generated and A- and S-motility phenotypes were analyzed (Figure 2-3). The motility assays were performed on different agar conditions, 1.5% and 0.5% agars, which favor the A- or S-motility respectively, and the colony morphology examined. Considering A-motility, an Δ*agmE* colony spreads less than a WT colony on 1.5% agar; however, single cells are still present at the edge of the colony, which is not the case for the control strain DK1217 (A-S+) (Figure 2-3A). These data suggest that the Δ*agmE* mutant is partially impaired in A-motility. Considering S-motility, a WT colony on 0.5% agar spreads in flares, which are hardly present in an Δ*agmE* mutant colony (Figure 2-3B). Therefore, the Δ*agmE* mutant is also partially impaired in S-motility. From this analysis, the Δ*agmE* mutant has both A- and S-motility defects in agreement with previous data (Youderian *et al.*, 2003) .

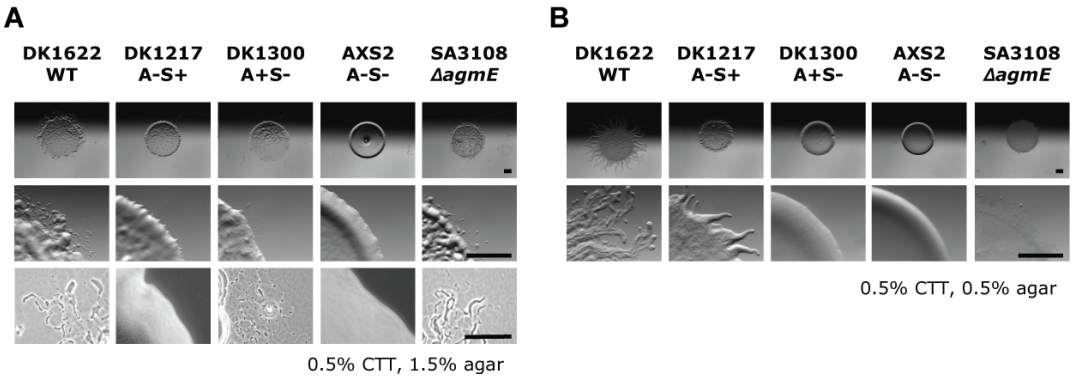


**Figure 2-3. Δ*agmE* is partially impaired in A- and S-motility. A)** A-motility phenotype of Δ*agmE* mutant compared with WT, DK1217 (A-S+), DK1300 *(*A+S-) and AXS2 (A-S-) in 0.5% CTT medium containing 1.5 % agar, conditions that favor A-motility. Scale bar on the upper and middle pictures is 1 mm (Leica MZ8 stereomicroscope). For the bottom pictures, the scale bar is 0.1 mm (Leica IMB/E inverted microscope). **B)** S-motility phenotype of Δ*agmE* mutant compared to WT, DK1217 (A-S+), DK1300 *(*A+S-) and AXS2 (A-S-) in 0.5% CTT medium containing 0.5 % agar, which favors S-motility. The scale bars represent 1 mm (Leica MZ8 stereomicroscope).

### 2.1.3 Genetic complementation of the Δ*agmE* mutant

To verify that the motility defects observed in the Δ*agmE* mutant are due to the *agmE* mutation, genetic complementation was performed. First, the *agmE* locus was mapped to determine whether *agmE* is in an operon with the two flanking genes encoding for hypothetical proteins using a reverse transcription-PCR approach (Figure 2-4). For this, total RNA was isolated from exponentially growing WT cultures and cDNA was synthesized (Materials and Methods). Primer pairs were designed to generate PCR products covering intergenic regions of the genes of interest as well as an internal region of *agmE* (Figure 2-4). The PCR product labeled **3**, which cover the internal region of *agmE* was obtained using genomic DNA and cDNA. With the primers pairs **1** and **2**, which cover the intergenic regions *agmE*-MXAN0636 and *agmE*-MXAN0634, respectively, PCR products were only obtained using genomic DNA as template. This data indicates that *agmE* is not in an operon with the flanking genes. Therefore, 400bp upstream the *agmE* gene were included as a promoter region in the construct for complementation of the *agmE* mutation. The construct was integrated at the myxophage Mx8 attachment site in the Δ*agmE* mutant. The motility phenotypes and AgmE expression levels using our specific AgmE antibodies (Materials and Methods) were then studied in the complementation strain (Δ*agmE*/*agmE*+) (Figure 2-5). AgmE is expressed at the same level as in WT in the complementation strain (Figure 2-5A). Moreover, the A- and S-motility defects were restored (Figure 2-5B & C). These data demonstrate that the *agmE* mutation is responsible for the motility defects.

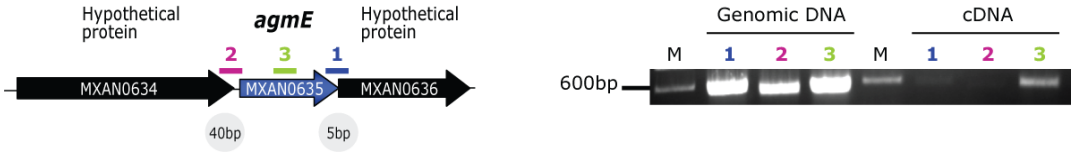


**Figure 2-4. *agmE* operon mapping.** Genomic and RNA were extracted from exponentially growing WT cells. RNA was converted to cDNA (see Material and Methods). To check whether *agmE* is in an operon with the two genes encoding for hypothetical proteins, primers were designed that their products (600 bp) cover the intergenic regions of *agmE-MXAN0636* and *agmE-MXAN0634* (**1** and **2**, respectively), and as control, primers binding an internal fragment in the *agmE* gene were used (**3**). M represents the marker.

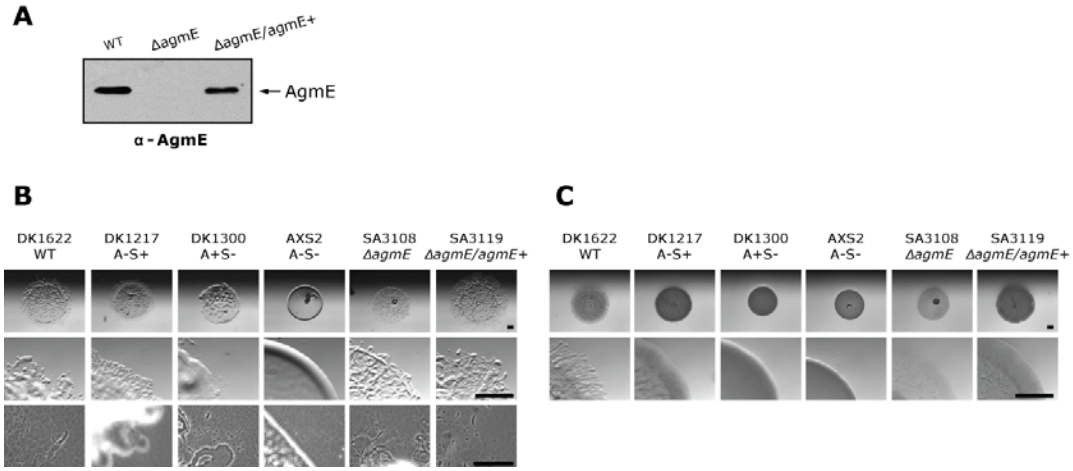


**Figure 2-5. *agmE* genetic complementation restores A- and S- motility. A)** Levels of AgmE in the complementation strain (Δ*agmE*/*agmE*+). Equal amount of total proteins were resolved on a SDS-PAGE and subjected to immunoblot analysis using anti-sera specific to AgmE. **B)** A-motility phenotype of Δ*agmE/agmE*+ compared with WT, DK1217 (A-S+), DK1300 *(*A+S-) and AXS2 (A-S-) in 0.5% CTT medium containing 1.5 % agar, conditions that favor A-motility. Scale bar on the upper and middle pictures is 1 mm (Leica MZ8 stereomicroscope). For the bottom pictures, the scale bar is 0.1 mm (Leica IMB/E inverted microscope). **C)** S-motility phenotype of Δ*agmE/agmE*+ compared to WT, DK1217 (A-S+), DK1300 *(*A+S-) and AXS2 (A-S-) in 0.5% CTT medium containing 0.5 % agar, which favors S-motility. The scale bars represent 1 mm (Leica MZ8 stereomicroscope).

### 2.1.4 RomR localization and pili levels are normal in the Δ*agmE* mutant

To investigate whether the partial A-motility defect was due to incorrect localization of A-motility proteins, the localization of RomR was determined in the Δ*agmE* mutant (Figure 2-6). RomR localizes in a bipolar asymmetric pattern with the large cluster at the lagging cell pole (Leonardy *et al.*, 2007). In an Δ*agmE* mutant, RomR-mCherry localizes in a bipolar asymmetric pattern as in the case of WT (Figure 2-6A). This result suggests that AgmE is not involved in the correct localization of RomR.

Since S-motility absolutely requires type IV pili, we also investigated the ability for the Δ*agmE* mutant to assemble pili by performing "shear pili assays" as described in Wall *et al.*, 1998 (Figure 2-6B). The Δ*agmE* mutant has pilin levels similar to WT, indicating that AgmE is not directly involved in S-motility. From these results, we conclude that the A- and S-motility defects observed in the Δ*agmE* mutant are not due to the incorrect localization of RomR or the lack of pili.

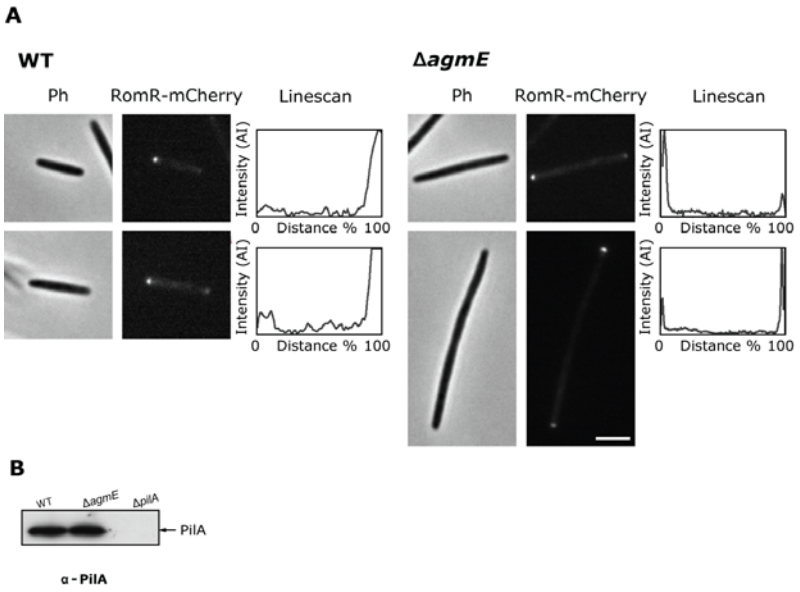


**Figure 2-6. RomR localization and pilin levels are normal in Δ*agmE*. A)** Subcellular localization of RomR-mCherry in WT and Δ*agmE* cells (n=100). Exponentially growing cells were placed on a thin TPM-1% agarose pad and visualized by light (phase contrast Ph) and fluorescence microscopy. The fluorescence intensities were measure using the linescan function of Metamorph® 7.5 (maximum value, scan width 10). Scale bar represents 5 µm. **B)** Shear pili assay. Cell were resuspended to 5 x $10^9$ cells/ mL and placed onto 0.5% CTT-agar for 4 hours at 32°C. Cells were then harvested in 0.4 mL TPM buffer and vortexed for three minutes. Then samples were centrifuged to separate the cells from the supernatant. The pili present in the supernatant were precipitated overnight at 4°C by addition of 100mM $MgCl_2$ and the precipitates were resuspended in SDS loading buffer. 10µL of each sample were loaded on a SDS-PAGE and subjected to immunoblot analysis using specific anti-sera to PilA.

## 2.2 AgmE is involved in other processes causing the motility defect?

During the analysis of the Δ*agmE* mutant motility defects, a striking feature caught our attention: Δ*agmE* cells show different cell lengths in comparison to WT cells (Figure 2-7A). By quantitative analysis (Figure 2-7B), we found that >95% of WT cells have a size between 2.6 to 10 µm whereas 44% of Δ*agmE* cells are longer than 10 µm. In contrast to WT cells, 4% of the Δ*agmE* mutant cells are very short with a length below 2.5 µm. In the complementation strain (Δ*agmE*/*agmE*+), the cell length distribution was restored back to that of WT (Figure 2-7), demonstrating that the Δ*agmE* mutation is responsible the cell length phenotype.

There are many motility mutants known in *M. xanthus*; however, none of them have been observed to make filamentous and/or very short cells. Moreover, induced filamentation by cephalexin treatment dramatically reduces the gliding speed of the S-motility system and only slighty reduces the gliding speed of the A-motility system (Sun *et al.*, 1999). These

observations led us to speculate that the Δ*agmE* mutation might affect DNA replication and/or segregation and/or cell division and in that way indirectly resulting in the motility defects.

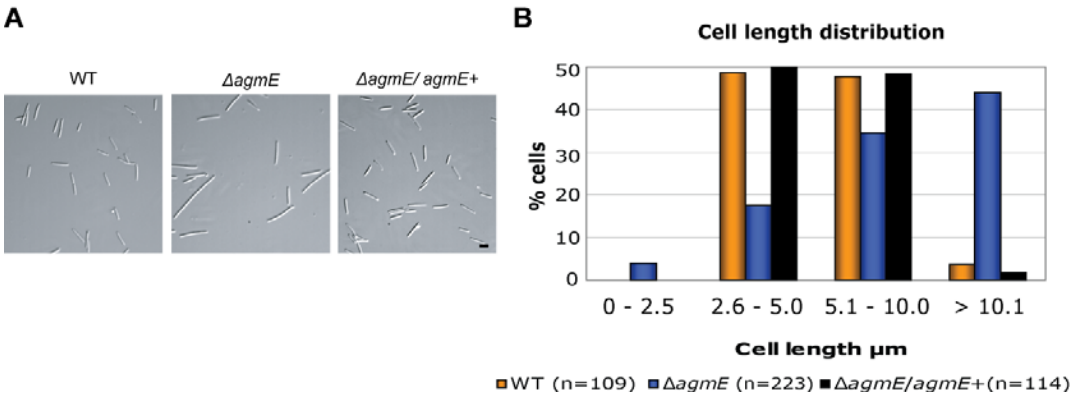


**Figure 2-7. Δ*agmE* cells have different cell lengths compared to WT cells. A)** WT, Δ*agmE* and Δ*agmE*/*agmE*+ cells taken during exponential growth and placed onto a thin TPM-1% agarose pads. Pictures were taken using Zeiss Axio Imager. M1 (Carl Zeiss). Scale bar represents 2µm. **B)** Cell length distributions of WT, Δ*agmE* and Δ*agmE*/*agmE*+ cells. Cell length was measured using the region measurement function of Metamorph® 7.5 and exported to Microsoft Excel to generate the graph.

### 2.2.1 AgmE is not involved in DNA replication or segregation

The first question was whether Δ*agmE* cells initiate rounds of chromosome replication with a normal frequency. To address this question, the DNA content in WT and Δ*agmE* cells was visualized by DAPI staining and the number of nucleoids counted. Because Δ*agmE* cells are longer than WT, the direct comparison of the number of nucleoids is not possible. To compensate for the cell length difference, WT cells were treated with the antibiotic cephalexin for two generations (8 h). Cephalexin blocks cell division without affecting DNA replication, DNA segregation or cell growth (Pogliano *et al.*, 1997). The number of nucleoids within Δ*agmE* cells was then compared to WT and cephalexin-treated WT cells.

WT cells contain one or two nucleoids in the absence of cephalexin (Figure 2-8A, **orange triangles**), whereas the number of nucleoids ranges from 0 up to 12 in Δ*agmE* cells (Figure 2-8A, **blue circles**). In cephalexin treated WT cells, the number of nucleoids was increased to 4 to 8 (Figure 2-8A, **yellow triangles**). When the number of nucleoids is plotted as function of cell length, it is evident that there is a similar correlation between cell length and the number of nucleoids in WT, cephalexin-treated WT and Δ*agmE* cells (Figure 2-8A).

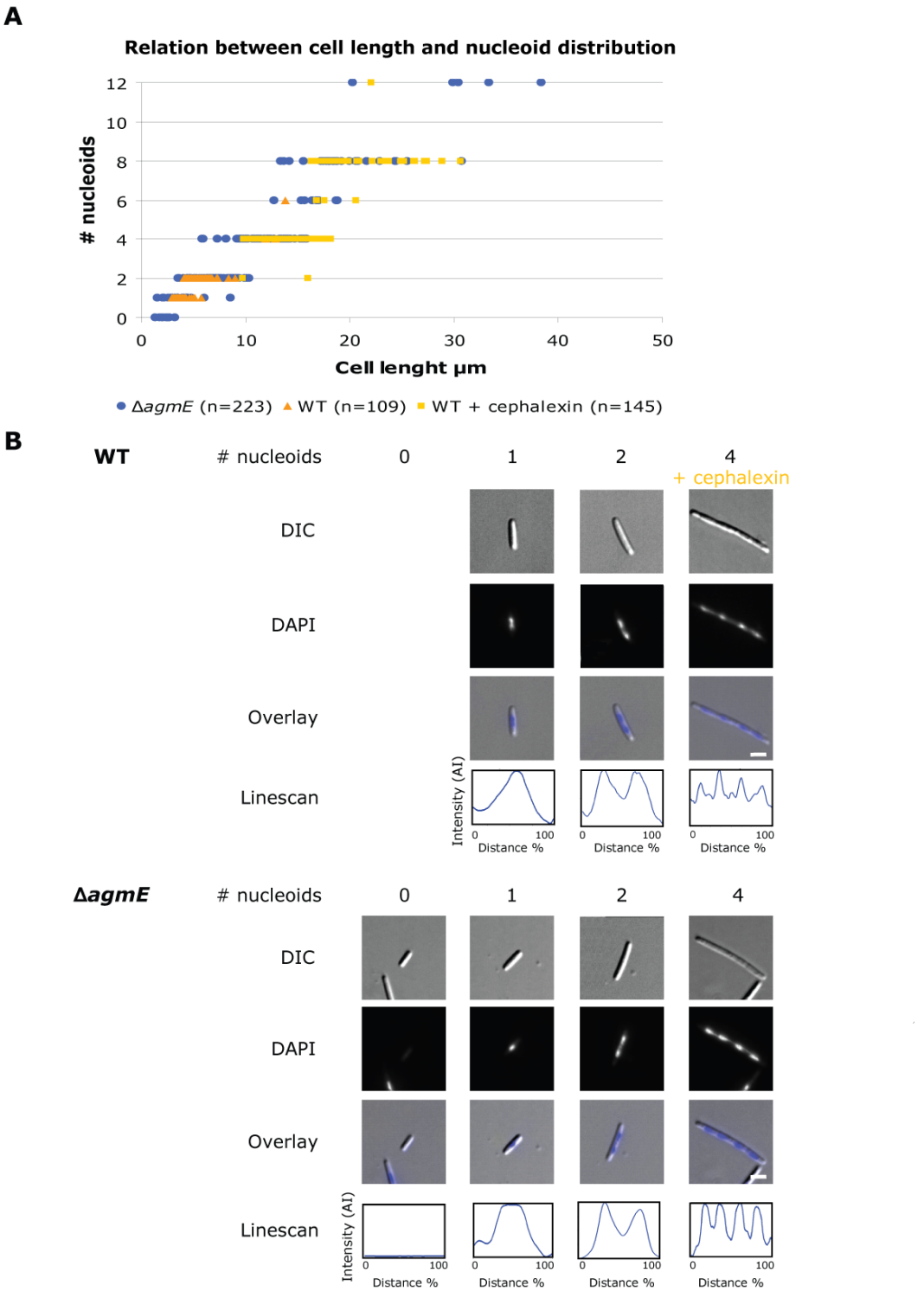


**Figure 2-8. AgmE is not involved in DNA replication or segregation**. **A)** Comparison of the number of nucleoids of exponentially growing WT, Δ*agmE* and cephalexin treated WT cells. Cephalexin treatment was carried out using 100 µM of cephalexin for two generations (8 h). Cells were DAPI stained (1 µg/ ml) for 10 min and the number of nucleoids were counted using the linescan function of Metamorph® 7.5 (maximum value, scan width 10) to measure the fluorescence intensity of the DAPI signal. One peak represents one nucleoid. **B)** Comparison of nucleoid positioning within WT, cephalexin treated WT and Δ*agmE* cells. The procedure was performed as described in A. Scale bars represent 2 µm.

These results imply that DNA replication is not affected in Δ*agmE* cells. During this analysis, we observed that 4% Δ*agmE* cells lacked a nucleoid, and these cells are consistenly the very short cells (Figure 2-8A).

To adress whether AgmE is involved in DNA segregation, the same type of analysis was used to determine nucleoid positioning (Figure 2-8B). In WT and Δ*agmE* cells, the nucleoids are positioned depending on their number. One nucleoid is located at mid-cell while two nucleoids are positioned at the ¼ and ¾ positions of the cell length. Cephalexin treated WT and longer Δ*agmE* cells also have their nucleoids evenly spaced. This result implies that the Δ*agmE* mutation does not affect DNA segregation.

### 2.2.2 AgmE might be involved in cell division

In the previous analyses, it was observed that 4% of the Δ*agmE* cells do not contain a nucleoid. These mini-cells, as well as filamentous cells, could be explained by the aberrant positioning of the septum in Δ*agmE* mutant cells (Figure 2-9). To explore this possibility, the positioning of septums was analysed in WT and Δ*agmE* cells. In WT cells, 9% of the cells (n=243) contain a septum which is located at mid-cell (100% of cell presenting a septum). However, in the absence of *agmE*, the cells divide less frequently and only 3% of the cells present a septum (n=421) and the placement of the septum seems to be more random e.g. 29% of the cells contained a septum close to a pole, which could lead to the formation of anucleated cells (4%). The less frequent division sites, the abnormal localization of the septum and the normal DNA replication and segregation suggests that AgmE have an important function in cell division.

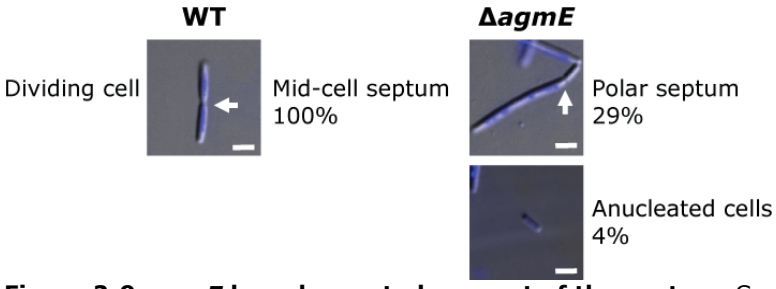


**Figure 2-9. *agmE* has aberrant placement of the septum**. Comparison of the placement of the septum in WT and Δ*agmE* cells. The white arrow shows the position of the septum. In WT, 9% of cells contain a septum (n=243), which is located at mid-cell (100% of cells containing a septum). In Δ*agmE* mutant, 3% of cells present a septum (n=421) from which 29% contain a septum close to a pole. Only in an Δ*agmE* mutant, mini-cells with no nucleoids are present (4%). Scale bars represent 2 µm.

## 2.3 FtsZ localization

Correct placement of the division site depends on the localization of the FtsZ protein. FtsZ is the first protein to localize at the division site and acts as a scaffold for other proteins, which later form the cytokinesis machinery (den Blaauwen *et al.*, 2008; Lutkenhaus and Addinall, 1997; Sackett *et al.*, 1998). Since the placement of the septum seems to be random in Δ*agmE* cells, we asked if this is due to the incorrect localization of FtsZ.

### 2.3.1 FtsZ localization

It has been described that FtsZ-GFP is unable to complement an *E. coli ftsZ* mutant (Ma *et al.*, 1996). Moreover, *ftsZ* is an essential gene in *M. xanthus* (Garcia-Moreno *et al.*, 2009). Therefore, an *ftsZ*-mCherry fusion under the control of its native promoter (400bp upstream the *ftsZ* gene) was constructed and placed at an exogenous site (Mx8 attachment site) in WT and Δ*agmE* cells. This strategy could lead to a slight cell division inhibition since it is known that altering FtsZ levels can result in filamentous cells in *E. coli* (Ma *et al.*, 1996). Therefore, the cell length distribution of strains containing an *ftsZ*-mCherry fusion and the expression levels were determined (Figure 2-10). In the WT strain containing FtsZ-mCherry, cells were slightly longer than WT cells but not filamentous. This strain was then used to analyze FtsZ localization. Furthermore, the cell size was also slighty increased in an Δ*agmE* strain containing FtsZ-mCherry compared to Δ*agmE* cells. Using our specific FtsZ antibodies (Materials and Methods), full length FtsZ-mCherry was detected in both strains with little or no degration; however the fusion proteins are expressed at lower levels than the WT protein (Figure 2-10B).

The timing of FtsZ assembly into the Z-ring is usually analyzed with reference to cell length in a random population of exponentally growing culture (Inoue *et al.*, 2009). In *M. xanthus* WT cells, FtsZ was observed to have two localization patterns, which correlate with cell length (Figure 2-11). In 51% of WT cells, corresponding to small-sized cells, FtsZ is localized in randomly distributed clusters along the cell body and these clusters do not cross the cell width, hereafter this pattern is termed speckled-pattern. In the remaining 49% of the cells, corresponding to large-sized cells, FtsZ is localized in a cluster spanning the cell width at mid-cell even before

constriction is visible (Figure 2-11). In contrast in Δ*agmE* cells, FtsZ is found mainly in speckled-pattern irrespectively of cell lenght (98%) (Figure 2-11). These observations indicate that the localization of FtsZ at mid-cell depends on AgmE. These data, then, strongly support that AgmE is involved in cell division.

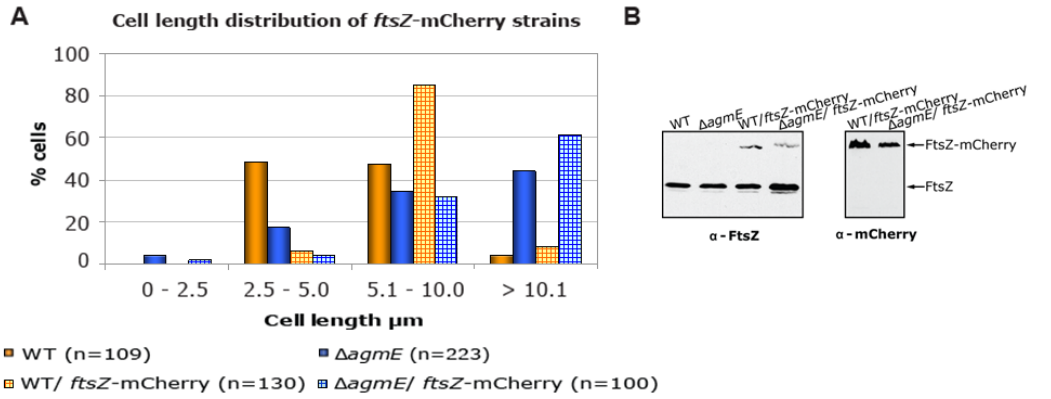


**Figure 2-10. Strains carrying *ftsZ*-mCherry fusion proteins show cell elongation. A)** Cell length distribution of strains carrying FtsZ-mCherry fusion protein compared to WT and Δ*agmE* cells. The cell length was measured using the region measurement function of Metamorph® 7.5. **B)** Levels of FtsZ-mCherry in WT and Δ*agmE* cells. Equal amounts of total protein were resolved on a SDS-PAGE and subjected to immunoblot analysis using anti-sera specific to FtsZ and DsRed. mCherry is a derivative of DsRed fluorescence protein, which is also recognized by the anti-sera specific for DsRed (gift from Patrick Viollier). For simplicity this anti-sera is name α-mCherry.

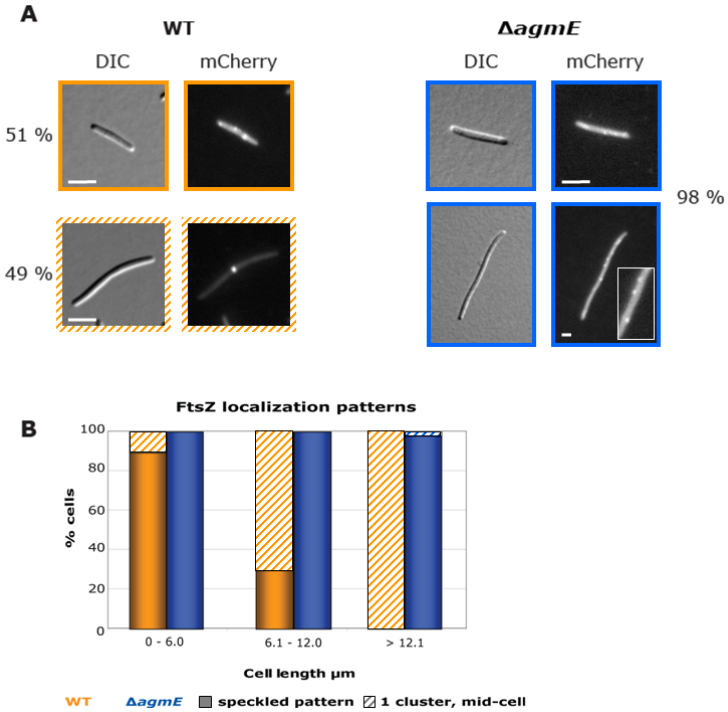


**Figure 2-11. FtsZ localization in WT and Δ*agmE* cells. A)** Subcellular localization of FtsZ-mCherry in WT and Δ*agmE* cells. Cells were taken in exponentially growth phase and were placed on a thin TPM- 1% agarose pad. FtsZ localization patterns were determined by

counting 130 WT and 100 Δ*agmE* cells, respectively. The scale bars represent 2 µm. The inner box in the lower picture for Δ*agmE* has been enlarged three fold to better observe the FtsZ "speckles". **B)** FtsZ localization patterns in function of the cell length in WT and Δ*agmE* mutant. For each cell length class, the number of cells was normalized to 100% and the percentage of cell presenting each localization pattern is shown.

### 2.3.2 FtsZ and cell cycle

Because FtsZ localization patterns correlate with cell size in WT, it was hypothesized that the two patterns might represent the status of the cell cycle. To verify this, the WT strain containing FtsZ-mCherry fusion protein was DAPI stained and the FtsZ localization patterns determined together with the number of nucleoids (Figure 2-12). When FtsZ localizes in a speckled-pattern, cells contain either one (52%) or two incompletely segregated nucleoids (48%). On the other hand, 100% cells containing two fully segregated nucleoids contained FtsZ at mid-cell. Hence, FtsZ localization patterns correlate with the different states of the cell cycle. FtsZ speckled-pattern localization correlates with cells that are replicating/segregating their nucleoids whereas FtsZ mid-cell localization correlates with cells that have completed nucleoid segregation.

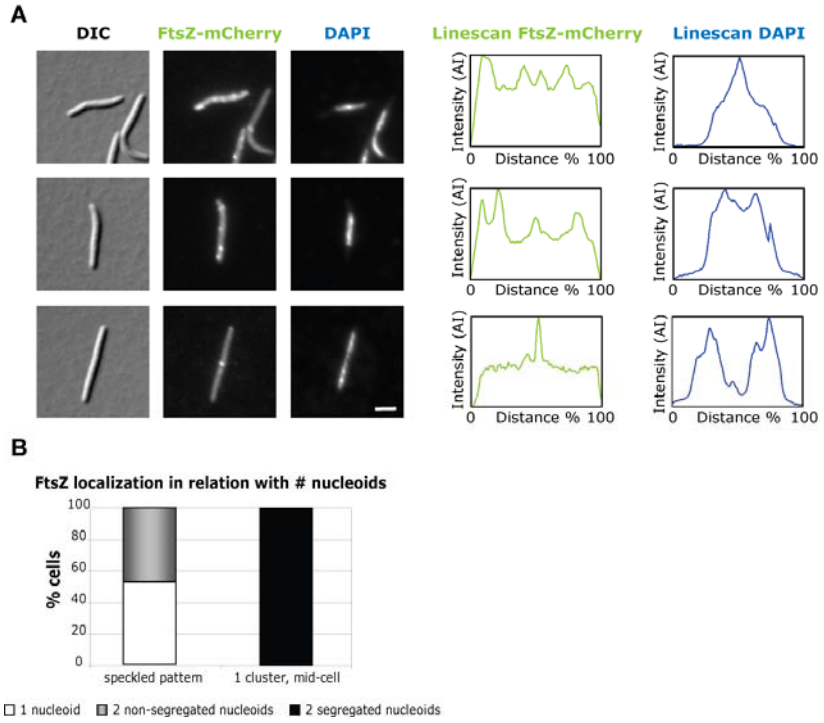


**Figure 2-12. FtsZ localization depends on the cell cycle. A)** Determination of number of nucleoids in WT/*ftsZ*-mCherry cells. Exponentially growing cells were DAPI stained (1 µg/mL) and FtsZ localization as well as the number of nucleoids were determined (n=100) using the linescan function of Metamorph® 7.5 (maximum value, scan width 10). Scale bar represents 2 µm. **B)** FtsZ localization patterns in relation with the number of nucleoids. For each localization pattern the number of cells counted was normalized to 100% and the percentage of cell presenting one or two non-fully segregated or two fully segregated nucleoids is shown.

Because the FtsZ localization patterns do not correlate with cell length in the Δ*agmE* mutant (Figure 2-11), it was interesting to analyze if FtsZ-rings (e.g. clusters crossing the cell width) are formed over the nucleoids in Δ*agmE* cells. As shown in Figure 2-13, FtsZ speckles can localize over the nucleoids, whereas FtsZ only forms a Z-ring that spans the cell width when it is localized between the nucleoids. This preliminary result (n < 100) suggests that *M. xanthus* possesses a nucleoid occlusion system which prevents cell division in the vicinity of the nucleoid (Wu and Errington, 2004).

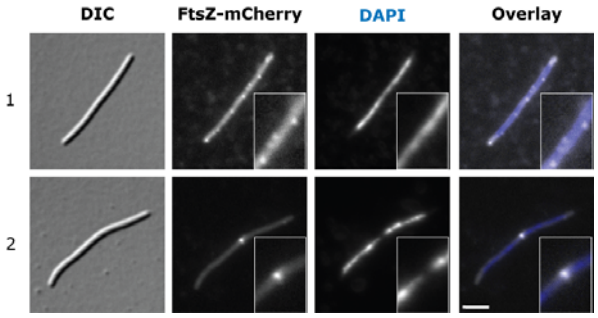


**Figure 2-13. FtsZ-ring can only form between nucleoids in Δ*agmE* cells.** Exponentially growing cells were DAPI stained (1μg/ml). 1) Cell presenting FtsZ speckled-pattern localization. FtsZ "speckles" localize over the nucleoid (n=20). 2) Cell presenting FtsZ localization close to mid-cell (n=5). The scale bar represent 5 μm and the inner boxes have been enlarged three fold to better visualized FtsZ localization.

### 2.3.3 FtsZ localization is dynamic

Time lapse microscopy was performed to determine whether the localization of FtsZ is dynamic. For this, exponentially growing cells were placed onto 0.25% CTT thin 1% agarose pads and FtsZ-mCherry localization followed for 20 minutes with frames captured every 5 minutes (Figure 2-14). The localization of the FtsZ speckles rapidly changed over time (Figure 2-14, cell 1). This implies that FtsZ localization is highly dynamic. Eventually these speckles concentrate to a focus at mid-cell (Figure 2-14, cell 2). Once FtsZ has reached mid-cell, it stably remains there, likely until cell division occurs (Figure 2-14, cell 3). These results suggest that FtsZ localization presents two dynamic patterns: 1) fast dynamics represented by the "speckles" moving rapidly within the cell; 2) slow dynamics where the "speckles" concentrate to one single focus at mid-cell during the course of the cell cycle.

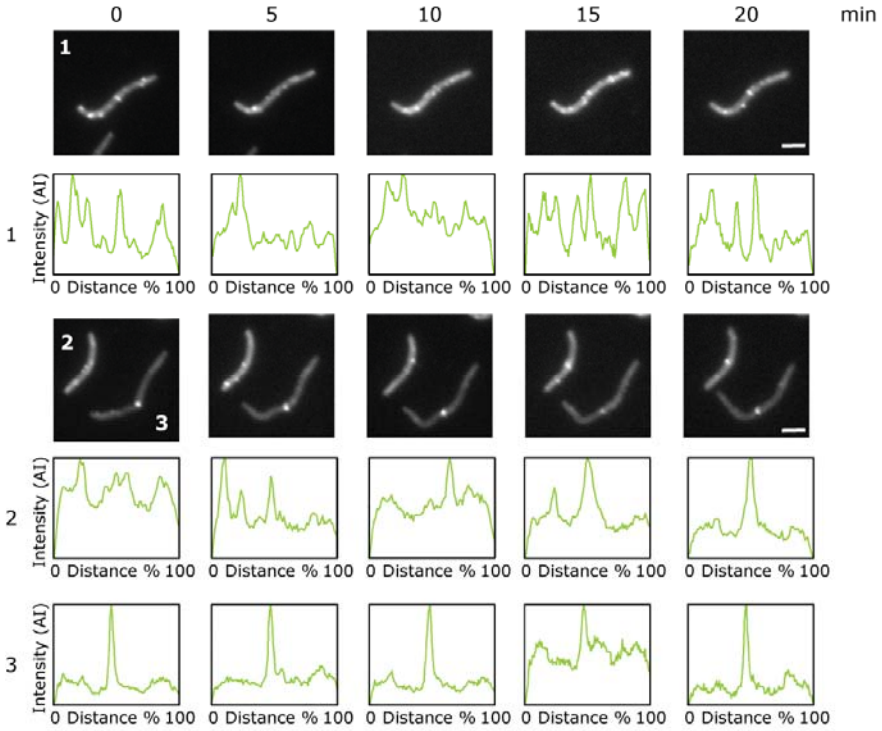


**Figure 2-14. FtsZ localization is dynamic.** Subcellular localization of FtsZ-mCherry during the time course. Exponentially growing cells were placed onto a thin 0.25% CTT 1% agarose pad (t = 0 min) and visualized at 5 min intervals by light and fluorescence microscopy. The fluorescence intensity of FtsZ-mCherry was measured using the linescan function of Metamorph® 7.5 (maximum value, scan width 10). 1) Cell presenting FtsZ "speckles" rapidly changing localization over time. 2) Cell presenting FtsZ "speckles" that concentrate at mid-cell. 3) Cell presenting stable FtsZ mid-cell cluster. At least 4 cells having each localization pattern were visualized. Scale bar represents 2 µm.

To summarize these results, in WT cells, FtsZ localizes in two different patterns which correlate with cell length and with the status of the cell cycle (e.g DNA replication/segregation). Moreover, the speckled-pattern localization is highly dynamic since the "speckles" change localization over a period of five minutes, and the "speckles" then concentrate to form a stable focus at mid-cell. In contrast in Δ*agmE* cells, FtsZ mostly localizes in a speckled-pattern regardless of cell size and cell cycle since DNA replication and segregation are normal in the Δ*agmE* mutant. Taken together these data support that AgmE is required for the proper localization of FtsZ. This implies two possibilities for the function of AgmE: AgmE is required for the localization of FtsZ at mid-cell or AgmE plays a role in the stabilization of the FtsZ-ring once it is formed.

## 2.4 AgmE localization

There are different ways to ensure that FtsZ localizes at mid-cell. One way is to inhibit FtsZ polymerization at the poles as in the case for the Min system in *E. coli* and *B. subtilis* or MipZ in *C. crescentus*, leaving only mid-cell free for FtsZ polymerization and subsequent assembly of the cytokinesis machinery (Lutkenhaus, 2007; Thanbichler and Shapiro, 2006). Another possibility is to positively regulate FtsZ polymerization at mid-cell, by either stabilizing FtsZ-ring at mid-cell (e.g. FtsA, ZipA, and ZapA) (Lutkenhaus, 2007) or by directing FtsZ to mid-cell. However, currently there is no example in the literature of a protein that localizes before FtsZ at mid-cell and directs FtsZ to mid-cell. To understand whether AgmE is acting negatively or positively on FtsZ localization, AgmE localization was investigated.

### 2.4.1 AgmE localization

To determine AgmE localization, an *agmE*-mCherry fusion was generated under the control of its native promoter and integrated at an exogenous site (Mx8 attachment site) in the Δ*agmE* mutant. To verify that the fusion protein is functional, the cell length distribution and the expression levels were determined (Figure 2-15). The cell length distribution of Δ*agmE*/*agmE*-mCherry strain is restored to that of WT (Figure 2-15A). Moreover, immunoblot analyses were performed and it was observed that the full length protein is present essentially at WT levels. In addition, the fusion protein undergoes a partial degradation as detected with AgmE antibodies (Figure 2-15B). These results imply that the fusion protein is functional. AgmE localization was studied using this strain.

AgmE localizes in three distinct patterns, which correlates with cell length: patchy, focus off-center and focus at mid-cell (Figure 2-16). In short cells, AgmE localized in a patchy pattern (24% of observed cells). As the cell size increased, AgmE localized in a single focus off-center (⅜ of the cell length) (26% of observed cells), and finally localized at mid-cell in larger cells even before constriction was visible (50% of observed cells). Because AgmE does not localize at the poles and localizes at mid-cell in 50% of the cells, we hypothesize that AgmE acts positively on FtsZ mid-cell localization.

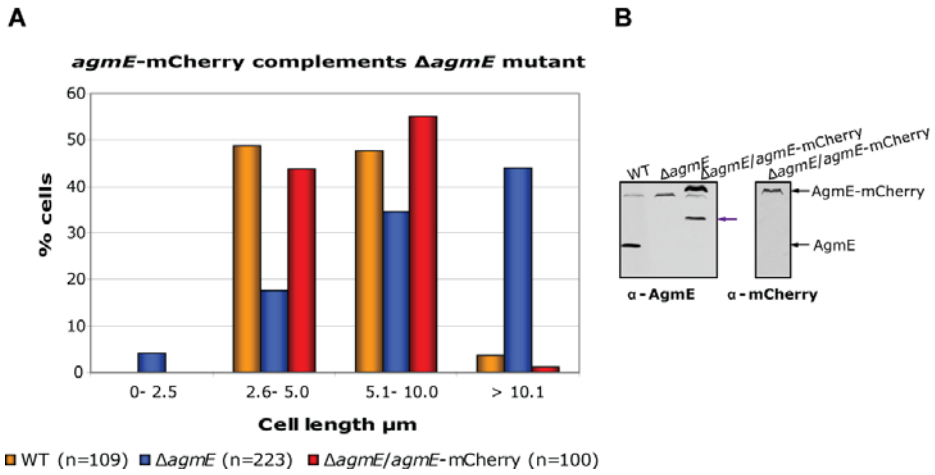


**Figure 2-15. *agmE*-mCherry fusion is functional. A)** Cell length distribution of Δ*agmE*/*agmE*-mCherry compared to WT and Δ*agmE* cells. The cell length measurements were performed using the region measurement function of Metamorph® 7.5. **B)** Levels of AgmE-mCherry. Equal amounts of total protein were resolved on a SDS-PAGE and subjected to immnunoblot analysis using anti-sera specific to AgmE and mCherry. The positions of AgmE-mCherry and AgmE are indicated by the black arrows. The partial degradation product detected only with AgmE antibodies is indicated by the purple arrow.

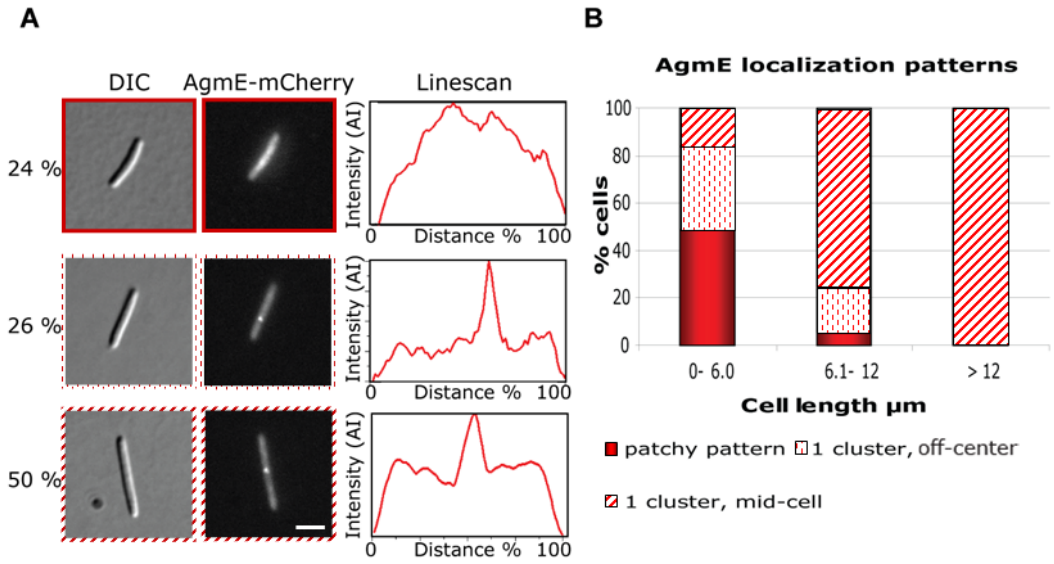


**Figure 2-16. AgmE has three localization patterns that depend on cell length. A)** Subcellular localization of AgmE-mCherry (n=100). Exponential growing cells were placed on TPM- 1% agarose and visualized by light and fluorescence microscopy. The fluorescence intensity was measure using the linescan function of Metamorph® 7.5 (maximum value, scan width 10). The scale bar represents 2 µm. **B)** AgmE localization patterns in function of the cell length. For each cell length class, the number of cells was normalized to 100% and the percentage of cell presenting each localization pattern is shown.

### 2.4.2 AgmE and cell cycle

Like for FtsZ, the AgmE localization patterns correlate with cell length, which implies that AgmE localization depends on the state of the cell during the cell cycle. In order to verify this, DAPI staining was performed in *ΔagmE*

strain containing an AgmE-mCherry fusion protein and the number of nucleoids determined (Figure 2-17). Cells with AgmE in the patchy localization pattern consistently contained one nucleoid (100%). Cells presenting AgmE in the off-center localization had either one nucleoid (40%) or two non-fully segregated nucleoids (60%). In 100% of cells presenting AgmE localization at mid-cell, the cells contained two fully segregated nucleoids. Therefore, AgmE localization clearly correlates with cell cycle.

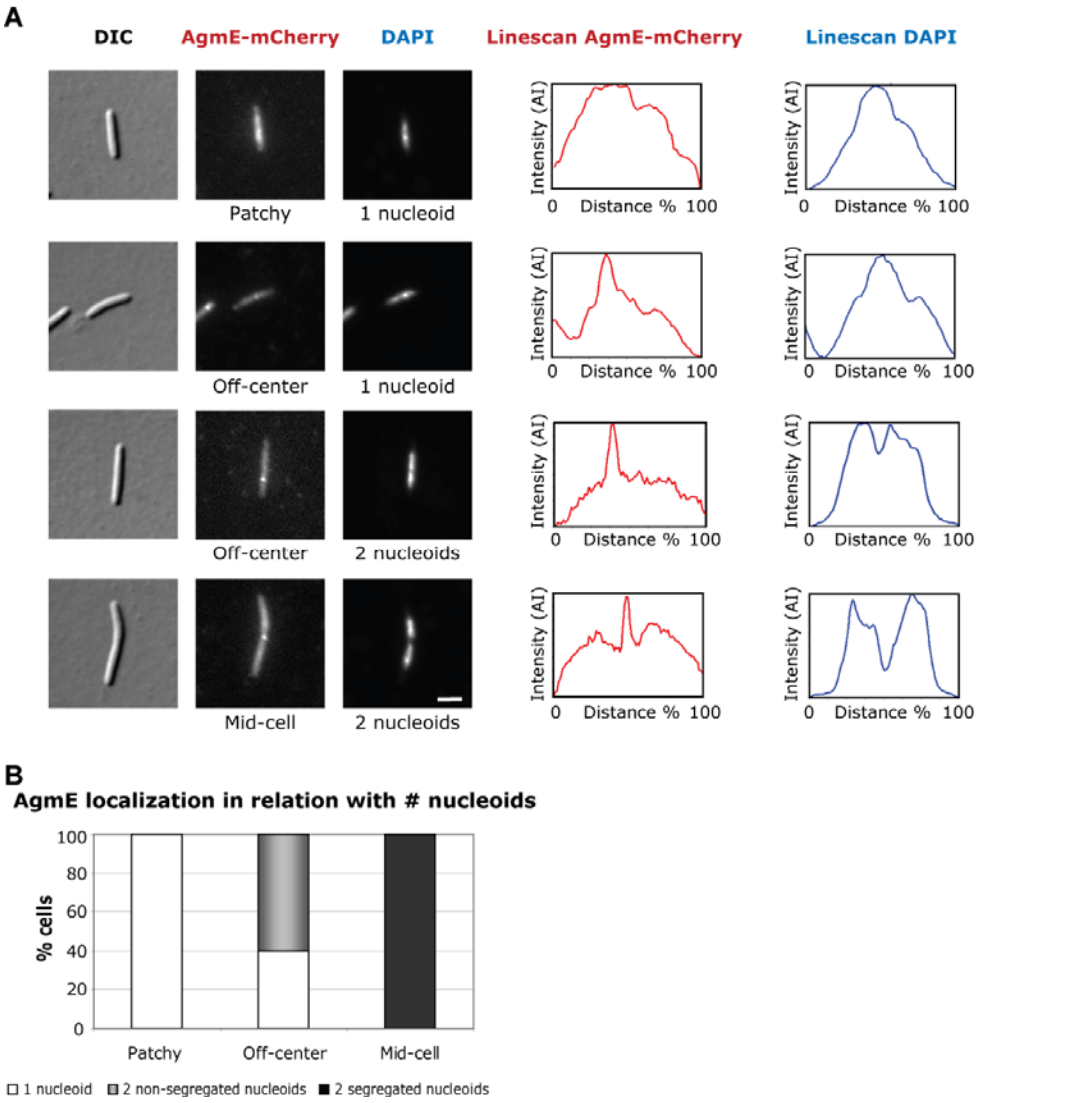


**Figure 2-17. AgmE localization depends of the cell cycle. A)** Correlation between AgmE localization pattern and the number of nucleoids. Cells were taken from exponentially growing culture, DAPI stained (1 µg/ml) and placed onto a thin TPM-1% agarose pad. The number of nucleoids and AgmE localization was determined (n=110) using the linescan function of Metamorph® 7.5 (maximum value, scan width 10). Scale bar represents 2 µm. **B)** AgmE localization patterns in relation with the number of nucleoids. For each localization pattern the number of cells counted was normalized to 100% and the percentage of cell containing one or two non-fully segregated or two fully segregated nucleoid is shown.

### 2.4.3 AgmE localization is dynamic during cell cycle

To investigate if AgmE localization is dynamic, time lapse microscopy was performed (Figure 2-18). For this, exponentially growing cells were placed onto 0.25% CTT thin 1% agarose pads and AgmE-mCherry localization followed for 15 minutes with frames captured every 5 minutes. During the course of the time lapse microscopy, most of the cells studied presented AgmE in a stable localization pattern (Figure 2-18, cells 1, 3 and 5). In other words, AgmE localization did not change during the time course irrespectively of whether cells displayed patchy, off-center or mid-cell localization patterns. This means that AgmE does not present fast dynamics as described for FtsZ "speckles" (section 2.3.3). Occasionally, however, AgmE localization changed from patchy to one off-center cluster or from one off-center cluster to a mid-cell cluster (Figure 2-18, cells 2 and 4). Therefore in contrast to the fast and slow dynamics of FtsZ localization, only slow dynamic localization was observed for AgmE.

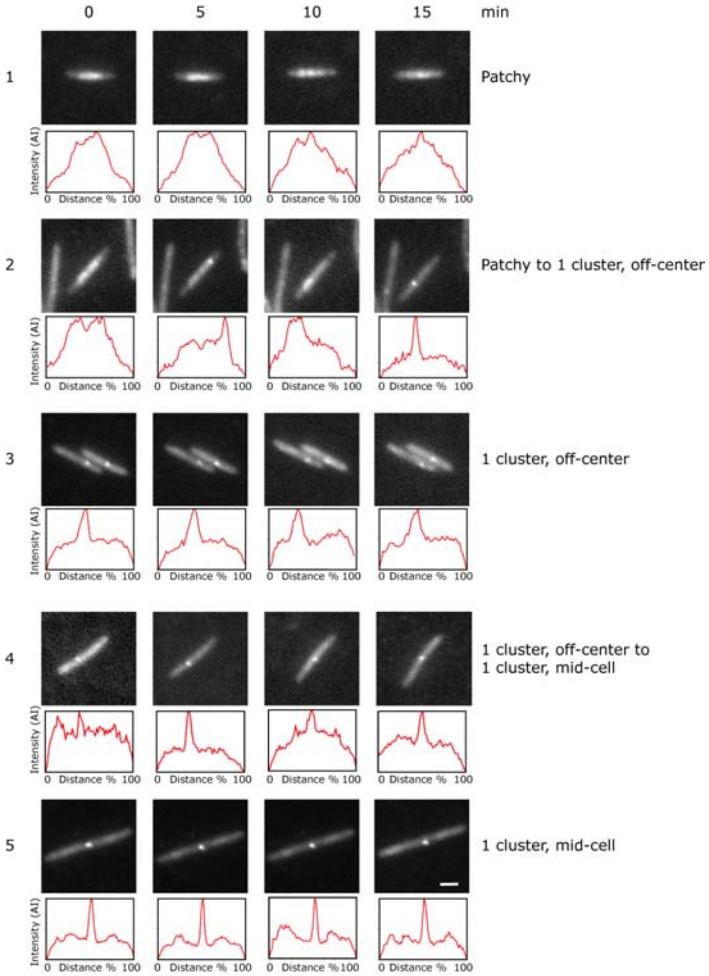


**Figure 2-18. AgmE localization is dynamic during the cell cycle.** Subcellular localization of AgmE-mCherry during the time course. Exponentially growing cells were placed onto a thin 0.25% CTT 1% agarose pad (t = 0 min) and visualized at 5 min intervals by light and fluorescence microscopy. The fluorescence intensity of AgmE-mCherry was measured using the linescan function of Metamorph® 7.5 (maximum value, scan width 10). At least 2 cells having each localization pattern were visualized.

### 2.4.4 Comparison of AgmE and FtsZ localization patterns

Both AgmE and FtsZ localization depend on the cell cycle: before cell initiate DNA replication and when the cells are replicating and/or segregating their DNA, AgmE and FtsZ are not localized at mid-cell and when DNA segregation is completed both proteins localize to mid-cell. To attempt a direct comparison of both AgmE and FtsZ localization, a "timeline" was constructed in which the localization patterns in the two strains containing AgmE-mCherry and FtsZ-mCherry were studied in relation to the cell length (Graph 2-1). To circumvent the slight difference in cell size in these strains, the cell length was converted to percentage (100% represents the longest cell of each strain). From this timeline, it evident that small cells contain AgmE and FtsZ in patchy and speckled patterns, respectively. As cell size increases both AgmE and FtsZ tend to localize at mid-cell. We, therefore, hypothesize that AgmE and FtsZ co-localize at mid-cell in cells with segregated chromosomes. However, from this analysis, it is not possible to conclude which protein localizes first at mid-cell.

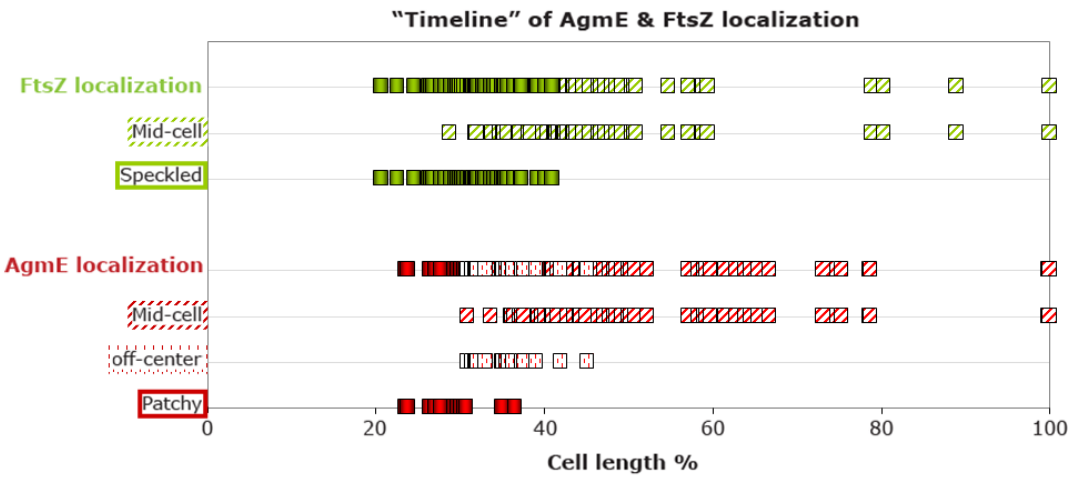


**Graph 2-1. "Timeline" of AgmE and FtsZ localizations.** The squares represent cells and the different colors show AgmE localization in **red** (n=100) and FtsZ localization in **green** (n=130). Filled squares symbolize patchy or speckled localization patterns, dotted squares represent AgmE off-center localization and stroked squares correspond to mid-cell localization. The localization patterns are shown in relation to the cell length, which is presented in percentage (100% represent the longest cell for each strain).

## 2.5 AgmE and FtsZ localization

The localization of AgmE at mid-cell implies that AgmE acts positively on the localization of FtsZ by directing FtsZ localization or stabilizing the FtsZ-ring at mid-cell. To distinguish between these models, co-localization studies were carried out.

### 2.5.1 AgmE and FtsZ localization

In order to localize FtsZ and AgmE within the same cell, a FtsZ-GFP fusion protein under the control of its native promoter was constructed and integrated at an exogenous site (Mx8 attachment site) while the construct coding for AgmE-mCherry integrated at another exogenous site via homologues recombination (*carS* locus). Both fusion proteins were then introduced in WT and Δ*agmE* cells. For both strains, the cell length distribution and localization patterns were analyzed and compared to the results obtained for WT/*ftsZ*-mCherry and Δ*agmE*/*agmE*-mCherry (Figure 4-1 and Figure 4-2 in supplementary results). Both fusion proteins behave as previously described (section 2.3.1 and 2.4.1). However, the fluorescence intensity of the FtsZ-GFP fusion was diminished compared to FtsZ-mCherry; thus the FtsZ "speckles" could no longer be observed and the localization pattern was, therefore, renamed to diffuse localization instead of speckled-pattern.

The localization patterns of AgmE and FtsZ were studied in WT cells. First, the cell length distribution of this strain and expression levels of AgmE-mCherry and FtsZ-GFP were determined (Figure 2-19). As previously shown for the WT strain containing an extra copy of FtsZ, cells were slightly elongated but not filamentous (Figure 2-19A) (section 2.3.1). The full length AgmE-mCherry fusion is present at slightly higher levels than WT. The full length FtsZ-GFP is present at lower levels than WT.

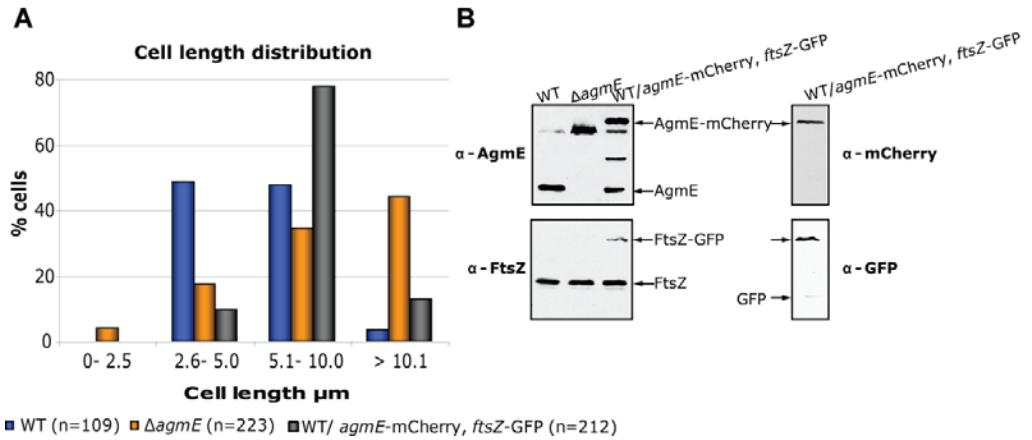


**Figure 2-19. Cell length distribution of WT carrying AgmE and FtsZ fusion proteins. A)** Cell length distribution of WT/*agmE*-mCherry, *ftsZ*-GFP compared to WT and Δ*agmE* cells. Cell length was measure using the region measurement function of Metamorph® 7.5. **B)** Levels of AgmE-mCherry and FtsZ-GFP fusion proteins. Equal amounts of total protein were resolved on a SDS-PAGE and subjected to immunoblot analysis using anti-sera specific to AgmE, FtsZ, GFP and mCherry.

Next, the localization patterns were analyzed (Figure 2-20). In cells with AgmE localizing in a patchy pattern or in an off-center cluster, FtsZ is localized in a diffuse pattern (21% and 22 %, respectively). As the cell size increased, AgmE localized at mid-cell and co-localized with FtsZ (45%). Intriguingly, 12% of cells displayed mid-cell localization of AgmE in the absence of mid-cell localization of FtsZ.

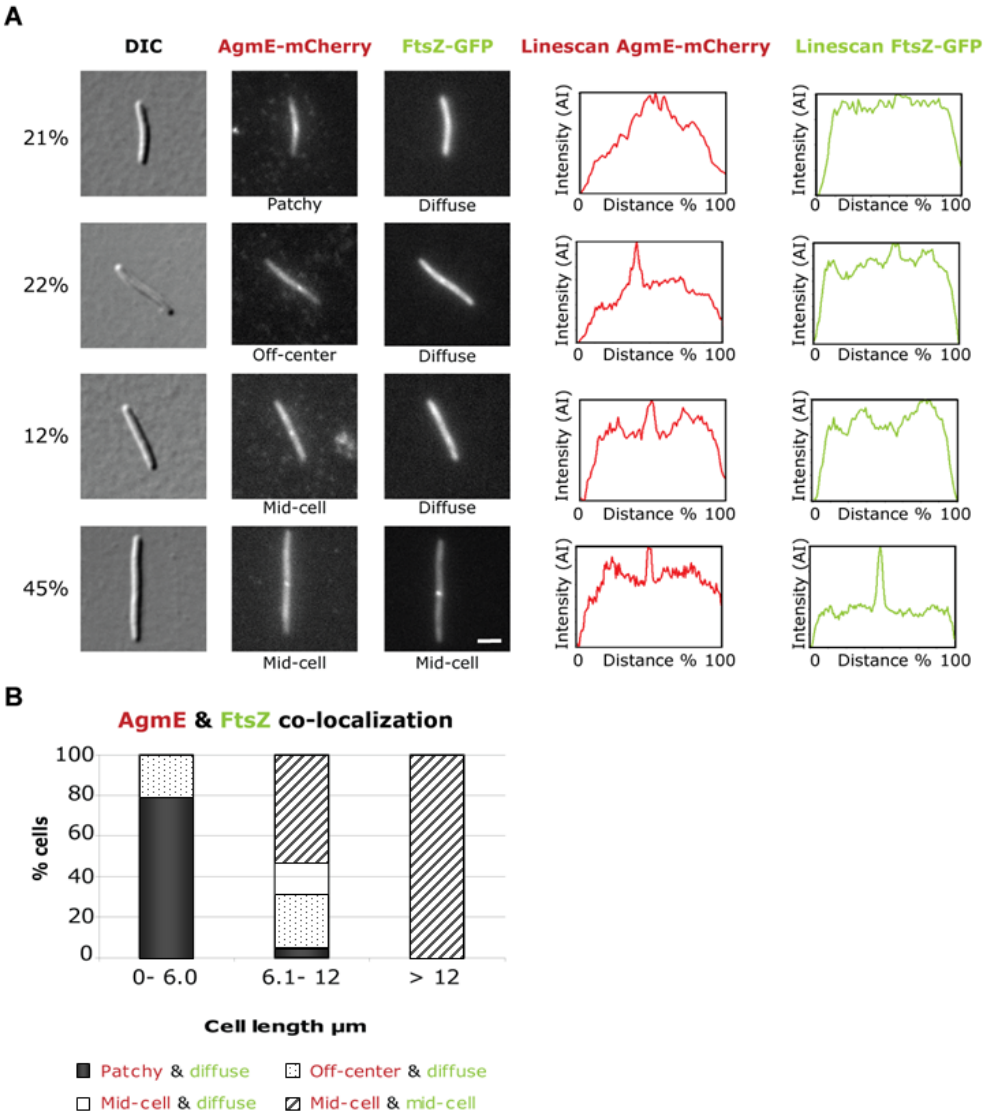


**Figure 2-20. AgmE and FtsZ localizations. A)** Subcellular localization of AgmE-mCherry and FtsZ-GFP (n=212). Exponential growing cells were place on TPM- 1% agarose and visualized by light and fluorescence microscopy. The fluorescence intensity were measured using linescan function of Metamorph® 7.5 (maximum value, scan width 10). The scale bar represents 2 µm. **B)** AgmE and FtsZ localization patterns in relation with cell length. For each cell length class, the number of cells was normalized to 100% and the percentage of cell presenting each localization pattern is shown.

The correlation between the different patterns of localizations and cell size is better visualized in Graph 2-2. Small cells have AgmE localized in a patchy pattern and FtsZ is diffusely localized, as the cell length increases AgmE localizes in one single off-center focus, and finally once the cells have reached a specific size AgmE localizes at mid-cell and FtsZ then seems to localize at mid-cell with AgmE in larger-sized cells.

On the basis of the localization of AgmE to mid-cell and the observation that AgmE localizes to mid-cell before FtsZ, we propose that AgmE is a novel cell division regulator that acts positively to directly place FtsZ at mid-cell. However, a stabilization function of AgmE on FtsZ-ring can not be excluded at this point.

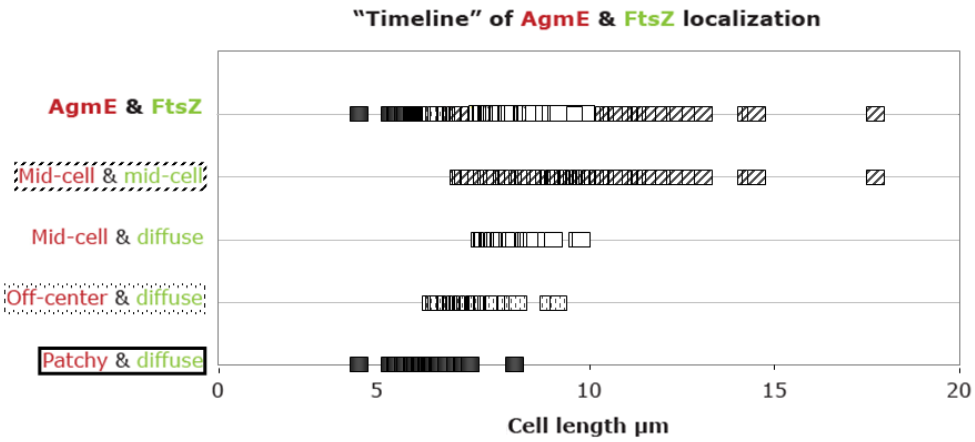


**Graph 2-2. " Timeline" of AgmE and FtsZ localization patterns in function of the cell length.** The squares represent cells that show AgmE and FtsZ localization (n=212). Filled squares symbolize patchy or diffuse localization patterns, dotted squares represent AgmE and FtsZ not mid-cell localization, non filled squares represent AgmE mid-cell localization while FtsZ is diffuse and stroked squares correspond to both proteins localized at mid-cell. The localization patterns are shown in relation to the cell length.

### 2.5.2 Localization of AgmE and FtsZ when cell division is inhibited

Previous data have shown that FtsZ localization at mid-cell is dependent on AgmE. In order to analyze this dependence, cell division was inhibited and the localization of AgmE and FtsZ determined (Figure 2-21). This preliminary experiment (n < 100) shows that FtsZ localized in one focus at or close to mid-cell and AgmE co-localized with FtsZ. This suggests that the completion of cell division is a requirement for the localization of FtsZ and AgmE to nascent division sites. AgmE also seem to localize in a patchy pattern as well as in one cluster when cell division is inhibited. Therefore, it would

seem that when cell division is inhibited AgmE is capable of localizing in two different patterns. Since the fluorescence of FtsZ-GFP is lower that FtsZ-mCherry, we can not exclude that FtsZ also localizes in a speckled-pattern.

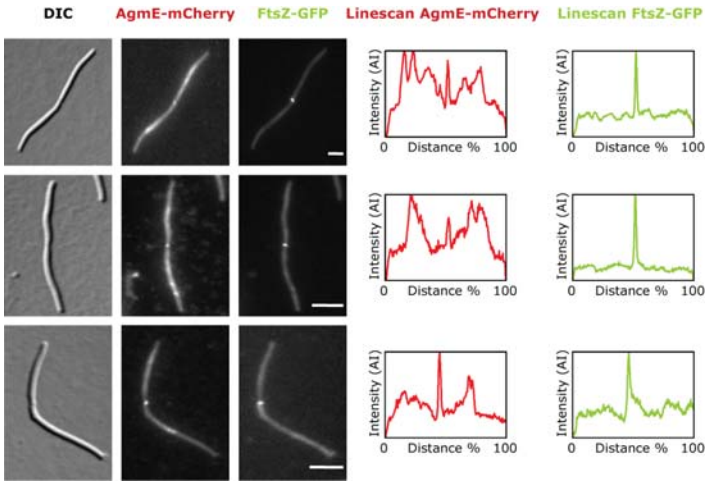


**Figure 2-21. Localization of AgmE and FtsZ during inhibition of cell division.** Subcellular localization of AgmE-mCherry and FtsZ-GFP (n=30). Exponentially growing cell were treated for two generations (8h) with 100 µM cephalexin and then were placed on TPM-1 % agarose and visualized by light and fluorescence microscopy. Fluorescence intensities were determined using linescan function (Metamorph® 7.5, maximum value, scan width 10). Scale bars represent 10 µm.

## 2.6 Understanding how AgmE functions

To understand how AgmE may functions, we first focused on the properties of ParA-like proteins. It has been described that the ATPase activity is important for their function. In addition, some ParA-like proteins are able to polymerize *in vitro* (Barilla *et al.*, 2005; Leonard *et al.*, 2005).

Second, we focused on the role of AgmE in cell division. It is known that for cell division to proceed properly correct levels of cell division regulators and stabilizing proteins for the FtsZ-ring are required (Dai and Lutkenhaus, 1992; de Boer *et al.*, 1992; Thanbichler and Shapiro, 2006). Therefore, the phenotype of cells overexpressing AgmE was investigated. Furthermore, AgmE and FtsZ co-localize at mid-cell (section 2.5), this suggests that AgmE might direct FtsZ to mid-cell or stabilize the formation of the FtsZ-ring at mid-cell. Either hypothesis requires AgmE to interact directly with FtsZ. Therefore, interaction studies were performed and a possible effect of AgmE on FtsZ polymerization determined.

### 2.6.1 ATP hydrolysis is important for the correct localization of AgmE

In order to test whether the ATPase activity is important for the function of AgmE, different point mutations (*agmE*$^{D90A}$, *agmE*$^{D175A}$ and *agmE*$^{K66Q}$) that are predicted to abolish ATP binding or hydrolysis were generated and the ability to complement the Δ*agmE* mutation analyzed (Figure 2-22). Of these three point mutant proteins, only AgmE$^{D90A}$ was detected and this protein accumulated at lower levels compared to WT AgmE protein. This amino acid substitution is predicted to abolish ATP hydrolysis but still allow ATP binding based on reports for Soj from *T. thermophilus* (Leonard *et al.*, 2005). The phenotypic analysis showed that *agmE*$^{D90A}$ did not complement the Δ*agmE* mutation with respect to cell length distribution. However, due to the lower accumulation levels, this result does not conclusively show whether ATPase activity is important for the function of AgmE.

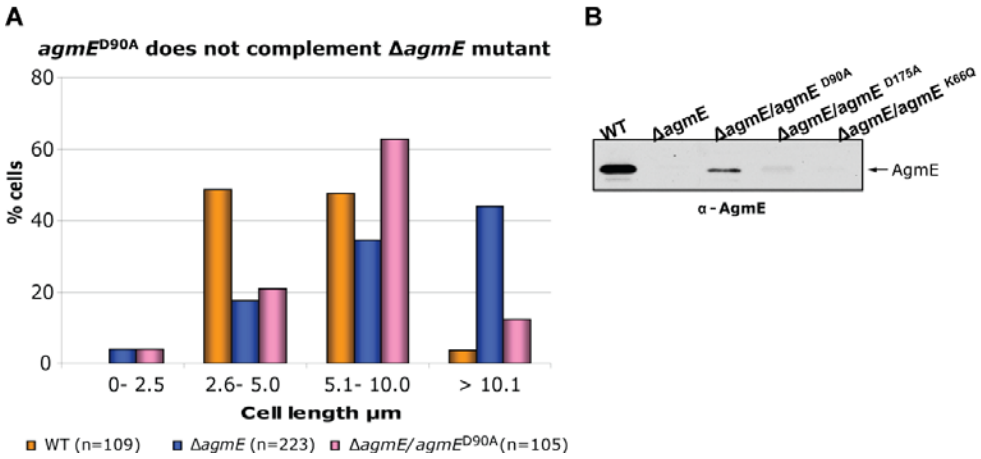


**Figure 2-22. Different point mutants predicted to abolish AgmE's ATPase activity. A)** Cell length distribution of Δ*agmE*/*agmE*$^{D90A}$ compared to WT and Δ*agmE* cells. Cell length was measured using the region measurement function (Metamorph® 7.5) **B)** Levels of AgmE point mutants in Δ*agmE* mutant. Equal amounts of total protein were resolved on a SDS-PAGE and subjected to immnunoblot analysis using anti-sera specific to AgmE.

Because AgmE$^{D90A}$ protein was the only AgmE mutant protein accumulating, the localization of AgmE$^{D90A}$ was studied in the Δ*agmE* mutant.

To verify that *agmE*$^{D90A}$-mCherry does not complement the Δ*agmE* mutant, the cell length distribution and the expression levels were determined (Figure 2-23). As expected, this point mutant does not complement the Δ*agmE* mutation. Moreover, the expression levels of the fusion protein were like WT and the AgmE-mCherry fusion. Therefore, this strain

(Δ*agmE*/*agmE*$^{D90A}$-mCherry) could be used to study the localization of the AgmE mutant protein.

In contrast to AgmE, AgmE$^{D90A}$ was localized in one focus in 80% of the cells. Intriguingly, this focus was found to localize at random positions within the cells and this localization was independent of cell length (Figure 2-24). This result suggests that ATPase hydrolysis is important for normal AgmE localization.

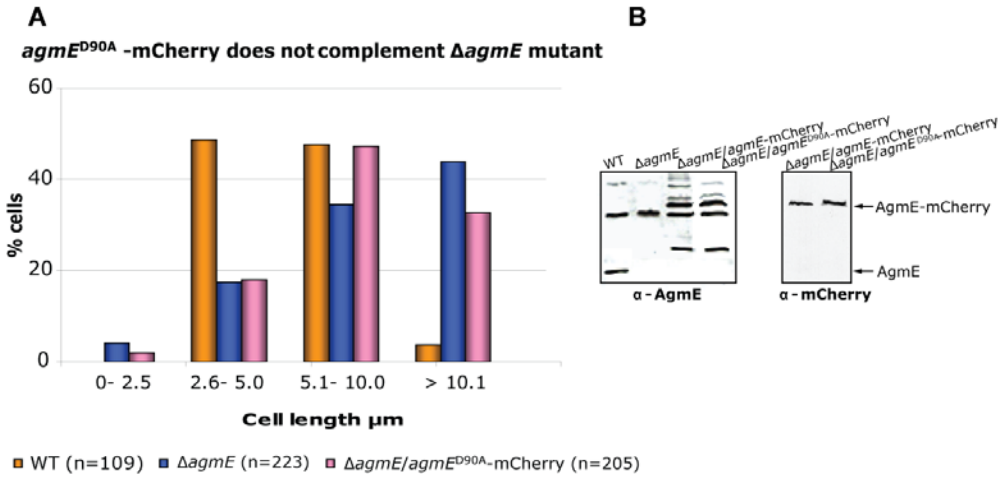


**Figure 2-23. ATPase hydrolysis is important for AgmE's function. A)** Cell length distribution of Δ*agmE*/*agmE*$^{D90A}$ compared to WT and Δ*agmE* cells. Cell length was measured using the region measurement function (Metamorph® 7.5) **B)** Levels of AgmE$^{D90A}$-mCherry. Equal amounts of total protein were resolved on a SDS-PAGE and subjected to immunoblot analysis using anti-sera specific to AgmE and mCherry.

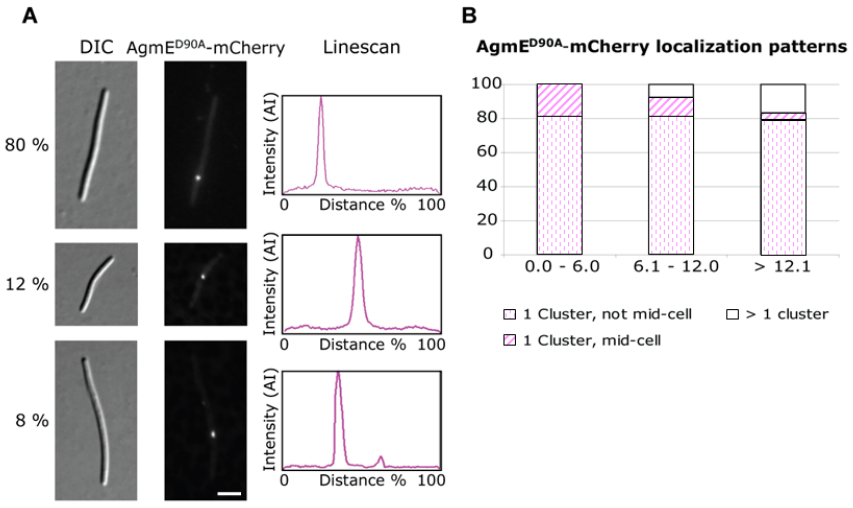


**Figure 2-24. Localization of AgmE$^{D90A}$ is independent of cell length. A)** Subcellular localization of AgmE$^{D90A}$-mCherry (n= 115). Exponential growing cells were placed on TPM-1% agarose and visualized by light and fluorescence microscopy. Fluorescence intensities were determined using linescan function (Metamorph® 7.5, maximum value, scan width 10). The scale bar represents 2 µm. **B)** AgmE$^{D90A}$ localization patterns in function of cell length. For each cell length class, the number of cells was normalized to 100 % and the percentage of cell presenting each localization pattern is shown.

AgmE$^{D90A}$-mCherry is mainly localized in one off-center focus. However, this focus is not located at the ⅜ position of the cell length as the WT AgmE protein. To begin to understand the localization of AgmE$^{D90A}$, the position of the nucleoids was visualized (Figure 2-25). AgmE$^{D90A}$-mCherry seems to localize in one cluster located over a nucleoid. From the Soj structure from *T. thermophilus* (Leonard *et al.*, 2005), AgmE$^{D90A}$ is likely capable of ATP binding but not hydrolysis. Therefore, we propose that AgmE localizes in one specific off-center focus over a nucleoid upon ATP binding and that ATP hydrolysis is important for mid-cell localization.

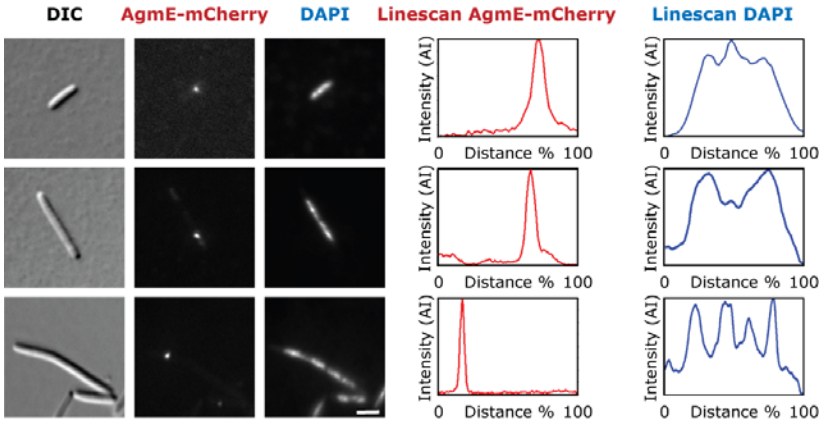


**Figure 2-25. Localization of AgmE$^{D90A}$ and nucleoids.** Exponentially growing cells were DAPI stained (1 µg/ml) and were placed on TPM-1% agarose and visualized by light and fluorescence microscopy. Fluorescence intensities were determined using linescan function (Metamorph® 7.5, maximum value, scan width 10).

To verify that AgmE has ATPase activity, *in vitro* ATPase assays were performed. Heterologous produced AgmE was purified by affinity chromatography and *in vitro* ATPase assay was performed using increasing concentrations of AgmE (Figure 2-26). However, *in vitro* AgmE ATPase activity could not be detected. This suggests that either the ATPase activity of AgmE is so low that it cannot be detected with the conditions used or that AgmE requires a co-factor to stimulate its ATPase activity.

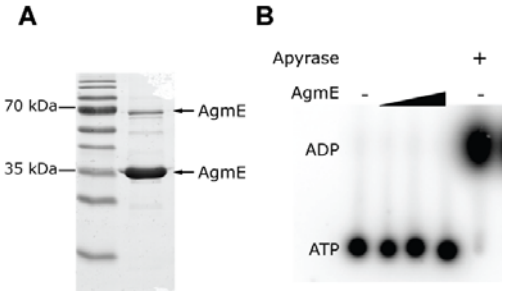


**Figure 2-26. AgmE in vitro ATPase assay.**
**A)** Purification of AgmE. Soluble His$_6$-AgmE was purified by $Ni^{2+}$ affinity chromatography as described in Materials and Methods. After SDS-PAGE, the proteins were stained with Coomassie Brilliant Blue. Molecular size markers are included on the left.
**B)** ATPase activity of AgmE. Autoradiogram of labeled adenosine phosphates after incubation of [α-$^{32}$P] ATP with the increasing concentration of His$_6$-AgmE (5µM, 10µM and 15µM) or Apyrase (2µM) followed by TLC. The positions of [α-$^{32}$P] ATP and [α-$^{32}$P] ADP are indicated.

### 2.6.2 AgmE forms polymers *in vitro*

To test whether AgmE has the ability to form polymers *in vitro*, pelleting assays based on ultracentrifugation and electron microscopy in the absence or presence of nucleotides were carried out (Figure 2-27). When alone, a small percentage of AgmE sedimented despite a clearing spin of the AgmE stock prior to starting the assay. Therefore, AgmE alone seems to have a tendency to form higher-order protein complexes (Figure 2-27A in the absence of nucleotides). After addition of nucleotides (ADP or ATP), AgmE sedimented almost completely (Figure 2-27A). To confirm that AgmE forms filaments and is not precipitating in the pelleting assay, electron microscopy was performed. As seen in Figure 2-27B, AgmE by itself did not form aggregates or filaments. However, when ATP was added, thin filaments were clearly seen, demonstrating that AgmE forms filaments *in vitro* in a nucleotide dependent manner.

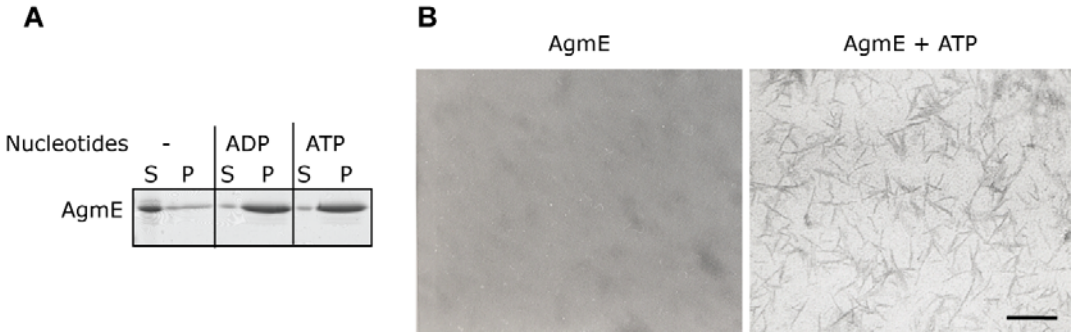


**Figure 2-27. AgmE forms polymers in a nucleotide dependent manner. A)** Nucleotide-dependent sedimentation of AgmE by ultracentrifugation. AgmE (10µM) was incubated in the absence or presence of nucleotides (2mM) and the reactions were subjected to ultracentrifugation (20 000 *x* g, 60 min, RT). The supernatants (S) and pellets (P) were analyzed by SDS-PAGE and stained with Coomassie Brilliant Blue**. B)** Negative stain electron microscopy shows that AgmE (10µM) forms filaments in the presence of ATP. Scale bar represent 125 nm.

### 2.6.3 *In vivo* overexpression of AgmE

It is known that correct levels of cell division regulators are required for cell division to proceed properly. To test whether increased levels of AgmE leads to a cell division defect, *agmE* was placed under the control of the *pilA* promoter, which leads to an estimated 10-fold increase in AgmE accumulation (Figure 2-28B). It has been described that the overexpression of cell division regulators such as MinC or stabilization proteins like FtsA leads to filamentation but not mini-cell formation (Dai and Lutkenhaus,

1992; de Boer *et al.*, 1992). Interestingly, AgmE overexpression leads to the formation of mini-cells as well as filamentous cells (Figure 2-28A).

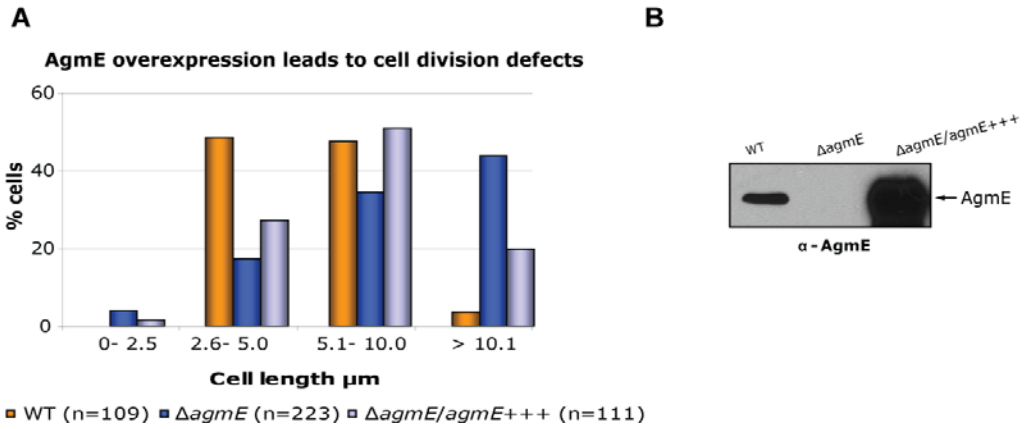


**Figure 2-28. AgmE overexpression leads to cell division defects. A)** Cell length distribution of AgmE overexpressing strain compared to WT and Δ*agmE* cells. Cell length was measured using the region measurement function of Metamorph® 7.5 **B)** Levels of AgmE when overexpressed *in vivo*. Equal amounts of total proteins were loaded on an SDS-PAGE and subjected to immunoblot analysis using anti-sera specific to AgmE.

To further characterize the AgmE overexpression phenotype, the localization of AgmE-mCherry under the *pilA* promoter was investigated. The cell length distribution was determined to confirm that the overexpression of this fusion protein also resulted in a cell division defect (Figure 2-29A). Moreover, the full length fusion protein accumulated showed by immunoblot analyses (Figure 2-29B); however, degradation products were also detected using AgmE and mCherry antibodies.

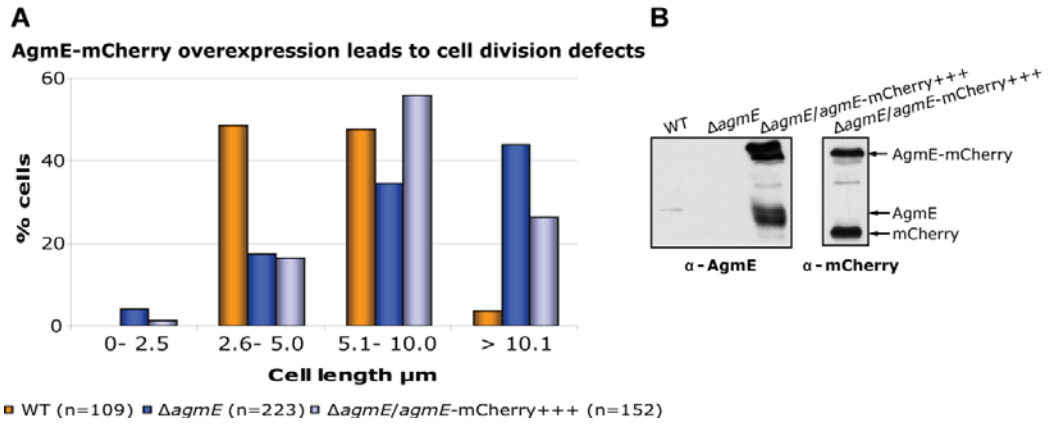


**Figure 2-29. Overexpression of AgmE-mCherry. A)** Cell length distribution of *agmE*-mCherry overexpression strain compared to WT and Δ*agmE* cells. Cell length was measured using the region measurement function of Metamorph® 7.5 **B)** Levels of AgmE-mCherry overexpression. Equal amounts of total protein were resolved in an SDS-PAGE and subjected to immunoblot analysis using anti-sera specific to AgmE and mCherry.

The localization of the overexpressed AgmE-mCherry and nucleoid positioning were determined (Figure 2-30). The overexpressed AgmE-mCherry co-localizes with the nucleoid (100%). However, overexpression of AgmE-mCherry led to DNA replication and/or segregation defects (lower panels of Figure 2-30). Large-size cells are expected to have more than 4 nucleoids, which are evenly spaced (section 2.2.1). However, that is not the case in large cells overexpressing AgmE-mCherry. Moreover, this phenotype is not due to the fusion protein since the overexpression of AgmE alone leads to the same phenotype (data not shown). This suggests that the overexpression of AgmE have pleiotropic effects. Nevertheless, these data provide evidence that it is important that AgmE is expressed at correct levels for correct cell division.

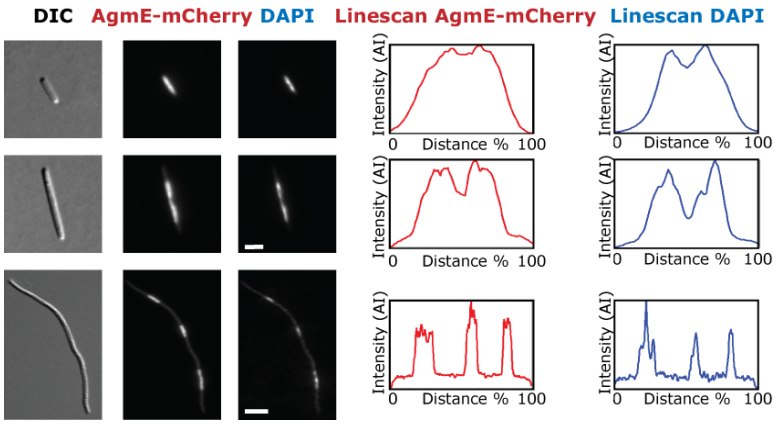


**Figure 2-30. Co-localization of AgmE-mCherry overexpression with nucleoid.** Exponentially growing cells were DAPI stained (1 µg/ml) and placed onto a thin TPM-1% agarose pad (n=100). Fluorescence intensities were determined using linescan function of Metamorph® 7.5 (maximum value, scan width 10). Scale bars represent 2 µm (upper and middle pictures) and 5 µm (lower picture)

### 2.6.4 AgmE DNA binding assay

The localization of AgmE$^{D90A}$ and overexpressed AgmE over the nucleoid made us consider whether AgmE has DNA binding capacity. In order to test this, DNA binding assays were performed in which the plasmid pMCS-2 was used as unspecific DNA and increasing amounts of AgmE added in the absence or presence of nucleotides (Figure 2-31). In the conditions tested, AgmE did not bind plasmid DNA. This could mean that either AgmE DNA binding requires a specific sequence or that AgmE indirectly binds DNA through an unidentified protein.

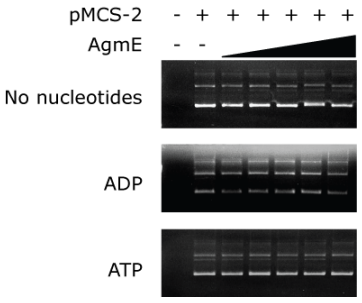


**Figure 2-31. Electrophoretic mobility shift assay of AgmE DNA binding.** The ability of AgmE to bind double stranded plasmid DNA (200 fmoles of pMCS-2) was assayed in the absence of nucleotides and in the presence of ADP or ATP (2 mM). Binding reactions were performed in 50 mM Tris-HCl pH 8.5, 5 mM $MgSO_4$ with increasing amounts of AgmE 0-100 pmol. Reactions were incubated for 10 min at 25°C, mixed with gel loading buffer and run on a 1 % agarose gel in 0.5 X TB + 1mM $MgSO_4$ buffer and stained with ethidium bromide.

### 2.6.5 AgmE interacts directly with FtsZ

To test whether AgmE interacts directly with FtsZ, pull down experiments were performed in which either purified $His_6$-AgmE or $His_6$-FtsZ were bound to the $Ni^{2+}$-NTA column and WT or Δ*agmE* cell extract added (Figure 2-32). As controls, only purified AgmE/FtsZ or only cell extract were added to the $Ni^{2+}$-NTA column. Any interactions were confirmed by immunoblot analysis and by identification of proteins by mass spectrometry (MS).

In the SDS-PAGE in Figure 2-32B, the band marked with an asterisk is only present in the eluate from the column where purified $His_6$-AgmE and WT cell extract were added. This protein was identified as FtsZ protein by MS. In immunoblot analysis, a faint FtsZ band was present, but also an extra band corresponding to the size of FtsZ and AgmE together was detected using FtsZ antibodies; however whether this band contains FtsZ is not known. The same experiment was performed using purified $His_6$-FtsZ. The band marked with an asterisk in Figure 2-32C was only present in the eluate from the column where both $His_6$-FtsZ and WT cell extract were added and this band was identified as the AgmE protein by MS. Moreover, immunoblot analysis using AgmE antibodies confirmed the presence of AgmE only in the eluate from the column having both purified FtsZ and WT cell extract.

These results were confirmed by the identification of all proteins present in the different elution fractions by nano-HPLC and MS/MS. (Table 5-1 in supplementary results). In the control samples with only cell extract, different proteins bind unspecifically to the column; however AgmE or FtsZ are not among of them. In the column where $His_6$-AgmE was bound to the column and WT cell extract was added, FtsZ was identified as the second most abundant protein present in this sample (after $His_6$-AgmE). For the column where $His_6$-FtsZ and WT cell extract were added, AgmE was also the second

most abundant protein identified (after $His_6$-FtsZ). These results suggest that AgmE and FtsZ interact *in vitro*.

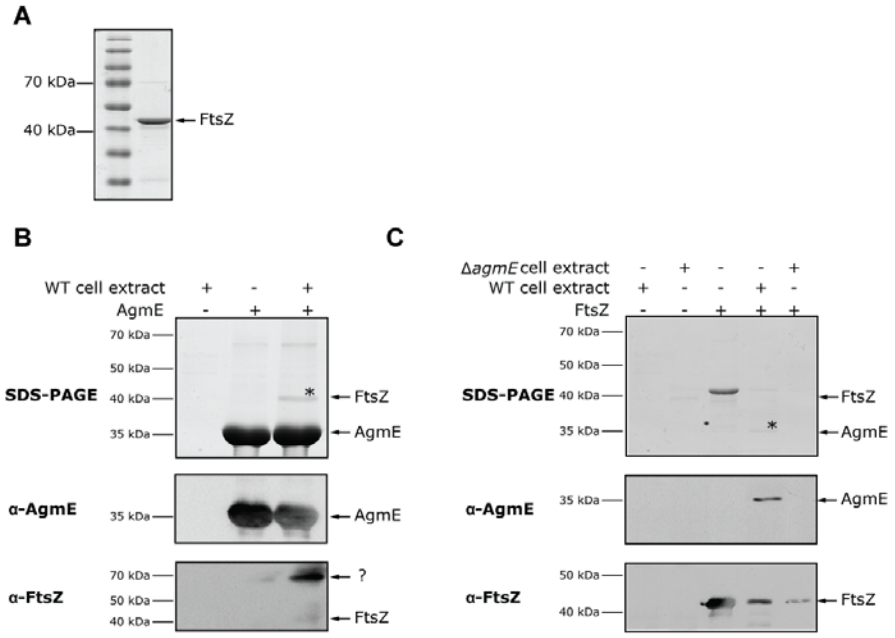


**Figure 2-32. AgmE and FtsZ interact *in vitro*. A)** Purification of FtsZ. Soluble $His_6$-FtsZ was purified by $Ni^{2+}$ affinity chromatography as described in Materials and Methods. After SDS-PAGE, proteins were stained with Coomassie Brilliant blue. Molecular size markers are included on the left. **B)** FtsZ is pulled down by $His_6$-AgmE. $His_6$-AgmE was incubated with or without WT cell extract, and pull down complexes were obtained by $Ni^{2+}$-NTA agarose column. Proteins were separated by SDS-PAGE (upper panel) and analyzed by immunoblot with α-AgmE and α-FtsZ antibodies (lower panels). The positions of the molecular size markers and of AgmE and FtsZ are indicated on the left and right, respectively. **C)** AgmE is pulled down by $His_6$-FtsZ. Procedure performed as in **B** only that $His_6$-FtsZ was used as bait. (*) means proteins that were pulled down and analyzed by MS/ MS.

### 2.6.6 Effect of AgmE on FtsZ polymerization

Preliminary studies were performed to test the ability of FtsZ to polymerize *in vitro*. Different conditions were tested for FtsZ *in vitro* polymerization assay in a similar manner as previously described (Mukherjee and Lutkenhaus, 1999). In the various conditions tested, FtsZ did not polymerize (Figure 2-33). This suggested that either purified FtsZ protein is not active or that FtsZ requires another factor to be able to polymerize in a nucleotide dependent manner. To test whether AgmE is the required factor to allow FtsZ polymerization, increasing concentration of AgmE were added to the FtsZ *in vitro* polymerization assay (Figure 2-33). However, it seems that AgmE does not have any significant effect on the polymerization of FtsZ. This suggests that either AgmE is not the factor missing for FtsZ to be

able to polymerize or that conditions have to be optimized for this assay, or as stated above FtsZ protein is not functional.

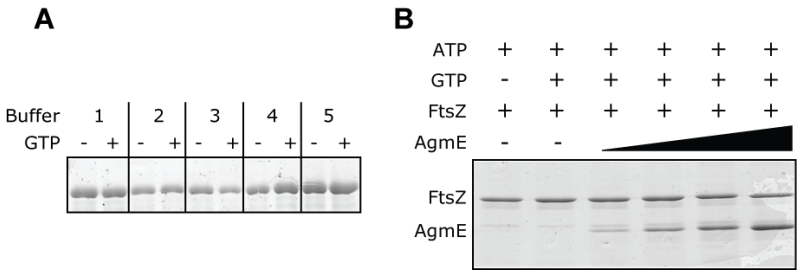


**Figure 2-33. AgmE has no effect in FtsZ polymerization. A)** FtsZ *in vitro* polymerization assay. Purified FtsZ (3 µM) was incubated in the absence or presence of GTP for 20 min at RT in different buffer conditions. 1) Buffer P: 50 mM HEPES, pH 7.2, 50 mM KCL, 10 mM $MgCl_2$, 1 mM β-mercaptoethanol. 2) Buffer P + 10 mM $CaCl_2$. 3) Buffer P1: 50 mM MES, pH 6.5, 50 mM KCL, 10 mM $MgCl_2$, 1 mM β-mercaptoethanol. 4) Buffer P1 + 10 mM $CaCl_2$. 5) Buffer P + 0.1mM $CuSO_4$. Samples subsequently centrifuged for 15 min at 200,000 x g. After immediate removal of the supernatant, pelleted proteins were dissolved in SDS sample buffer and incubated for 10 min at 95°C. Pelleted proteins were subjected to SDS-PAGE and visualized by Coomassie brilliant blue. **B)** Effect of AgmE in FtsZ polymerization. FtsZ (3 µM) was incubated for 30 min, RT with increasing concentrations of AgmE (0, 1.5, 6, and 12 µM). The samples were processed as described in **A**.

## 2.7 Understanding cell division in *Myxococcus xanthus*

Since the *agmE* mutation is not lethal, we speculate that there is at least one other system involved in the regulation of cell division in *M. xanthus*. To better understand cell division in *M. xanthus*, orthologues of the known regulators of Z-ring assembly and of the cytokinesis machinery, as well as possible interacting partners of AgmE were sought by bioinformatics analyses.

### 2.7.1 Components of the cytokinesis machinery in *M. xanthus*

By performing BLAST analysis using *E. coli* and *B. subtilis* cell division proteins and according to the annotation of the *M. xanthus* genome, most of the components of the cytokinesis machinery are present with a few exceptions (Table 2-1). *M. xanthus* FtsN was not found by sequence similarity but MXAN3502 is a structural homologue of FtsN that localizes late at the division site in *M. xanthus* (Möll and Thanbichler, submitted). Surprisingly, most of the regulators of Z-ring assembly known in *E. coli* and *B. subtilis* are not present in *M. xanthus*. This suggests that cell division regulators are yet to be discovered in *M. xanthus.* Interestingly, *M. xanthus* has a DivIVA homologue, a coiled-coiled protein involved in the polar localization of MinCD in *B. subtilis* (Marston *et al.*, 1998).

**Table 2-1. Components of the cytokinesis machinery and regulators of Z-ring assembly in *M. xanthus*.** The table shows the known cell division regulators in *E. coli* and *B. subtilis* in *M. xanthus*. Homologues were identified by BLAST search (confidence level > $10^{-6}$, probability that the sequence similarities would occur by chance alone) and using the annotation of the *M. xanthus* genome. * indicates that the protein was not found by BLAST analysis but by searching for structural homologues (Möll and Thanbichler, submitted)

| Cytokinesis machinery | | Regulators of Z-ring assembly | |
|---|---|---|---|
| FtsZ | MXAN5597 | MinC | No significant hit |
| FtsA | MXAN5599 | MinD | No significant hit |
| FtsQ | MXAN5600 | MinE | No significant hit |
| DdlB | MXAN5601 | DivIVA | MXAN 3112 |
| MurB | MXAN5602 | SlmA | No significant hit |
| MurC | MXAN5603 | NoC | No significant hit |
| MurG | MXAN5604 | ZipA | No significant hit |
| FtsW | MXAN5605 | SepF | No significant hit |
| MurD | MXAN5606 | ZapB | No significant hit |
| MraY | MXAN5607 | ZapA | No significant hit |
| MurF | MXAN5608 | ClpX | MXAN2015 |
| MurE | MXAN5609 | SulA | No significant hit |
| FstI | MXAN5610 | YneA | No significant hit |
| MraW | MXAN5612 | | |
| MraZ | MXAN5614 | | |
| EnvA | MXAN4967 | | |
| EnvC | MXAN4449 | | |
| FtsK | MXAN1460 | | |
| FtsE | MXAN5748 | | |
| FtsX | MXAN5747 | | |
| FtsB | MXAN3704 | | |
| AmiC | MXAN3886 | | |
| FtsN* | MXAN3502 | | |

In order to check whether DivIVA is important for cell division, an in frame deletion, a Δ*agmE,*Δ*divIVA* double mutant and an *in vivo* DivIVA overexpression construct were generated (Figure 2-34). We expected that if DivIVA is involved in cell division in *M. xanthus*, a Δ*divIVA* mutant would present mini-cells and moderately filamentous cells and overexpression of DivIVA would lead to filamentous cells similar to the phenotype for the DivIVA ortholog in *B. subtilis* (Cha and Stewart, 1997). Moreover, in *B. subtilis* single deletion of the MinCD or the nucleoid occlusion system leads to viable cells, whereas the double deletion leads to severe defects in cell division (Wu and Errington, 2004). Therefore, we expect that if DivIVA is involved in cell division, the double deletion mutant Δ*agmE,*Δ*divIVA* would not be viable. The *M. xanthus* Δ*divIVA* deletion mutant showed only a slight elongation of cell length but no filamentation and no mini-cells were generated (Figure 2-34). In addition, DivIVA *in vivo* overexpression did not lead to cell division defects. However, the level of the overexpression was not determined since DivIVA antibodies were not generated. Furthermore,

the double deletion mutant Δ*agmE,*Δ*divIVA* was viable and behaved like the single deletion of *agmE*. Based on these observations, we conclude that *M. xanthus* DivIVA has no major role in cell division. However, because of the slight elongation of the Δ*divIVA* cells, it is possible that DivIVA plays a minor role in cell division. Therefore, the localization of DivIVA-mCherry was studied in WT and in Δ*agmE* mutant (Figure 2-35). It has been described that *B. subtilis* DivIVA localizes at the poles and late in the cell cycle localizes at the septum (Edwards and Errington, 1997). This is not the case for *M. xanthus* DivIVA, which was found to localize in a speckled-pattern in WT as well as in the Δ*agmE* mutant. These data strongly support the notion that DivIVA is not involved in cell division.

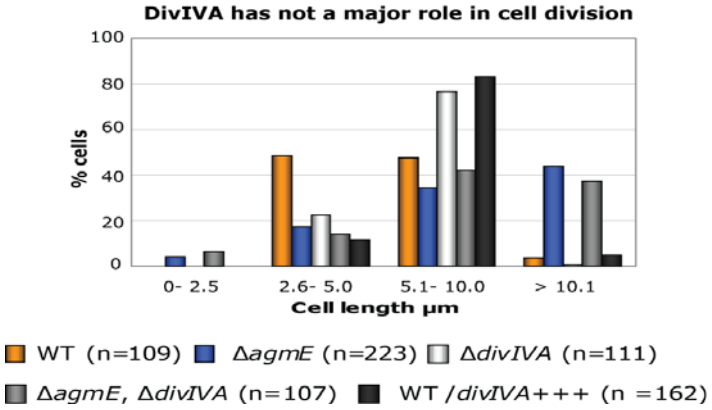


**Figure 2-34. DivIVA has no major role in cell division.** Cell length distribution of Δ*divIVA,* Δ*divIVA,*Δ*agmE* and WT/*divIVA*+++ compared to WT and Δ*agmE*. Cell length was measured using the region measurement function of Metamorph® 7.5.

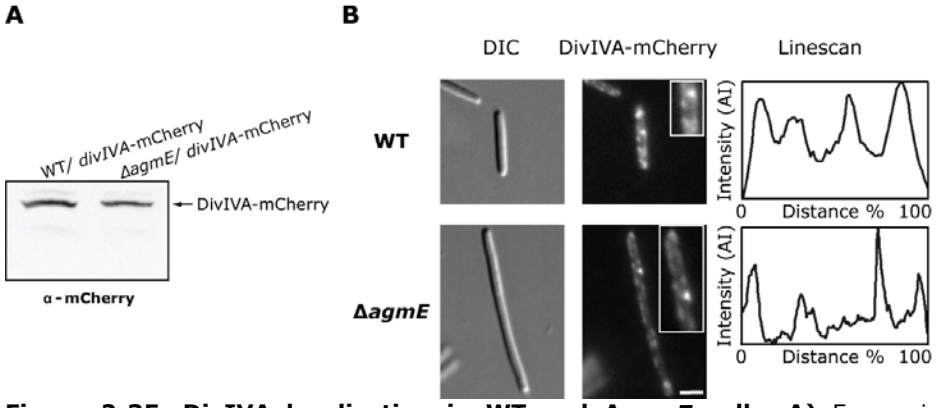


**Figure 2-35. DivIVA localization in WT and Δ*agmE* cells. A)** Expression levels of DivIVA-mCherry in WT and Δ*agmE* mutant. Equal amounts of total protein were resolved in an SDS-PAGE and subjected to immunoblot analysis using anti-sera specific to mCherry. **B)** Subcellular localization of DivIVA-mCherry in WT and Δ*agmE* cells. Cells were taken in exponentially growth phase and were placed on a thin TPM- 1% agarose pad. DivIVA localization was determined by counting 100 and 51 cells for WT and Δ*agmE* cells, respectively. The scale bars represent 2µm. The inner boxes have been enlarged three fold to better observe the speckles

### 2.7.2 Other cell division proteins in *M. xanthus*

A bioinformatics approach was taken to identify candidates involved in cell division acting together with AgmE. Initially, we focused on the two genes coding for hypothetical proteins flanking the *agmE* gene. Because a conserved genetic organisation suggests that the corresponding gene products act in the same process, the conservation of the *agmE* locus was studied by performing BLASTp analysis. The *agmE* locus was only conserved in the close relatives of *M. xanthus*: *S. aurantica* and *A. dehalogenans* (Figure 2-36A). We further analyzed the two hypothetical proteins using SMART analysis to find any conserved domains (Figure 2-36B). MXAN0634 has HEAT repeats which, consist of 3 to 36 units forming a rod-like helical structure that appear to function as protein-protein interaction surfaces. MXAN0636 has a DUF827 domain, which has been found in several plant proteins with unknown function according to the PFAM family description. To analyze the possible function of these two hypothetical proteins, position specific iterated BLAST searches were performed using the full length proteins and truncated versions (data not shown). Unfortunately, only proteins with unknown function containing HEAT domains and coiled-coil domains were found for MXAN0634 and MXAN0636, respectively. A coiled-coil search was performed to confirm that MXAN0636 is a coiled-coil protein (Figure 2-36B). Coiled-coil proteins such as DivIVA from *B. subtilis* and ZapB from *E. coli* have been implicated in cell division (Cha and Stewart, 1997; Ebersbach *et al.*, 2008). Therefore, I first studied *MXAN0636,* which is the gene downstream of *agmE*.

To check whether MXAN0636 is involved in cell division, several analyses were performed: construction and phenotypic analysis of an insertion mutant, genetic complementation, *in vivo* overexpression and an Δ*agmE,MXA0636::km* double mutant (Figure 2-37). The *MXAN0636* insertion mutation and the overexpression of MXAN0636 led to cell division defects giving rise to filamentous and mini-cells. Moreover, the *MXAN0636* mutation is responsible for this phenotype since an exogenous copy of MXAN0636 restores the cell length distribution to WT. Thus, the *MXAN0636* mutation phenocopies *agmE* mutation suggesting that MXAN0636 is also involved in cell division.

The level of the *in vivo* overexpression of MXAN0636 can not be determined since the antibodies generated do not specifically recognize MXAN0636 in *M. xanthus* (data not shown). Interestingly, the purified $His_6$-MXAN0636 protein runs as a protein double its predicted size in SDS-PAGE, which suggests that MXAN0636 is able to form dimers.

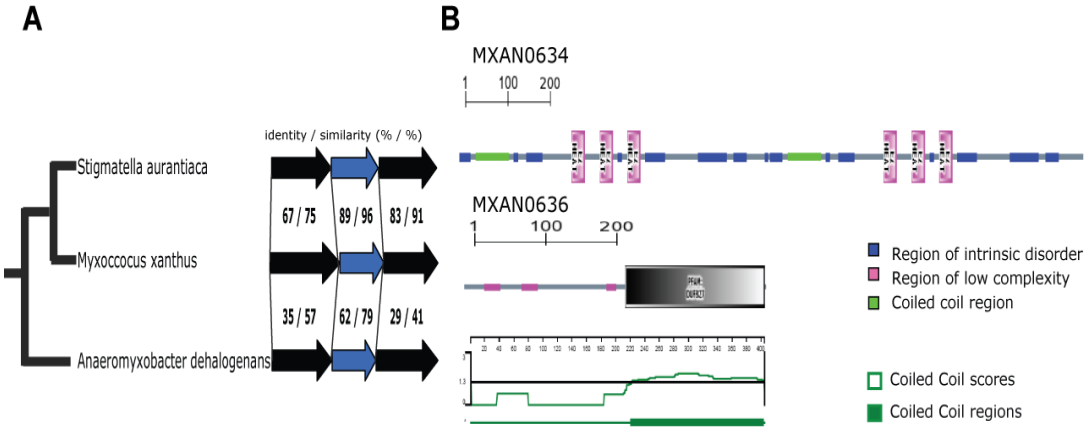


**Figure 2-36. Bioinformatics analyses of *agmE* locus. A)** Conservation of *agmE* locus. BLASTp analyses were performed to identify orthologs of MXAN0634, AgmE and MXAN0636 present in the same genetic context in all available bacteria proteomes (confidence level > $10^{-4}$, probability that the sequence similarities would occur by chance alone). **B)** SMART analyses to show the domains present in MXAN0634 and MXAN0636. Additionally, Coiled-coil search was performed on MXAN0636 using Coil server *(*www.ch.embnet.org/software/COILS_form.html*)* and the graph was generated using DNAstar protean function.

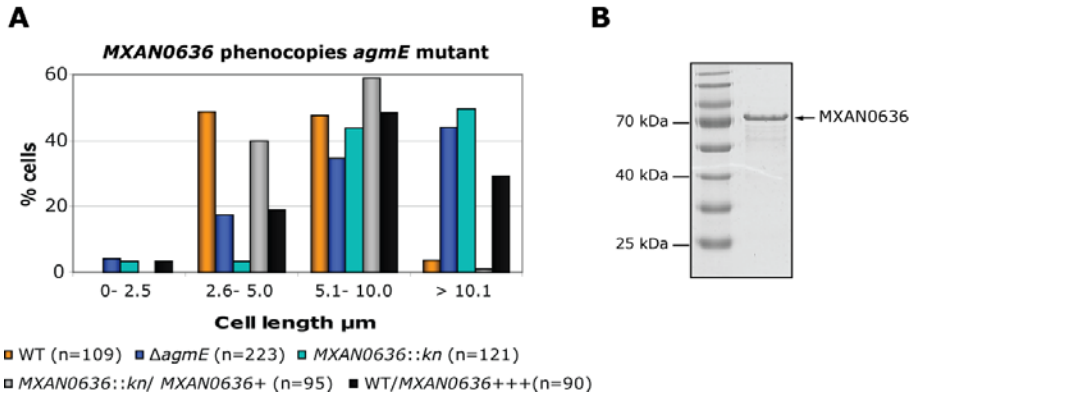


**Figure 2-37. MXAN0636 seems to be involved in cell division. A)** Cell length distribution of MXAN0636, *MXAN0636::kn*/*MXAN0636*+ and WT/*MXAN0636*+++ compared to WT and Δ*agmE* cells. Cell length was measured using the region measurement function of Metamorph® 7.5. **B)** Soluble $His_6$-MXAN0636 was purified by $Ni^{2+}$ affinity chromatography as described in Materials and Methods. After SDS-PAGE, proteins were stained with Coomassie Brilliant Blue. Molecular size markers are included on the left

To characterize the role of MXAN0636 in cell division, the localization of FtsZ and AgmE were studied in *MXAN0636* mutant (Figure 2-38): 1) The full length FtsZ-mCherry is expressed in *MXAN0636* mutant and FtsZ localizes

in a speckled-pattern (99%) (Figure 2-38A & B). Therefore, FtsZ localization is dependent of MXAN0636. 2) The full length AgmE-mCherry is expressed in *MXAN0636* mutant and AgmE is localized in a patchy pattern in *MXAN0636* mutant (100%) (Figure 2-38B & D), which suggests that MXAN0636 is important for AgmE localization.

These results suggest that MXAN0636 is involved in cell division by correctly localizing AgmE, and therefore FtsZ. In the *MXAN0636* mutant, AgmE is no longer localized, therefore FtsZ can not longer localize at mid-cell and this results in the formation of filamentous and mini-cells. Importantly, a double mutant Δ*agmE*, *MXAN0636*::km could not be generated. In fact, the *MXAN0636* insertion mutant could only be obtained in the presence of an exogenous copy of MXAN0636 in the Δ*agmE* mutant. Therefore, it seems that mutation of *MXAN0636* in combination with the Δ*agmE* mutation is lethal. Taken together, these data suggest that MXAN0636 and AgmE act to ensure correct cell division

So far, a functional MXAN0636 fusion protein has not been generated to analyze its localization during the cell cycle. For MXAN0634, the generation of an in frame deletion is currently in progress.

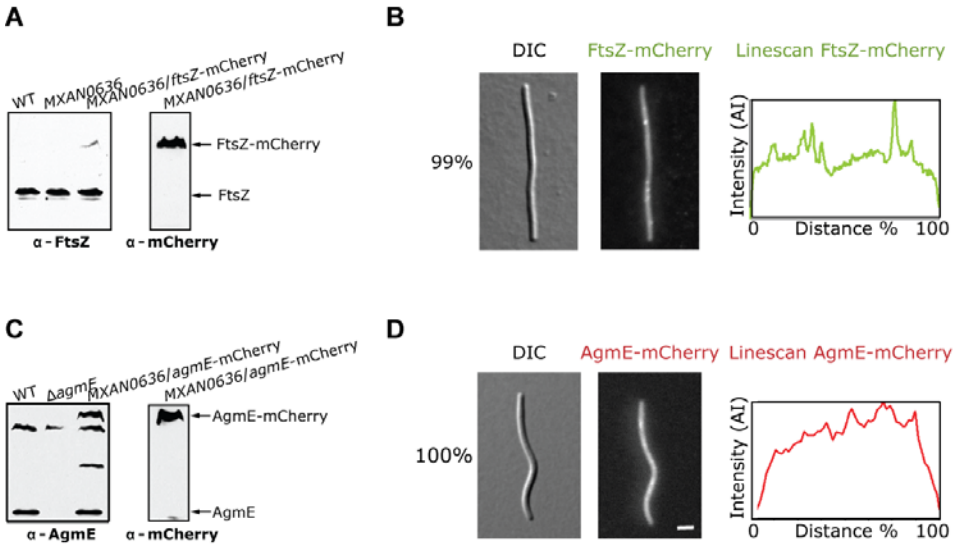


**Figure 2-38. MXAN0636 is important for FtsZ and AgmE localizations. A & C)** Levels of FtsZ-mCherry and AgmE-mCherry fusion proteins**.** Equal amounts of total protein were resolved on a SDS-PAGE and subjected to immunoblot analysis using anti-sera specific to AgmE, FtsZ and mCherry**. B & D)** FtsZ-mCherry and AgmE-mCherry localization in *MXAN0636*::km (n=50 for each). Exponential growing cells were place on TPM- 1% agarose and visualized by light and fluorescence microscopy. Fluorescence intensities were determined using linescan function (Metamorph® 7.5, maximum value, scan width 10). The scale bar represents 5 µm.

# 3 Discussion

Correct positioning of the division plane is a prerequisite for the generation of daughter cells with a normal chromosome complement and with a correct size. To achieve this, bacteria have developed an array of regulatory systems that ensure the correct positioning of the FtsZ protein. FtsZ, a structural tubulin homologue, forms a ring-like structure at mid-cell called the Z-ring that marks the cell division site and acts as a scaffold for the assembly of the cytokinesis machinery (Bi and Lutkenhaus, 1991; Dajkovic and Lutkenhaus, 2006). In *E. coli* and *B. subtili*s, the spatial regulation of the Z-ring assembly is controlled by two systems: nucleoid occlusion and the Min system (Bernhardt and de Boer, 2005; Wu and Errington, 2004). In contrast, *C. crescentus* lacks homologues of these two systems. In *C. crescentus*, the orphan ParA-like protein MipZ functions as a temporal and spatial cell division regulator, which ensures the correct positioning of the Z-ring (Thanbichler and Shapiro, 2006). In *M. xanthus,* however, the mechanisms regulating the positioning of the cell division plane have not been studied.

In this study, we have characterized the orphan ParA-like protein AgmE. AgmE was found in an screen designed to identify A-motility proteins (Youderian *et al.*, 2003). The Δ*agmE* in-frame deletion mutant has both A- and S-motility defects. We have shown that these defects are neither due to the incorrect localization of the A-motility protein RomR nor to the lack of pili. However, the defect in S-motility in an Δ*agmE* mutant could be due to the abnormal elongation observed in these cells. It has previously been shown that induced filamentation of *M. xanthus* cells by cephalexin treatment results in a dramatic decrease in S-motility, whereas cell elongation results in a slight reduction of A-motility (Sun *et al.*, 1999). These results strongly suggest that the motility defects in an Δ*agm*E mutant are indirect and due to the effect of the *agmE* mutation on cell division.

## 3.1 AgmE is involved in cell division

In addition to motility defects, the Δ*agmE* mutant is characterized by filamentous cells and mini-cells. This phenotype is characteristic for mutations in genes important for chromosome segregation (Lasocki *et al.*, 2007; Yamaichi *et al.*, 2007) or genes involved in regulation of the positioning of the cell division site (Bernhardt and de Boer, 2005; Thanbichler and Shapiro, 2006; Wu and Errington, 2004). The cell length phenotype did not allow us to distinguish in which process AgmE is involved. Therefore, we investigated DNA replication and segregation in the Δ*agmE* mutant. Our data indicate that DNA replication as well as DNA segregation are normal in an Δ*agmE* mutant. Importantly, we observed that constrictions indicating nascent division sites were rarely formed in the Δ*agmE* mutant. In addition, polar cell divisions were present in an Δ*agmE* mutant suggesting that the possible defect of an Δ*agmE* mutant is the inability to correctly place the division site at mid-cell.

## 3.2 AgmE affects FtsZ localization

In order to investigate if AgmE plays a direct role in cell division, the localization of FtsZ in WT and Δ*agmE* mutant cells was determined because FtsZ is the first (known) protein to localize at mid-cell in model organisms such as *E. coli* and *B. subtilis* and, therefore, marks the division site (den Blaauwen *et al.*, 2008; Lutkenhaus and Addinall, 1997; Sackett *et al.*, 1998). In *M. xanthus* WT cells, we found FtsZ has two different patterns of localization that correlate with the cell length and, thus with the cell cycle. In small-sized cells containing either one or two incompletely segregated nucleoids (i.e. cells that are replicating and segregating their nucleoids), FtsZ is localized in a speckled-pattern. Moreover, we have shown by time-lapse microscopy that these speckles are highly dynamic and their positions change over a period of 5 minutes. After DNA replication/segregation is complete, FtsZ speckles concentrate at mid-cell to form the Z-ring. Therefore, cells containing two fully-segregated nucleoids have FtsZ localized at mid-cell. Once the Z-ring is formed at mid-cell in *M. xanthus*, it is stably maintained likely until cell division occurs.

Overall, FtsZ dynamic localization in *M. xanthus* WT cells are similar to those described for *E. coli* and *B. subtilis* where FtsZ exhibits rapid movements in helix-like patterns that concentrate at mid-cell and assemble into the Z-ring (Peters *et al.*, 2007; Thanedar and Margolin, 2004).

FtsZ in an *ΔagmE* mutant, in contrast to WT, is mainly localized in a speckled-pattern which does not correlate with cell length or cell cycle. These "speckles" likely correspond to non-functional structures unable to assemble into the Z-ring and therefore unable to support the assembly of the cytokinesis machinery. Moreover, the FtsZ "speckles" were observed to localize over the nucleoids in WT as well as in Δ*agmE* cells. In Δ*agmE* cells Z-rings were rarely formed. However, when formed these Z-rings could occasionally initiate the assembly of the cytokinesis machinery, which would result in cell division. Moreover, in Δ*agmE* cells the Z-ring assembly can occur randomly in cell regions not containing a nucleoid occasionally leading to the observed polar cell divisions when the Z-ring was formed close to a pole. The above observations have two implications: 1) The primary defect in an Δ*agmE* mutant is the inability to correctly localize and concentrate FtsZ to mid-cell. In other words, the presence of AgmE is required for the establishment of a single and functional Z-ring at mid-cell. 2) *M. xanthus* possesses a nucleoid occlusion system as in *E. coli* and *B. subtilis* for the inhibition of Z-ring formation over the nucleoids and that system does not involve AgmE.

In principle, AgmE could act either negatively or positively on FtsZ localization. In the negative regulation model, FtsZ polymerization is inhibited at the poles as in the case for the Min system in *E. coli* and *B. subtilis* or MipZ in *C. crescentus*, therefore leaving only mid-cell free for FtsZ polymerization and subsequent assembly of the cytokinesis machinery (Lutkenhaus, 2007; Thanbichler and Shapiro, 2006). In the positive regulation model, FtsZ polymerization at mid-cell is stimulated by either stabilizing the FtsZ-ring at mid-cell as it has been described for FtsA, ZipA, and ZapA (Lutkenhaus, 2007) or by directing FtsZ to mid-cell (currently there are no known examples). By determining where AgmE is localized, we could distinguish between the negative regulation and positive regulation models.

## 3.3 AgmE acts positively on FtsZ mid-cell localization

AgmE localizes in three distinct patterns, which correlate with cell size and cell cycle. When the cells are small-sized and contain only one nucleoid, AgmE is localized in a patchy pattern. As cell size increases, cells start to replicate and segregate their nucleoids. In these cells, AgmE localizes in one single focus located at the ⅜ position of the cell length (off-center cluster). Once the cells have elongated and DNA replication/segregation is complete, AgmE localizes at mid-cell even before constriction is visible. Consistent with the cell cycle dependent localization of AgmE, we showed by time-lapse microscopy that AgmE localization is dynamic during the cell cycle. The observations that AgmE is not localized at the poles and, importantly, that AgmE localizes at mid-cell when nucleoids have segregated and even before constriction is visible like FtsZ strongly indicates that AgmE acts positively on FtsZ localization.

Z-ring stabilizing factors such as FtsA and ZipA in *E. coli* have been shown to localize simultaneously with FtsZ at mid-cell in a manner that depends on FtsZ (Den Blaauwen *et al.*, 1999; Hale and de Boer, 1999). Consistent with this observation, FtsA in *B. subtilis* has been shown to interact with FtsZ prior Z-ring assembly (Jensen *et al.*, 2005). In addition, FtsA localizes at mid-cell later than FtsZ during the cell cycle in *C. crescentus* (Möll and Thanbichler, submitted). Furthermore, the remaining components of the cytokinesis machinery in *E. coli* localize in a sequential and interdependent manner at the division site after Z-ring is assembled (den Blaauwen *et al.*, 2008). Therefore, the precise timing of AgmE and FtsZ localization at mid-cell would provide an indication for the function of AgmE. In co-localization studies, we found that when AgmE is localized in a patchy pattern or in one off-center cluster, FtsZ is localized in a diffuse/speckled-pattern. As cell size increases, AgmE localizes at mid-cell and co-localizes with FtsZ. This result confirms that AgmE and FtsZ co-localize at mid-cell. Intriguingly, some cells displayed mid-cell localization of AgmE in the absence of FtsZ mid-cell localization, which suggests that AgmE directs FtsZ to mid-cell. Finally, we showed that AgmE directly interacts with FtsZ *in vitro* in pull down assays as it has been shown for proteins involved in the correct localization and stabilization of the Z-ring (Cordell *et al.*, 2003; Dajkovic *et al.*, 2008; de Boer *et al.*, 1992; Flynn *et al.*, 2003; Gueiros-Filho and Losick, 2002;

Haeusser *et al.*, 2004; Pichoff and Lutkenhaus, 2002; Thanbichler and Shapiro, 2006; Weart *et al.*, 2005). Because AgmE localizes to nascent division site before FtsZ, we suggest that AgmE directs FtsZ to mid-cell. AgmE is the first example of a protein that positively regulates the localization of FtsZ. It has been shown that Z-rings can form in the absence of stabilizing proteins such as ZipA and FtsA in *E. coli* (Addinall *et al.*, 1996; Pichoff and Lutkenhaus, 2002). This is, however, not the case in an Δ*agmE* mutant because FtsZ mainly localizes in a speckled-pattern and very rarely forms Z-rings. Therefore, a stabilization function of AgmE on Z-ring assembly is less likely suggesting that the main function of AgmE is to direct FtsZ to mid-cell.

## 3.4 ATPase hydrolysis is required for AgmE localization and function

Because AgmE localizes in three patterns that correlate with the cell cycle, we hypothesized that the nucleotide bound state of AgmE would be important to achieve these localization patterns. Therefore, we generated an AgmE$^{D90A}$ mutant. This amino acid substitution is predicted to be impaired in ATP hydrolysis based on reports for the ParA ortholog (Soj) in *T. thermophilus* (Leonard *et al.*, 2005). AgmE$^{D90A}$ is inactive i.e. an Δ*agmE* mutant is not complemented by an exogenous copy of *agmE*$^{D90A}$. Moreover, AgmE$^{D90A}$ localizes mainly in one single cluster located at random positions over a nucleoid and this localization does not correlate with the cell cycle. This strongly suggests that ATPase hydrolysis is required for the proper localization of AgmE at mid-cell and for coupling AgmE localization to the cell cycle. Interestingly, the ParA ortholog (Soj) in *B. subtilis* requires ATPase activity for its correct localization. Several point mutations predicted to abolish ATP binding or hydrolysis were generated and each point mutant localizes in a different pattern (Murray and Errington, 2008). Moreover, because AgmE$^{D90A}$ is predicted to be able to bind ATP but not hydrolyzed it, we propose that ATP binding to AgmE triggers the off-center localization and that ATP hydrolysis is required for the AgmE mid-cell localization. Unfortunately, the ATPase activity has not been successfully shown *in vitro*. It is known that ParA-like proteins are weak ATPases (Hayes and Barilla, 2006); therefore, it is possible that AgmE ATPase activity could not be

detected under the conditions used. Furthermore, it has been demonstrated that ParB enhances the ATPase activity of their cognate ParA proteins (Davis *et al.*, 1992; Easter and Gober, 2002; Leonard *et al.*, 2005; Watanabe *et al.*, 1992). Therefore, it is possible that a co-factor is needed to stimulate the ATPase activity of AgmE *in vitro*.

In addition, we have demonstrated that AgmE forms polymers *in vitro* in an nucleotide-dependent manner, which has also been observed for other ParA-like proteins (Barilla *et al.*, 2005; Ebersbach *et al.*, 2006; Leonard *et al.*, 2005; Lim *et al.*, 2005). Moreover, ATP hydrolysis is not required for polymer formation but for its dynamics (Leonard *et al.*, 2005). Therefore, we propose that AgmE mid-cell localization requires dynamic polymer formation.

## 3.5 Model for AgmE function during cell division

Taken together, we propose the following model for how AgmE functions in cell division (Figure 3-1): New born cells in G1 phase and containing one nucleoid have AgmE localized in a patchy pattern (Figure 3-1A). This patchy pattern would represent AgmE in an ADP bound form. In response to an unknown cell cycle signal (e.g. initiation of DNA replication), AgmE binds ATP and relocalizes to a single off-center focus during S phase (Figure 3-1B). In response to a second unknown cell cycle signal (e.g. termination of DNA replication) but after DNA replication/ segregation is complete (i.e. G2 phase), AgmE localizes at mid-cell where it forms polymers (Figure 3-1C). AgmE polymers would then direct FtsZ to mid-cell to form the Z-ring. The Z-ring in turn recruits the cytokinesis machinery in late G2 phase (Figure 3-1D). Upon completion of cell division, both AgmE and FtsZ delocalize from mid-cell (Figure 3-1E), and we suggest that cell division leads to accumulation of the ADP bound form of AgmE.

The cell cycle signals are not known, in our model we propose that initiation of DNA replication, completion of DNA replication/segregation and cell division are the possible signals triggering AgmE to relocalize. These hypotheses are based on the observation that AgmE localization is cell cycle dependent. Coupling AgmE localization to a specific signal of the cell cycle would allow the correct timing for Z-ring formation.

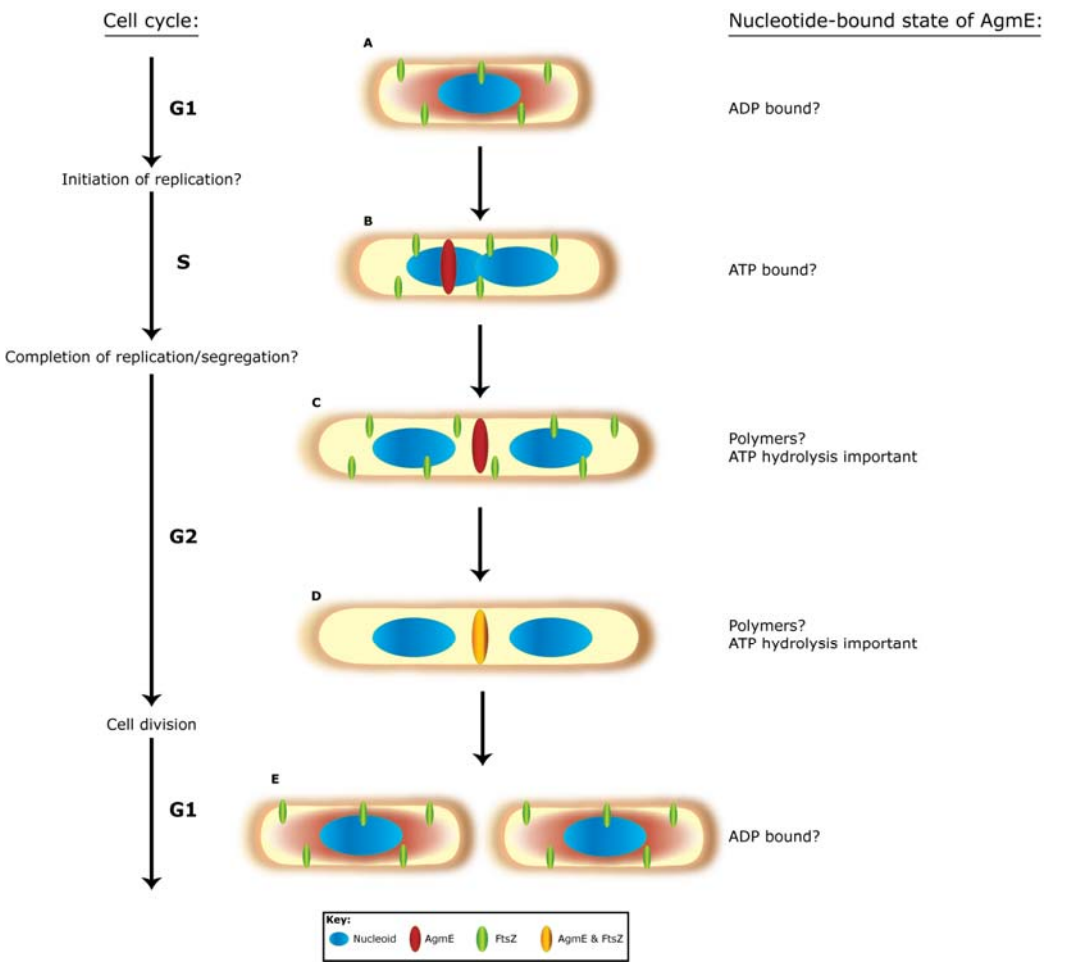


**Figure 3-1. AgmE positively regulates the positioning of FtsZ. A)** New born cells contain one nucleoid. AgmE and FtsZ are localized in a patchy and speckled-pattern, respectively. **B)** Upon receiving a signal (e.g. initiation of replication), AgmE relocalizes to the off-center cluster and FtsZ remains localized in a speckled-pattern. **C)** After a second signal (e.g. completion of DNA replication/segregation), AgmE relocalizes at mid-cell while FtsZ remains localized in a speckled-pattern. **D)** Once AgmE is at mid-cell, it forms polymers that direct FtsZ to mid-cell. Then, FtsZ assemble into the Z-ring and and in turn recruits the cytokinesis machinery. **E)** Cell division leads to the generation of two daughter cells and delocalization of AgmE and FtsZ from mid-cell.

## 3.6 Open questions

Our model suggests that FtsZ localization depends on AgmE and that AgmE localizes to mid-cell independently of FtsZ. The last assumption has not been tested directly. The *ftsZ* gene is essential in *M. xanthus* (Garcia-Moreno *et al.*, 2009) and since depletion experiments are not possible in *M. xanthus* due to the lack of tight inducible promoters, we propose to inhibit FtsZ polymerization *in vivo* by using known FtsZ polymerization inhibitors described for other bacteria (Stokes *et al.*, 2005). We expect that

if AgmE localization is independent of FtsZ, then AgmE could still localize at mid-cell in the absence of Z-ring formation.

In our model, we have proposed that cell cycle signals trigger AgmE relocalization. To test if DNA replication is a signal for AgmE to relocalize, we propose to block the initiation of DNA replication by using nalidixic acid, which specifically inhibits DNA synthesis without affecting protein synthesis or cell growth (Kimchi and Rosenberg, 1976). In this experiment, we expect that AgmE would be mainly localized in a patchy pattern. Since there are no known antibiotics or compounds capable of blocking termination of DNA replication or DNA segregation, testing whether these are signals for AgmE relocalization is more complicated. However, a *parA* mutant (MXAN7477) has recently been obtained in a transposon mutagenesis screen designed to identify genes important for development (Anna Konovalova and Sigrun Wegener-Feldbrügge, unpublished data). This *parA* gene is part of the typical *parAB* operon which has been implicated in DNA segregation in other bacteria (Lasocki *et al.*, 2007; Yamaichi *et al.*, 2007). We expect that if DNA segregation is a signal for AgmE relocalization, AgmE would be mainly localized in an off-center focus in a *parA* mutant.

The most intriguing question is why *M. xanthus* needs a positive regulator of FtsZ localization while in other bacteria FtsZ localization is negatively regulated? A possible reason is that *M. xanthus* cells are much longer than *E. coli* cells. Therefore, inhibiting *M. xanthus* polar regions, which are as large as individual *E. coli* cells, would require mechanisms capable of inhibiting Z-ring formation in relatively large cellular regions that would only allow Z-ring assembly at mid-cell. Therefore, localizing a positive regulator of FtsZ localization at the right time and right place could be a more productive strategy. Consistent with this idea, in human cells it has been shown that PRC1, which is a midzone-associated protein required for cytokinesis, is an essential factor in controlling the spatiotemporal formation of the midzone (Zhu *et al.*, 2006).

## 3.7 Conclusions

Bacteria have evolved an array of regulatory systems ensuring the proper partition of their genetic material and for the correct positioning of the cell division site. *M. xanthus* lacks the known cell division regulators present in *E. coli* and *B. subtilis*. In this study we could show that *M. xanthus* possesses an orphan ParA-like protein AgmE, which is involved in cell division. Based on the abnormal FtsZ localization in an Δ*agmE* mutant, on the observation that AgmE localizes to mid-cell before FtsZ and that FtsZ and AgmE interact *in vitro*, we propose that AgmE is a novel cell division regulator that acts positively to direct FtsZ localization to mid-cell. AgmE is the first example of a protein shown to positively regulate the localization of FtsZ. Thus, AgmE represent a fundamentally novel system for regulating the site of cell division in a bacterial system. Interestingly, most of the δ-proteobacteria from which genome sequences are available lack homologues of the Min system and nucleoid occlusion (Rothfield *et al.*, 2005)(data not shown) suggesting that these bacteria have evolved a different mechanism for regulating cell division that might include ParA-like proteins.

# 4 Supplementary results

## 4.1 AgmE and FtsZ localization: checking the constructs

### 4.1.1 AgmE-mCherry at *carS* locus

Because of the change where the AgmE-mCherry is integrated in the chromosome (*carS* locus), the cell length distribution, the expression levels and the localization patterns were determined (Figure 4-1). AgmE-mCherry integregated at *carS* locus is able to complement *agmE* mutation, although the cell size has slightly increased. Moreover, the full length fusion protein is expressed. AgmE localizes in thee distinct patterns as previously shown and these localization patterns correlated with the cell length (section 2.4.1). Therefore, we conclude that AgmE-mCherry integrated at *carS* locus behaves like AgmE-mCherry at the attachment site.

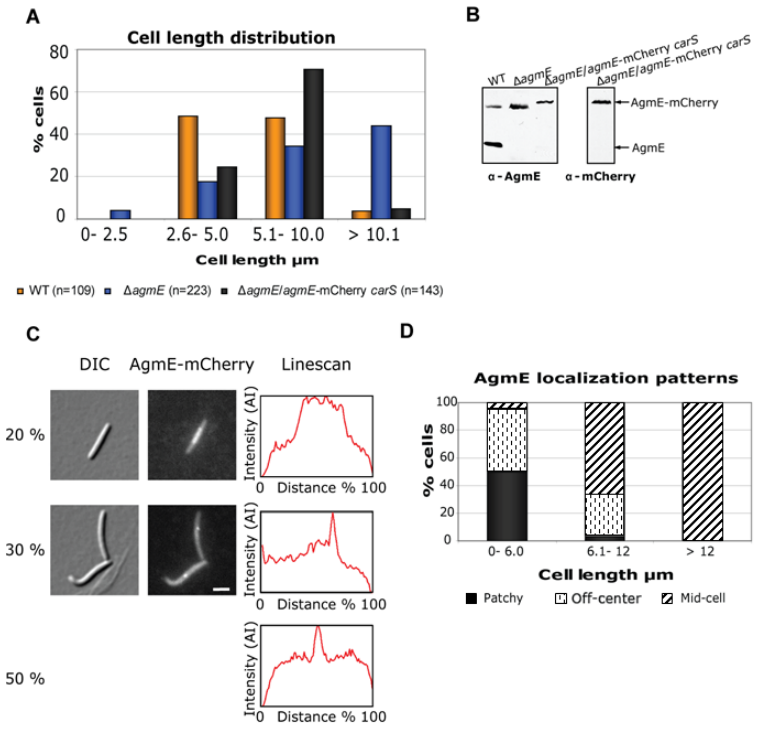


**Figure 4-1. AgmE-mCherry at *carS* locus behaves like AgmE-mCherry Mx8 attachment site. A)** Cell length distribution of Δ*agmE*/*agmE*-mCherry at *carS* in comparison with WT and Δ*agmE* cells. **B)** Levels of AgmE-mCherry. Equal amount of total proteins were resolved in an SDS-PAGE and subjected to immunoblot analysis using anti-sera specific to AgmE and mCherry. **C)** Subcellular localization of AgmE-mCherry (n= 143). The scale bar represents 2 µm. **D)** AgmE-mCherry localization patterns in function of the cell length. For each cell length class, the number of cells was normalized to 100 % and the percentage of cell presenting each localization pattern is shown.

### 4.1.2 FtsZ-GFP at Mx8 attachment site

The same analysis was performed for FtsZ-GFP fusion protein (Figure 4-2). WT strain carries the full length FtsZ-GFP and present elongated cells as previously shown (section 2.3.1). For FtsZ-GFP, speckled-pattern can no longer be observed, which can be due to the lower overall signal of this fusion. However the localization patterns are like the previously described (section 2.3.1). FtsZ localizes in a diffuse pattern in 53% and at mid-cell in 47% and these localization patterns correlate with the cell length. Therefore, besides for the reduction of the fluorescence signal, FtsZ-GFP behaves like FtsZ-mCherry fusion protein.

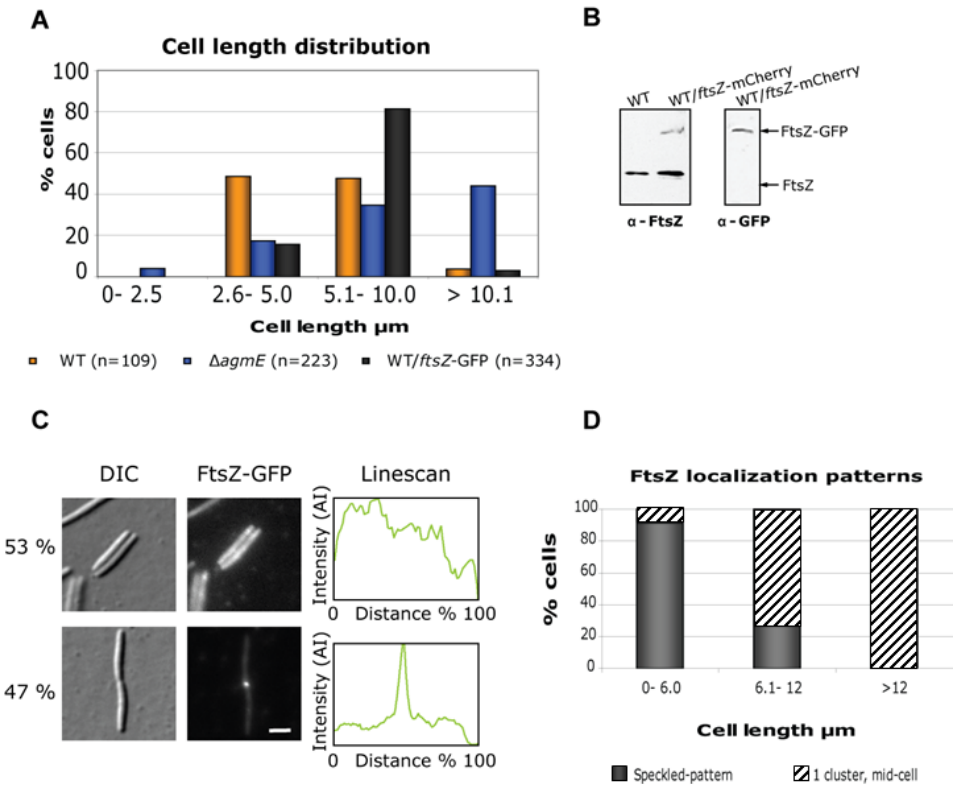


**Figure 4-2. FtsZ-GFP behaves like FtsZ-mCherry. A)** Cell length distribution of WT/*ftsZ*-GFP-mCherry in comparison with WT and Δ*agmE*. **B)** Levels of FtsZ-GFP. Equal amount of total proteins were resolved in an SDS-PAGE and subjected to immunoblot analysis using anti-sera specific to FtsZ and GFP. **C)** Subcellular localization of FtsZ-GFP. The scale bar represents 2 µm. **D)** FtsZ-GFP localization patterns in function of the cell length. For each cell length class, the number of cells was normalized to 100 % and the percentage of cell presenting each localization pattern is shown.

## 4.2 AgmE localization in WT background

When we investigated the localization of AgmE$^{D90A}$-mCherry in the Δ*agmE* mutant, we also placed this construct in WT background to check whether AgmE$^{D90A}$ is dominant negative. Therefore, here I compare the localization of AgmE-mCherry with the localization of AgmE$^{D90A}$ both in WT backgrounds.

### 4.2.1 AgmE localization in WT background

The construct *agmE*-mCherry under the control of its native promoter was placed at the Mx8 attachment site in WT cells. The cell length distribution and the expression levels were analyzed. The introduction of an extra copy of AgmE results in a slight elongation of the cells compared to *agmE*-mCherry in the Δ*agmE* mutant (Figure 4-3, A). The expression levels of this construct are slighty higher than WT (Figure 4-3, B). AgmE-mCherry localizes in three distinct patterns correlating with the cell length as previously described (Figure 4-3, C & D). From these analyses, we conclude that AgmE-mCherry in WT background behaves like AgmE-mCherry in the Δ*agmE* mutant.

### 4.2.2 AgmE$^{D90A}$ is dominant negative in WT

The construct *agmE*$^{D90A}$-Cherry under the control of its native promoter was placed at the Mx8 attachment site in WT cells. The cell length distribution and the expression levels were analyzed. The introduction of AgmE$^{D90A}$-mCherry results in the generation of filamentous and mini-cells (Figure 4-4**, A**). The expression levels of this construct are slighty higher than WT (Figure 4-4, B). AgmE$^{D90A}$-mCherry mainly localizes in one off-center cluster and this does not correlate with the cell length as previously described (Figure 4-4, C &D). From these analyses, we conclude AgmE$^{D90A}$-mCherry is dominant negative in WT which could mean that AgmE$^{D90A}$ is able to interact with the WT AgmE or that AgmE$^{D90A}$ titrates out the downstream components of the cell division machinery and therefore cell division is impaired.

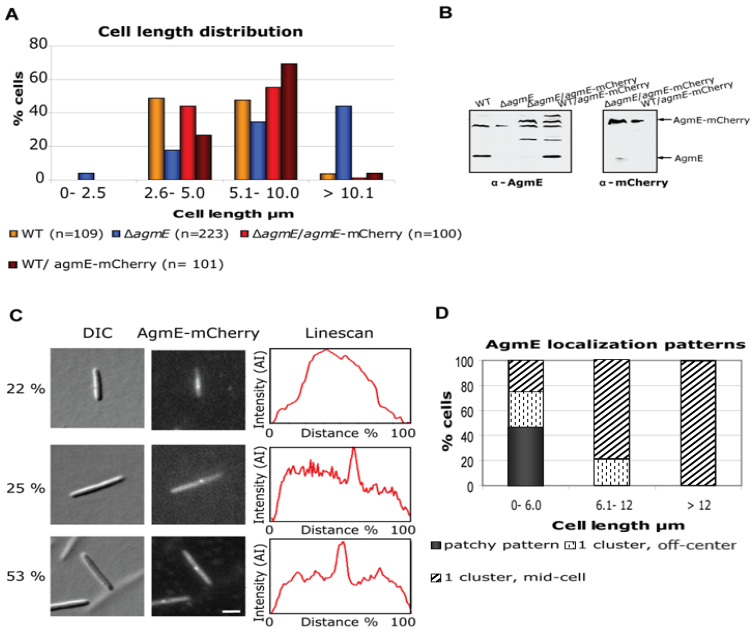


**Figure 4-3. AgmE-mCherry in WT behaves like AgmE-mCherry in Δ*agmE*. A)** Cell length distribution of *agmE*-mCherry in WT compared to WT, Δ*agmE* and Δ*agmE*/ *agmE*-mCherry cells. Cell length was measure using the region measurement function of Metamoph® 7.5. **B)** Levels of AgmE-mCherry. Equal amount of total proteins were resolved in an SDS-PAGE and subjected to immunoblot analysis using anti-sera specific to AgmE and mCherry. **C)** Subcellular localization of AgmE-mCherry in WT background. Exponentially growing cells were placed on TPM-agarose and visualized by light and fluorescence microscopy. The fluorescence intensity was measure using the line scan function of Metamorph® 7.5 (maximum value, scan width 10) (n= 101). The scale bar represents 2 µm. **D)** AgmE-mCherry localization patterns in WT background in function of the cell length. For each cell length class, the number of cells was normalized to 100 % and the percentage of cell presenting each localization pattern is shown.

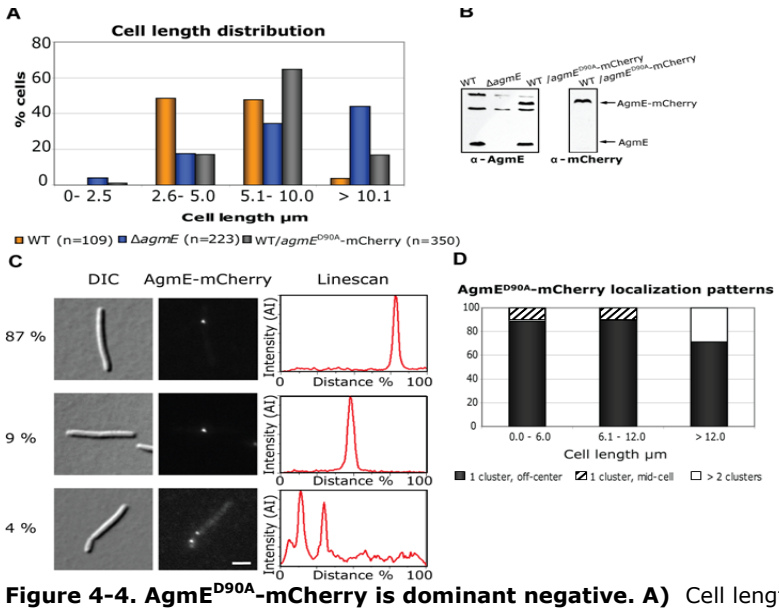


**Figure 4-4. AgmE$^{D90A}$-mCherry is dominant negative. A)** Cell length distribution of *agmE*$^{D90A}$-mCherry in WT compared to WT, Δ*agmE* and Δ*agmE*/ *agmE*-mCherry cells. **B)** Levels of AgmE$^{D90A}$-mCherry. Equal amount of total proteins were resolved in an SDS-PAGE and subjected to immunoblot analysis using anti-sera specific to AgmE and mCherry. **C)** Subcellular localization of AgmE$^{D90A}$-mCherry in WT background (n=55)**.** The scale bar represents 2 µm. **D)** AgmE$^{D90A}$-mCherry localization patterns in WT background **i**n function of the cell length. For each cell length class, the number of cells was normalized to 100 % and the percentage of cell presenting each localization pattern is shown.

## 4.3 Identification of proteins in pull down assays by MS/MS

The identification of the proteins from the pull down assays in section 2.6.5 is presented here. Each fraction was trypsin digested and the peptides were separated by nano-HPLC and identified by MS/MS.

**Table 4-1. Identification of putative interacting proteins of AgmE and FtsZ.** After trypsin digestion, peptides were separated by nano-HPLC and proteins were identified by MS/MS. Only proteins having more than two peptides and minimum score of 100 are considered as present in the sample. Proteins highlighted in yellow represent putative interacting partners.

| MXAN # | gene name | Annotation | # peptides | Score |
|---|---|---|---|---|
| Ni-NTA+ WT cell extract | | | | |
| MXAN3298 | | Tuf translation elongation factor | 13 | 761 |
| MXAN4895 | | chaperonin | 8 | 662 |
| MXAN2759 | | moaB Molybdenum cofactor biosynthesis | 7 | 526 |
| MXAN4293 | | Hypothetical protein | 6 | 448 |
| MXAN6923 | | atpD ATP synthase F1, beta subunit | 8 | 443 |
| MXAN5040 | | aldehyde dehydrogenase family protein | 4 | 290 |
| MXAN3519 | | gltA citrate synthase | 4 | 286 |
| MXAN0457 | | sigma 54 modulation protein | 4 | 251 |
| MXAN3345 | | cold-shock domain family protein-related protein | 3 | 238 |
| MXAN4467 | | groEL TCP-1/cpn60 chaperonin family superfamily | 5 | 237 |
| MXAN4219 | | alpha keto acid dehydrogenase complex, E3 component, lipoamide dehydrogenase | 3 | 169 |
| MXAN5310 | | cold-shock domain family protein-related protein | 2 | 164 |
| MXAN4295 | | Patatin-like phospholipase family | 2 | 148 |
| MXAN3206 | | membrane protein, putative | 4 | 145 |
| MXAN1564 | | ahpC alkyl hydroperoxide reductase C | 2 | 145 |
| MXAN3582 | | cold-shock domain family protein-related protein | 2 | 142 |
| MXAN0672 | | cold-shock domain family protein-related protein | 2 | 131 |
| MXAN4327 | | Glu/Leu/Phe/Val dehydrogenase family protein | 3 | 125 |
| MXAN7028 | | atpA ATP synthase F1, alpha subunit | 3 | 121 |
| MXAN6037 | | cold-shock domain family protein-related protein | 2 | 105 |
| **Ni-NTA + AgmE** | | | | |
| MXAN0635 | *agmE* | ATPase, ParA family, putative | 31 | 3212 |
| **Ni-NTA +AgmE + WT cell extract** | | | | |
| MXAN0635 | *agmE* | ATPase, ParA family, putative | 89 | 7561 |
| MXAN5597 | *ftsZ* | Cell division protein FtsZ | 10 | 1124 |
| MXAN3519 | | gltA citrate synthase | 10 | 1001 |
| MXAN3298 | | tuf translation elongation factor Tu | 10 | 805 |
| MXAN0457 | | sigma 54 modulation protein, putative | 7 | 682 |
| MXAN4293 | | hypothetical protein | 7 | 551 |
| MXAN3302 | | rplB ribosomal protein L2 | 7 | 344 |
| MXAN2759 | | moaB molybdenum cofactor biosynthesis protein | 5 | 249 |
| MXAN1564 | | ahpC alkyl hydroperoxide reductase C | 3 | 152 |
| MXAN4895 | | chaperonin | 2 | 143 |
| MXAN3327 | | rplQ ribosomal protein L17 | 2 | 135 |
| **Ni-NTA + FtsZ** | | | | |
| MXAN5597 | *ftsZ* | Cell division protein FtsZ | 45 | 3960 |
| **Ni-NTA+ FtsZ+ WT cell extract** | | | | |

| | | | | |
|---|---|---|---|---|
| MXAN5597 | *ftsZ* | Cell division protein FtsZ | 94 | 8852 |
| MXAN0636 | *agmE* | ParA family, putative | 34 | 2481 |
| MXAN3298 | | tuf translation elongation factor Tu | 18 | 1404 |
| MXAN3519 | | gltA citrate synthase | 17 | 1262 |
| MXAN2759 | | moaB molybdenum cofactor biosynthesis protein | 12 | 1115 |
| MXAN4293 | | hypothetical protein | 10 | 998 |
| MXAN4895 | | chaperonin | 9 | 981 |
| MXAN4295 | | Patatin-like phospholipase family | 12 | 931 |
| MXAN6923 | | atpD ATP synthase F1, beta subunit | 11 | 897 |
| MXAN6106 | *fibA* | matrix-associated zinc metalloprotease FibA | 9 | 707 |
| MXAN3206 | | membrane protein, putative | 9 | 563 |
| MXAN0457 | | sigma 54 modulation protein, putative | 6 | 553 |
| MXAN4467 | | groEL TCP-1/cpn60 chaperonin family superfamily | 6 | 430 |
| MXAN1529 | | hypothetical protein | 6 | 411 |
| MXAN2985 | | Fic family protein | 6 | 385 |
| MXAN4219 | | lpdA alpha keto acid dehydrogenase complex, E3 component, lipoamide dehydrogenase | 4 | 358 |
| MXAN3305 | | rpsC ribosomal protein S3 | 4 | 333 |
| MXAN0212 | | aminotransferase, class I and II family protein | 5 | 317 |
| MXAN3549 | | rplS ribosomal protein L19 | 5 | 292 |
| MXAN2536 | | AMP-binding family protein | 5 | 289 |
| MXAN4289 | | hypothetical protein | 4 | 284 |
| MXAN4900 | | lipoprotein, putative | 4 | 261 |
| MXAN5040 | | aldehyde dehydrogenase family protein | 3 | 255 |
| MXAN1528 | | long-chain-fatty-acid CoA ligase, putative | 4 | 248 |
| MXAN7028 | | atpA ATP synthase F1, alpha subunit | 3 | 245 |
| MXAN3077 | | rpoB DNA-directed RNA polymerase, beta subunit | 5 | 241 |
| MXAN3543 | | nucleoside diphosphate kinase | 4 | 240 |
| MXAN3302 | | rplB ribosomal protein L2 | 3 | 238 |
| MXAN3793 | | rpsA ribosomal protein S1 | 3 | 231 |
| MXAN3296 | | rpsG ribosomal protein S7 | 3 | 230 |
| MXAN7039 | | lipoprotein, putative | 3 | 212 |
| MXAN6079 | | molybdopterin oxidoreductase, iron-sulfur binding subunit, putative | 2 | 209 |
| MXAN3410 | | ribBA 3,4-dihydroxy-2-butanone 4-phosphate synthase/GTP cyclohydrolase II | 3 | 208 |
| MXAN5783 | *pilA* | pilA pilin | 2 | 202 |
| MXAN2408 | | fusA translation elongation factor G | 2 | 195 |
| MXAN4327 | | Glu/Leu/Phe/Val dehydrogenase family protein | 4 | 193 |
| MXAN3345 | | old-shock domain family protein-related protein | 3 | 192 |
| MXAN7110 | | peptidyl-prolyl cis-trans isomerase, FKBP-type | 3 | 189 |
| MXAN3311 | | rplE ribosomal protein L5 | 2 | 185 |
| MXAN3129 | | peptidase, S9A (prolyl oligopeptidase) subfamily | 2 | 175 |
| MXAN5344 | | rpsB ribosomal protein S2 | 3 | 168 |
| MXAN2720 | | hypothetical protein | 2 | 168 |
| MXAN2786 | | hppD 4-hydroxyphenylpyruvate dioxygenase | 2 | 167 |
| MXAN3537 | | icd isocitrate dehydrogenase, NADP-dependent | 2 | 163 |
| MXAN1564 | | ahpC alkyl hydroperoxide reductase C | 3 | 159 |
| MXAN1994 | | rpsI ribosomal protein S9 | 2 | 151 |
| MXAN3582 | | cold-shock domain family protein-related protein | 2 | 149 |
| MXAN5310 | | cold-shock domain family protein-related protein | 2 | 146 |
| MXAN2730 | | NADH dehydrogenase I, C subunit | 3 | 145 |
| MXAN4564 | | 2-oxoisovalerate dehydrogenase complex, E1 component, alpha subunit | 2 | 138 |
| MXAN0672 | | cold-shock domain family protein-related protein | 2 | 130 |
| MXAN5933 | | peptidase, M48 (Ste24 endopeptidase) family | 2 | 130 |
| MXAN0133 | | hypothetical protein | 3 | 129 |
| MXAN1453 | | hypothetical protein | 2 | 126 |
| MXAN3325 | | rpsD ribosomal protein S4 | 2 | 117 |

| | | | | |
|---|---|---|---|---|
| MXAN1469 | | rplU ribosomal protein L21 | 2 | 114 |
| MXAN3192 | dnaK | chaperone protein DnaK | 2 | 113 |
| MXAN5078 | | ribosomal protein S6, putative | 2 | 112 |
| MXAN5319 | | TPR domain protein | 2 | 108 |

**Ni-NTA + Δ*agmE* cell extract**

| | | | | |
|---|---|---|---|---|
| MXAN3112 | | probable cell-division initiation protein, putative | 23 | 1677 |
| MXAN3519 | | gltA citrate synthase | 21 | 1586 |
| MXAN3298 | | tuf translation elongation factor Tu | 17 | 1465 |
| MXAN6923 | | atpD ATP synthase F1, beta subunit | 10 | 817 |
| MXAN0457 | | sigma 54 modulation protein, putative | 9 | 730 |
| MXAN2759 | | moaB molybdenum cofactor biosynthesis protein | 7 | 720 |
| MXAN4295 | | Patatin-like phospholipase family | 5 | 556 |
| MXAN4293 | | hypothetical protein | 8 | 536 |
| MXAN4467 | | groEL TCP-1/cpn60 chaperonin family superfamil | 5 | 432 |
| MXAN3206 | | membrane protein, putative | 6 | 402 |
| MXAN1529 | | hypothetical protein | 5 | 319 |
| MXAN4895 | | chaperonin | 5 | 303 |
| MXAN7039 | | lipoprotein, putative | 4 | 287 |
| MXAN6106 | fibA | matrix-associated zinc metalloprotease FibA | 3 | 267 |
| MXAN3702 | | transcriptional regulator, FurR family | 2 | 262 |
| MXAN1624 | | peptidase, M16 (pitrilysin) family | 4 | 234 |
| MXAN3461 | | oxidoreductase, short chain dehydrogenase/reductase family | 3 | 231 |
| MXAN3345 | | cold-shock domain family protein-related protein | 3 | 220 |
| MXAN3793 | | rpsA ribosomal protein S1 | 3 | 205 |
| MXAN2408 | | fusA translation elongation factor G | 2 | 172 |
| MXAN3582 | | cold-shock domain family protein-related protein | 2 | 171 |
| MXAN6079 | | molybdopterin oxidoreductase, iron-sulfur binding subunit, putative | 2 | 170 |
| MXAN7028 | | atpA ATP synthase F1, alpha subunit | 2 | 169 |
| MXAN5310 | | cold-shock domain family protein-related protein | 2 | 168 |
| MXAN4219 | | lpdA alpha keto acid dehydrogenase complex, E3 component, lipoamide dehydrogenase | 2 | 160 |
| MXAN2985 | | Fic family protein | 2 | 148 |
| MXAN0672 | | cold-shock domain family protein-related protein | 2 | 140 |
| MXAN6037 | | cold-shock domain family protein-related protein | 2 | 136 |
| MXAN3192 | | dnaK chaperone protein DnaK | 2 | 133 |
| MXAN3077 | | rpoB DNA-directed RNA polymerase, beta subunit | 4 | 132 |
| MXAN4900 | | lipoprotein, putative | 2 | 129 |
| MXAN4327 | | Glu/Leu/Phe/Val dehydrogenase family protein | 3 | 126 |
| MXAN4296 | | non-ribosomal peptide synthetase | 2 | 121 |
| MXAN3764 | | peptidyl-prolyl cis-trans isomerase, cyclophilin-type, putative | 2 | 119 |
| MXAN3537 | | icd isocitrate dehydrogenase, NADP-dependent | 1 | 111 |
| MXAN3410 | | ribBA 3,4-dihydroxy-2-butanone 4-phosphate synthase/GTP cyclohydrolase II | 2 | 110 |
| MXAN2906 | | penicillin acylase family protein | 1 | 106 |

**Ni-NTA + FtsZ + Δ*agmE* cell extract**

| | | | | |
|---|---|---|---|---|
| MXAN5597 | ftsZ | cell division protein FtsZ | 47 | 4330 |
| MXAN3298 | | tuf translation elongation factor Tu | 24 | 2203 |
| MXAN6923 | | atpD ATP synthase F1, beta subunit | 12 | 1013 |
| MXAN2759 | | moaB molybdenum cofactor biosynthesis protein B | 8 | 816 |
| MXAN3112 | | probable cell-division initiation protein, putative | 11 | 743 |
| MXAN4895 | | chaperonin, 60 kDa | 9 | 666 |
| MXAN3077 | | rpoB DNA-directed RNA polymerase, beta subunit | 9 | 635 |
| MXAN4293 | | hypothetical protein | 6 | 614 |
| MXAN6106 | fibA | matrix-associated zinc metalloprotease FibA | 7 | 587 |
| MXAN4295 | | Patatin-like phospholipase family | 8 | 515 |
| MXAN4467 | | groEL TCP-1/cpn60 chaperonin family | 5 | 460 |

| | | | | |
|---|---|---|---|---|
| | | superfamily | | |
| MXAN1529 | | hypothetical protein | 5 | 399 |
| MXAN3326 | | rpoA DNA-directed RNA polymerase, alpha subunit | 6 | 293 |
| MXAN1564 | | ahpC alkyl hydroperoxide reductase C | 3 | 240 |
| MXAN4289 | | hypothetical protein | 4 | 238 |
| MXAN2730 | | NADH dehydrogenase I, C subunit | 4 | 227 |
| MXAN3519 | | gltA citrate synthase | 3 | 197 |
| MXAN1624 | | peptidase, M16 (pitrilysin) family | 3 | 194 |
| MXAN3345 | | cold-shock domain family protein-related protein | 2 | 179 |
| MXAN3582 | | cold-shock domain family protein-related protein | 2 | 143 |
| MXAN6037 | | cold-shock domain family protein-related protein | 2 | 141 |
| MXAN5310 | | cold-shock domain family protein-related protein | 2 | 140 |
| MXAN3206 | | membrane protein, putative | 3 | 136 |
| MXAN7028 | | atpA ATP synthase F1, alpha subunit | 2 | 131 |
| MXAN0212 | | aminotransferase, class I and II family protein | 2 | 126 |
| MXAN0672 | | cold-shock domain family protein-related protein | 2 | 125 |
| MXAN3461 | | oxidoreductase, short chain dehydrogenase/reductase family family | 2 | 118 |
| MXAN0133 | | hypothetical protein | 2 | 109 |
| MXAN3192 | dnaK | chaperone protein DnaK | 2 | 106 |

# 5 Materials and Methods

## 5.1 Reagents, technical equipment and software

Reagents, enzymes and antibiotics used in this study are listed in Table 5-1 together with their suppliers. Specific chemicals are described in the text. Technical equipment and its manufacturers are listed in Table 5-2 and specific software applied for data analysis is listed in Table 5-3.

**Table 5-1.** Sources of reagents, enzymes, antibiotics and kits

| **Reagents** | **Vendor** |
|---|---|
| Media components, Agar | Roth (Karlsruhe)<br>Merck (Darmstadt)<br>Difco (Heidelberg)<br>Invitrogen (Karlsruhe) |
| Pure chemicals | Roth (Karlsruhe)<br>Merck (Darmstadt)<br>Sigma-Aldrich (Taufkirchen) |
| SDS-PAGE size standards | MBI Fermentas (St. Leon-Rot) |
| Agarose gel electrophoresis size standards | Bioline (Luckenwalde) |
| Oligonucleotides | Invitrogen (Karlsruhe)<br>Thermo scientific (Dreieich) |
| Rabbit Antisera | Eurogentec (Seraing, Belgium) |
| Buffer J | Epicentre (Hess.-Oldendorf) |
| **Enzymes** | |
| Platinum®Pfx DNA-polymerase | Invitrogen (Karlsruhe) |
| DnaseI (Rnase-free) | Ambion (Huntington, UK) |
| Eppendorf® MasterMix | Eppendorf (Hamburg) |
| Other nucleic acid modifying enzymes (restriction endonucleases, T4 DNA ligase, antarctic phosphatase®) | New England Biolabs (Frankfurt a.M.)<br>MBI Fermentas (St. Leon-Rot) |
| **Antibiotics** | |
| Kanamycinsulfate, Chloramphenicol, Ampicillin sodiumsalt, Gentamycin, Oxytetracycline dehydrate, Tetracycline | Roth (Karlsruhe) |
| **Kits** | |
| PCR purification, gel extraction, plasmid preparation | Qiagen (Hilden)<br>Zymo research (Hiss diagnostics, Freiburg) |
| BigDye® Terminator v. 3.1 cycle | Applied Biosystems (Darmstadt) |
| MasterPure™ DNA purification | Epicentre (Hess.-Oldendorf) |

**Table 5-2.** Equipment used in this study

| Application | Device | Manufacturer |
|---|---|---|
| Centrifugation | RC 5B plus<br>Ultra Pro 80<br>Multifuge 1 S-R<br>Biofuge fresco<br>Biofuge pico | Sorvall / Thermo scientific (Dreieich)<br>Heraeus / Thermo scientific (Dreieich) |
| PCR | Mastercycler personal<br>Mastercycler epgradient | Eppendorf (Hamburg) |
| DNA sequencing | 3130 Genetic analyzer | Applied Biosystems (Darmstadt) |
| Cell disruption | French® pressure cell press<br>Branson Sonifier | SLM instruments (Urbana, IL)<br>Heinemann (Schwäbisch Gmünd) |
| FPLC protein purification | ÄktaTM UnicornTM 5.0 | Amersham Biosciences (Munich) |
| Protein electrophoresis | Mini-PROTEAN® 3 cell | Bio-Rad (Munich) |
| Western blotting | TE77 semidry transfer unit | Amersham Biosciences (Munich) |
| Chemiluminescence detection | Fuji Photo Film FPM 100A | Fujifilm (Düsseldorf) |
| Microscopy | Zeiss Axio Imager. M1<br>DM6000B microscope<br>MZ 8 stereo microscope<br>DME light microscope | Carl Zeiss (Jena)<br>Leica Microsystems (Wetzlar) |
| Electroporation | Gene pulser xcell | Bio-Rad (Munich) |
| Determination of optical densities | Ultrospec 2100 pro | Amersham Biosciences (Munich) |
| Determination of nucleic acids absorption | Nanodrop ND-1000 UV-Vis spectrophotometer | Nanodrop (Wilmington) |
| DNA illumination and documentation | UVT 20 LE UV table | Herolac (Wiesloch) |
| Incubation of reactions | Thermomixer compact<br>Thermomixer comfort | Eppendorf (Hamburg) |
| Incubation of bacterial culture | Innova 4000® incubator shaker<br>Innova44® incubator shaker<br>B6420 incubator<br>9020-0075 cooled incubator | New Brunswick Scientific (NJ, USA)<br>Heraeus (Langenselbold)<br>Binder (Tuttlingen) |
| Steam sterilization | 2540E<br>FVS MK 6.5 | Tuttnauer (Breda, Netherlands)<br>Fedegari Autoclavi (Albuzzano, Italy) |

**Table 5-3.** Software for data analysis

| Application | Program | Vendor |
|---|---|---|
| Fluorescence microscopy image analyses | Metamorph® v 7.5 | Molecular Devices (Union city, CA) |
| Checking sequencing | Vector NTI software suite | Invitrogen (Karlsruhe) |
| Sequence aligments | 10 | |

## 5.2 Media

Culture media for *Escherichia coli* were prepared as described in Sambrook & Russel, 2000. (Table 5-4). Antibiotics and/or X-gal were added when needed (Table 5-5).

**Table 5-4.** Growth media for *E. coli*

| Medium | Composition |
|---|---|
| Luria-Bertani (LB) | 1% (w/v) tryptone, 0.5% (w/v) yeast extract, 1% (w/v) NaCl |
| LB agar plates | LB-medium, 1% (w/v) Agar |
| 2YT | 16g bacto trypton, 5g Yeast extract, 5g NaCl, pH 7.2 |

**Table 5-5.** Additives for *E. coli* cultures

| Additive | Final concentration | Dissolved in |
|---|---|---|
| Ampicillin sodium salt | 100µg/mL | $H_2O$ |
| Chloramphenicol | 50µg/mL | 99.99% ethanol |
| Kanamycin sulfate | 100µg/mL | $H_2O$ |
| Tetracyclin | 15µg/mL | 99.99% ethanol |
| X-Gal | 40µg/mL | DMF |

*M. xanthus* strains were grown in 1% CTT (Table 5-6). Antibiotics were added when needed on the 1 % CTT plates (Table 5-7).

**Table 5-6.** Growth media for *M. xanthus.*

| Medium | Composition |
|---|---|
| 1% CTT (Hodgkin & Kaiser, 1977) | 1% (w/v) BactoTM Casitone, 10mM Tris-Cl pH 8.0, 1mM potassium phosphate buffer pH 7.6, 8mM MgSO4 |
| 1% CTT agar plates | 1% CTT medium, 1.5% agar |
| CTT soft agar | 1% CTT medium, 0.75% agar |

**Table 5-7.** Additives for *M. xanthus* plates

| Additive | Final concentration | Dissolved in |
|---|---|---|
| Kanamycin sulfate | 40µg/mL | $H_2O$ |
| Oxytetracycline | 10µg/mL | 0.1M HCl |

For *M. xanthus* motility assays, microscopy and time lapse microscopy media were prepared as follows:

**Table 5-8.** Media for *M. xanthus* assays

| Medium | Composition |
|---|---|
| A-motility plates (ref)<br>Prepared 24h prior use | 0.5% CTT, 1.5% agar |
| S-motility plates (ref)<br>Prepared 24h prior use | 0.5% CTT, 0.5% agar |
| TPM agarose<br>Prepared just before use | 10mM Tris-Cl pH 7.6, 1mM potassium phosphate buffer pH 7.6, 8mM $MgSO_4$, 1% (w/v) agarose |
| CTT agarose<br>Prepared just before use | 0.25% CTT, 1% (w/v) agarose |

## 5.3 Microbiological methods

### 5.3.1 *Escherichia coli* strains

**Table 5-9.** *E. coli* strains used in this study

| *E. coli* strain | Genotype | Reference |
|---|---|---|
| TOP10 | F- mcrA Δ(*mrr-hsdRMS-mcrBC*) 80*lacZΔM15ΔlacX*74 r*ecA1 deoR araD139* Δ(*ara-leu*)7697 *galU galK*, *rpsL strR*) *endA1 nupG* | Invitrogen (Karlsruhe) |
| Rosetta 2(DE3) | F- *ompT hsdSB*(*rB-mB*) *gal dcm*(DE3) pRARE2 ($Cm^R$) | Novagen/Merck (Darmstadt) |

### 5.3.2 *Myxococcus xanthus* strains

**Table 5-10.** *M. xanthus* strains used in this study. $Km^R$ and $Tc^R$ indicate kanamycin and tetracycline resistance, respectively.

| Strains | Genotype | Reference |
|---|---|---|
| DK1622 | Wild-type | (Kaiser, 1979) |
| DK1217 | *aglB1* | (Hodgkin and Kaiser, 1979) |
| DK1300 | *sglG1* | (Hodgkin and Kaiser, 1979) |
| ASX2 | Δ*cglB*/*ΔpilA* | (Rodriguez and Spormann, 1999) |
| SA2811 | *romR*::nptI | (Leonardy *et al.*, 2007) |
| SA2088 | *aglZ*-GFP, (pGFy148), $Km^R$ | S. Leonardy |
| SA2028 | *frzS*-GFP, (pFGBJ), $Km^R$ | S. Leonardy |
| SA3108 | Δ*MXAN0635* (*ΔagmE*) | This study |
| SA3109 | *MXAN0635::nptI* | This study |
| SA3111 | *MXAN0636::nptI* | This study |
| SA3112 | *ΔagmE*, *romR::nptI* | This study |

| | | |
|---|---|---|
| SA3113 | WT, *attB*:: *romR*-mDsRed (pSL113), $Tc^R$ | This study |
| SA3115 | *ΔagmE*, *pilA::Tc* | This study |
| SA3116 | *ΔagmE*, *attB*:: *romR*-mDsRed (pSL113), $Tc^R$ | This study |
| SA3117 | *ΔagmE*, *aglZ*-GFP (pGFy148), $Km^R$ | This study |
| SA3118 | *ΔagmE*, *frzS*-GFP (pFGBJ), $Km^R$ | This study |
| SA3119 | *ΔagmE*/Pnat *agmE*$^+$ (pKA26), $Tc^R$ | This study |
| SA3120 | WT/Pnat *agmE*$^+$ (pKA26), $Tc^R$ | This study |
| SA3121 | *ΔagmE*/ PpilA *agmE*$^+$ (pKA19), $Km^R$ | This study |
| SA3122 | *ΔagmE*/PpilA *agmE*-GFP (pKA20), $Km^R$ | This study |
| SA3123 | *divIVA*-mCherry (pKA25), $Km^R$ | This study |
| SA3124 | *ΔagmE*, *divIVA*-mCherry (pKA25), $Km^R$ | This study |
| SA3125 | WT/ PpilA *agmE*$^+$ (pKA19), $Km^R$ | This study |
| SA3126 | WT/PpilA *agmE*-GFP (pKA20), $Km^R$ | This study |
| SA3127 | Δ*MXAN3112* (Δ*diVIA*) | This study |
| SA3128 | WT/ Pnat *agmE*$^{D175A+}$ (pKA37), $Tc^R$ | This study |
| SA3129 | WT/ Pnat *agmE*$^{K66Q+}$ (pKA38), $Tc^R$ | This study |
| SA3130 | *ΔagmE*/Pnat *agmE*$^{D90A+}$ (pKA36), $Tc^R$ | This study |
| SA3131 | *ΔagmE*/Pnat *agmE*-mCherry (pKA28), $Tc^R$ | This study |
| SA3132 | WT/Pnat *agmE*-mCherry (pKA28), $Tc^R$ | This study |
| SA3133 | *ΔagmE*/Pnat *ftsZ*-mCherry at *carS* (pKA33), $Km^R$ | This study |
| SA3134 | WT/Pnat *ftsZ*-mCherry at *carS* (pKA33), $Km^R$ | This study |
| SA3135 | *MXAN0636*-mCherry (pKA21), $Km^R$ | This study |
| SA3136 | *MXAN0636::nptI*, Pnat *agmE*-mCherry (pKA28), $Km^R$, $Tc^R$ | This study |
| SA3137 | *MXAN0636::nptI*/Pnat *MXAN0636*$^+$ (pKA42), $Km^R$ ,$Tc^R$ | This study |
| SA3138 | *ΔagmE*/ Pnat *MXAN3112* (pKA40), $Tc^R$ | This study |
| SA3139 | Pnat *ftsZ*-mCherry (pKA32), $Tc^R$ | This study |
| SA3140 | WT/PpilA MXAN3112 (pKA39), $Km^R$ | |
| SA3141 | Pnat *MXAN0636*$^+$ (pKA41), $Km^R$ | This study |
| SA3142 | *ΔagmE*/ Pnat *ftsZ*-mCherry (pKA32), $Tc^R$ | This study |
| SA3143 | *MXAN0636*::*nptI*/ Pnat *ftsZ*-mCherry (pKA32), $Tc^R$, $Km^R$ | This study |
| SA3144 | *MXAN0636*::*nptI*/ P*pilA MXAN0636*$^+$ (pKA41), $Km^R$ ,$Tc^R$ | This study |
| SA3146 | *ΔagmE*/Pnat *agmE*$^{D90A}$-mCherry (pKA43), $Tc^R$ | This study |
| SA3147 | *ΔagmE*/P*pilA agmE*-mCherry (pKA45), $Km^R$ | This study |
| SA3148 | *ΔagmE*/Pnat *ftsZ*-mCherry at *carS* (pKA30), $Km^R$ | This study |
| SA3149 | WT/ Pnat *ftsZ*-mCherry at *carS* (pKA30), $Km^R$ | This study |
| SA3150 | WT/ Pnat *agmE*$^{D90A+}$ (pKA36), $Tc^R$ | This study |
| SA3152 | *ΔagmE*/ Pnat *agmE*$^{D175A+}$ (pKA37), $Tc^R$ | This study |
| SA3153 | *ΔagmE*/ Pnat *agmE*$^{K66Q+}$ (pKA38), $Tc^R$ | This study |

| | | |
|---|---|---|
| SA3154 | WT/Pnat *agmE*$^{D90A}$-mCherry (pKA43), Tc$^R$ | This study |
| SA3155 | WT/ Pnat *ftsZ*-GFP (pKA51), Tc$^R$ | This study |
| SA3156 | *ΔagmE*/Pnat *ftsZ*-GFP (pKA51), Tc$^R$ | This study |
| SA3157 | WT/Pnat *agmE*-mCherry at *carS* (pKA53), Km$^R$ | This study |
| SA3158 | *ΔagmE*/Pnat *agmE*-mCherry at *carS* (pKA53), Km$^R$ | This study |
| SA3159 | WT/Pnat *ftsZ*-GFP (pKA51), Pnat *agmE*-mCherry at *carS* (pKA53), Km$^R$ ,Tc$^R$ | This study |
| SA3160 | *ΔagmE*/ Pnat *ftsZ*-GFP (pKA51), Pnat *agmE*-mCherry at *carS* (pKA53), Km$^R$ ,Tc$^R$ | This study |
| SA3161 | *ΔagmE, ΔdiVIA* | This study |
| SA3162 | *ΔagmE*/ Pnat *MXAN0636* (pKA42), Tc$^R$ | This study |
| SA3163 | *ΔagmE*, *MXAN0636*::*nptI*/ Pnat *MXAN0636* (pKA42), Tc$^R$ | This study |
| SA3164 | Δ*MXA3112*/PpilA *MXAN3112* (pKA39), Km$^R$ | This study |

### 5.3.3 Cultivation of bacteria

Media and solutions were autoclaved for 20 minutes at 121°C and 1 bar over pressure. Heat sensitive liquids as antibiotic were filtered using 0.22µm pore size filters (Millipore, Schwalbach) and added after media have cooled to 55°C. Other equipment (such as glass ware, metal tools and ceramics) was sterilized at 180°C for three hours.

*M. xanthus* was cultivated aerobically at 32°C on 1% CTT agar in the dark. *M. xanthus* liquid cultures were inoculated by dispersion of single colonies by resuspending in a 1.5 ml Eppendorf tube containing 1ml liquid medium. Liquid cultures were grown on horizontal shakers at 240rpm at 32°C. Optical densities of *M. xanthus* liquid cultures were monitored at 550nm ($OD_{550}$) using 1cm path length.

*E. coli* was incubated aerobically on Luria-Bertani (LB-) agar at 37°C. *E. coli* liquid cultures were inoculated directly from single colonies into liquid medium and cultivated on horizontal shakers at 37°C and 240rpm. The optical density was determined at 600nm ($OD_{600}$).

### 5.3.4 Storage of transformed *M. xanthus* and *E. coli* strains

*M. xanthus* and *E. coli* cultures on solid media were stored up to three weeks at 18 or 4°C, respectively. For long term storage, 2ml cultures of *M. xanthus* were harvested at $OD_{550}$=0.5-0.9 by centrifugation and resuspended in 1ml CTT medium. The stocks were made with the

*M. xanthus* culture by adding glycerol to 4% and the mixtures were frozen in liquid nitrogen and stored at -80°C.

*E. coli* strains were supplemented with 200 µL of 50% glycerol (10% final concentration) and stored at -80°C.

### 5.3.5 Motility assay of *M. xanthus*

Motility assays were performed on different agar plates favoring either A- or S-motility (Table 5-8). Cells were grown to $OD_{550}$ 0.5 to 0.9, harvested, and resuspended in CTT medium to a calculated density of 5.0 $\times 10^9$ cells/ml. 5µl of cell suspension were placed on the two different motility plates and incubated at 32°C. After 24 h, colony morphology and colony edges were observed visually in a Leica MZ8 stereomicroscope and a Leica IMB/E inverted microscope and visualized using a Leica DFC280 CCD camera (Leica Microsystems).

## 5.4 Molecular biological methods

### 5.4.1 Oligonucleotides and plasmids

All oligonucleotide primers used in this study were synthesized by Invitrogen (Karlsruhe) or Thermo Scientific (Dreieich). Red sequences show restriction sites used for cloning. Blue sequences indicate complementary sequences that were used to fuse PCR products. **Bold** sequences specify addition of extra stop codon. Purple sequences indicate the addition of a linker.

**Table 5-11**. Primers used to generate in frame deletions, insertion mutants and to check integrations.

| Name | Description | Sequence (5' → 3') |
|---|---|---|
| **Generation of *MXAN0635* in frame deletion** | | |
| KA-200 | Primer A forward | ccgGAATTCCCTGCGCCAACTCCTCAG |
| KA-201 | Primer B reverse | CTTCGTCTGAATCTGCTTCGGGGACAC |
| KA-202 | Primer C forward | AAGCAGATTCAGACGAAGGGCACCCAG |
| KA-203 | Primer D reverse | gcgGGATCCCCGCTGCACCTCCACCTC |
| KA-212 | Primer E forward | CGACGTTGCCTGTGAAGCC |
| | Check insertion | |
| KA-213 | Primer F reverse | GCCTTCAGTCGCTCACGG |
| | Check insertion | |
| KA-214 | Primer G forward | CGACATCTGGGAGCTGCG |
| | Check in frame deletion | |
| KA-215 | Primer H reverse | TTGAAGGTGGCGTTGAAGG |

| | | |
|---|---|---|
| | Check in frame deletion | |
| **Generation of *MXAN3112* in frame deletion** | | |
| KA-295 | Primer A forward | ccgGAATTCGGTTAGAAGGGCCTCCAT |
| KA-296 | Primer B reverse | GCCGTTGGCCTTGTCGAGCGGAGTGATTTTCAT |
| KA-297 | Primer C forward | CCGCTCGACAAGGCCAACGGCGACTCC |
| KA-298 | Primer D reverse | gcgGGATCCCCGGAAGAGGGCGGAGTAGTG |
| KA-323 | Primer E forward | TTCATCGAACCTTGCTCCC |
| | Check insertion | |
| KA-324 | Primer F reverse | TGCTCGAAGTGGAACACGC |
| | Check insertion | |
| KA-333 | Primer G forward | ATCCGGCAGAAGCGGTTCG |
| | Check in frame deletion | |
| KA-334 | Primer H reverse | CTTCTTCTGGGACAGATACGC |
| | Check in frame deletion | |
| **Generation of *MXAN0634* in frame deletion** | | |
| KA-371 | Primer A forward | ccgGAATTCCGACGAGCAGTTGAGCACCAG |
| KA-372 | Primer B reverse | gcgTCTAGACACGCGGCGCGGCCTGCG |
| KA-373 | Primer C forward | gcgTCTAGAGTCACCCCAAGCCATTCC |
| KA-374 | Primer D reverse | gccAAGCTTCCTTGAAGTTCAGGAAGAGC |
| KA-375 | Primer E forward | GGGTCTCCGCTGTATCGC |
| | Check insertion | |
| KA-376 | Primer F reverse | GGCAGCGAGGACTTCTGG |
| | Check insertion | |
| KA-377 | Primer G forward | GGAACCAGATGATGGACAAGC |
| | Check in frame deletion | |
| KA-378 | Primer H reverse | TCGTGGATGGCTTCCTCG |
| | Check in frame deletion | |
| **Generation of *MXAN0635* insertion mutant** | | |
| KA-224 | Forward | gcgGGATCCTCCACGTCCTACGCCTGG |
| KA-225 | Reverse | gccAAGCTTCGGATAGTGCGTCTGGAG |
| **Generation of *MXAN0636* insertion mutant** | | |
| KA-250 | Forward | ccgGAATTCGAGGCGTTGCTCGACACC |
| KA-251 | Reverse | gcgGGATCCGGCCAGCAGCTTCACCCG |
| KA-284 | Forward | GCTCCAGACGCACTATCCG |
| | Check insertion | |
| KA-285 | Reverse | AGGACGGGAAGTAGCCAGG |
| | Check insertion | |

**Table 5-12.** PCR primers used for generation of complementation under native and *pilA* promoter

| **Name** | **Description** | **Sequence** |
|---|---|---|
| ***agmE* under native promoter** | | |
| KA-314 | Forward | gcgGGATCCGTCACCCCAAGCCATTCC |

| | | |
|---|---|---|
| KA-207 | Reverse | gccAAGCTTTCATCAGCCGGCCTGCTGGGT |
| ***agmE* under *pilA* promoter** | | |
| KA-207 | Reverse | gccAAGCTTTCATCAGCCGGCCTGCTGGGT |
| KA-288 | Forward | gcgTCTAGAATGGAAGCGCCGACGTAC |
| ***MXAN0636* under native promoter** | | |
| KA-347 | Forward | gcgGGATCCGCTCGCGGACTTCCTGTCC |
| KA-348 | Reverse | gccAAGCTTTCAGCGCACCGTGGCCTG |
| ***MXAN0636* under *pilA* promoter** | | |
| KA-349 | Forward | gcgTCTAGAATGAAGAAAGCCTTTGAACAGAACG |
| KA-348 | Reverse | gccAAGCTTTCAGCGCACCGTGGCCTG |
| ***MXAN3112* under *pilA* promoter** | | |
| KA-337 | Forward | gcgTCTAGAATGAAAATCACTCCGCTCG |
| KA-338 | Reverse | gccAAGCTTTCAGGAGTCGCCGTTGGC |

**Table 5-13.** PCR primers used for generation of fusion proteins

| Name | Description | Sequence |
|---|---|---|
| ***agmE*-GFP at native site** | | |
| KA-289 | Forward | ccgGAATTCATGGAAGCGCCGACGTAC |
| KA-219 | Reverse | gcgGGATCCGGCGGAGCCGCCGGCCTGCTGGGTGCC |
| ***agmE*-mCherry under native promoter for *attB* and *carS*** | | |
| KA-327 | Forward | ccgGGTACCGTCACCCCAAGCCATTCC |
| KA-219 | Reverse | gcgGGATCCGGCGGAGCCGCCGGCCTGCTGGGTGCC |
| ***agmE*-mCherry under *pilA* promoter for *attB*** | | |
| KA-219 | Reverse | GCGGGATCCGGCGGAGCCGCCGGCCTGCTGGGTGCC |
| KA-288 | Forward | GCGTCTAGAATGGAAGCGCCGACGTAC |
| ***ftsZ*-GFP and *ftsZ*-mCherry under native promoter for *attB*** | | |
| KA-335 | Forward | ATCGCTCATATGGAACAACCGCCGCGTGGG |
| KA-336 | Reverse | CGGGGTACCCGGCAGTTCCGTCTGGCC |
| ***divIVA*-mCherry at native site** | | |
| KA-299 | Forward | attgcgCCCGGGATGAAAATCACTCCGCTCGAC |
| KA-300 | Reverse | gcgGGATCCGGCGGAGCCGGAGTCGCCGTTGGCCTT |

**Table 5-14**. PCR primers used for overexpression of protein constructs in pET45b+ unless indicated. For AgmE point mutants, primers binding the desired amino acid substitution are shown here. These same AgmE primers were used to generate amino acid substitution for *in vivo* complementation.

| Name | Description | Sequence |
|---|---|---|
| **Overexpression construct *agmE*** | | |
| KA-206 | Forward | gcgGGATCCCATGGAAGCGCCGACGTAC |
| KA-207 | Reverse | gccAAGCTT**TCA**TCAGCCGGCCTGCTGGGT |
| **Overexpression construct *agmE*$^{D90A}$** | | |
| KA-236 | Forward | GACCTCGCCAGCCAGGGC |
| KA-237 | Reverse | GCCCTGGCTGGCGAGGTC |

| | | |
|---|---|---|
| **Overexpression construct *agmE*$^{D170A}$** | | |
| KA-238 | Forward | GAGGCCCAGTACGCCGTC |
| KA-239 | Reverse | GACGGCGTACTGGGCCTC |
| **Overexpression construct *agmE*$^{D175A}$** | | |
| KA-240 | Forward | GTCTTCGCCGCGCCGCCG |
| KA-241 | Reverse | CGGCGGCGCGGCGAAGAC |
| **Overexpression construct *agmE*$^{K66Q}$** | | |
| KA-242 | Forward | ACCGGCCAGACGTCGCTG |
| KA-243 | Reverse | CAGCGACGTCTGGCCGGT |
| **Overexpression construct *ftsZ*** | | |
| KA-342 | Forward | gcgGGATCCCATGGACCAGTTCGATCAGAACAAG |
| KA-343 | Reverse | gccAAGCTT**TCA**TTACGGCAGTTCCGTCTGGC |
| **Overexpression construct *MXAN0636*** | | |
| KA-344 | Forward | gcgGGATCCCATGAAGAAAGCCTTTGAACAGAACG |
| KA-345 | Reverse | gccAAGCTT**TCA**TCAGCGCACCGTGGCCTG |
| **Overexpression of *MXAN3112*** | | |
| KA-318 | Forward | gcgGGATCCgATGAAAATCACTCCGCTCGACATC |
| KA-319 | Reverse for pET24b+ | gccAAGCTTGGAGTCGCCGTTGGCCTT |
| KA-320 | Reverse | gccAAGCTT**TCA**TCAGGAGTCGCCGTTGGC |

**Table 5-15.** Primers used to verify integration at *attB* locus

| Name | Description | Sequence |
|---|---|---|
| *attB* rechts | Genome specific *attB* forward primer | GGAATGATCGGACCAGCTGAA |
| *attB* links | Genome specific *attB* downstream primer | CGGCACACTGAGGCCACATA |
| *attP* rechts | Plasmid specific *attP* forward primer | GCTTTCGCGACATGGAGGA |
| *attP* links | Plasmid specific *attP* reverse primer | GGGAAGCTCTGGGTACGAA |

**Table 5-16.** Primers used to verify integration at *carS* locus for constructs containing mCherry fusions

| Name | Description | Sequence |
|---|---|---|
| KA-403 | Primer binding pCT2 plasmid forward | TCGGCTGCAACTTTGTCATGCTTGACAC |
| KA-316 | mCherry internal primer reverse | CTTGAAGCCCTCGGGGAAGGA |
| KA-404 | Forward primer binding the kanamycin cassette | TTTTTTTTCATATGAGCCATATTCAACGGGAAACGTC |
| KA-405 | Reverse primer binding the kanamycin cassette | ATAAGCTTTTAGAAAAACTCATCGAGCATCAAATGAAAC |

**Table 5-17**. Primers used for sequencing

| Name | Description | Sequence |
|---|---|---|
| M13 fwd | General sequencing primer forward | CGCCAGGGTTTTCCCAGTCACGAC |
| M13 rv | General sequencing primer reverse | ATGCTCACTCATTAGGCACCCCAG |
| KA-231 | Sequencing pSWU30 forward | GGATGTGCTGCAAGGCGATTAAGTTGG |
| KA-232 | Sequencing pSWU30 reverse | GCTTTACACTTTATGCTTCCGGCTCG |
| KA-233 | GFP forward | CACATGGTCCTGCTGGAGTTCG |
| KA-234 | GFP reverse | TGTGGCCGTTTACGTCGCCGTCCAGCTC |
| KA-254 | PilA promoter seq reverse | GTGCGCACCTGGGTTGGCATGCG |
| KA-255 | PilA promoter seq forward | TGAGGGAGCCACGGTTGATGAG |
| KA-276 | pET45b+ forward | TGGCGCCGGTGATGCCGGCC |
| KA-277 | pET45b+ reverse | ATCCGGATATAGTTCCTCCT |
| KA-308 | pCT2 seq forward | CGCGTTCAATCGGACCAGCGGAGG |
| KA-309 | pCT2 seq reverse | CGCGGATGCCGTCGCGCTCACCCG |
| KA-316 | mCherry reverse | CTTGAAGCCCTCGGGGAAGGA |
| KA-317 | mCherry forward | CCTCCCTGCAGGACGGCGAGT |
| KA-406 | Internal primer of FtsZ for sequencing forward | CGTGCAGGGCATCAGCGACC |
| KA-407 | Internal primer of FtsZ for sequencing reverse | GGTCGCTGATGCCCTGCACG |

**Table 5-18.** Primers used to map *agmE* locus

| Name | Description | Sequence |
|---|---|---|
| KA-278 | Intergenic region *agmE* and *MXAN0636* forward | GCTCCAGACGCACTATCCG |
| KA-279 | Intergenic region *agmE* and *MXAN0636* reverse | CTCGGTGTCGAGCAACGC |
| KA-280 | Intergenic region *agmE* and *MXAN0634* forward | GTGGAATCCCTCTGCTCG |
| KA-281 | Intergenic region *agmE* and *MXAN0634* reverse | CTTCTCGAAGTCCTCGCC |
| KA-282 | Internal region of *agmE* forward | TCCCACGTCCTACGCCTGG |
| KA-283 | Internal region of *agmE*reverse | CGGATAGTGCGTCTGGAG |

**Table 5-19**. List of plasmid used in this study.

| Plasmids | Genotype | Reference |
|---|---|---|
| pBluescript II SK- | Vector for cloning, blue/white selection, $Amp^R$ | Fermentas (St. Leon-Rot) |
| pBGS18 | Vector for insertion mutants, $Km^R$ | (Spratt *et al.*, 1986) |
| pBJ114 | Vector for in frame deletion, $Km^R$ | (Julien *et al.*, 2000) |
| pSWU30 | Vector for inserting at *attB* | (Wu *et al.*, 1997) |
| pSW105 | Vector for inserting at attB containing *pilA* promoter | S. Weiss (MPI-Marburg) |
| pFGBJ | *frzS*-GFP, $Km^R$ | (Mignot *et al.*, 2005) |

| | | |
|---|---|---|
| pCT2 | Vector for inserting at *carS* locus | (Mignot *et al.*, 2007a) |
| pGFy148 | *aglZ*-GFP, $Km^R$ | G. Freymark (MPI-Marburg) |
| pET45b+ | Expression vector , T7 promoter, N-term $His_6$-tag, $Amp^R$ | Novagen/Merck (Darmstadt) |
| pET24b+ | Expression vector , T7 promoter, N-term $His_6$-tag, $Km^R$ | Novagen/Merck (Darmstadt) |
| pMT935 | Derivative of pCT2 containing mCherry fusion protein | M. Thanbichler (MPI-Marburg) |
| pFCrGFP | GFP fusion protein from *Chlamydomonas* | Biocat (Heilderberg) |
| pKA1 | pBJ114-*agmE* in-frame deletion, $Km^R$ | This study |
| pKA2 | pBGS18-*agmE* insertion fragment, $Km^R$ | This study |
| pKA3 | pET45b+ - *agmE* with extra stop codon, $Amp^R$ | This study |
| pKA10 | pBJ114- *agmE*-GFP fusion | This study |
| pKA12 | pET45b+ - $agmE^{D90A}$ with extra stop codon, $Amp^R$ | This study |
| pKA13 | pET45b+ - $agmE^{D170A}$ with extra stop codon, $Amp^R$ | This study |
| pKA14 | pET45b+ - $agmE^{D175A}$ with extra stop codon, $Amp^R$ | This study |
| pKA15 | pET45b+ - $agmE^{K66Q}$ with extra stop codon, $Amp^R$ | This study |
| pKA16 | pBJ114- C-term GFP with linker, $Km^R$ | This study |
| pKA18 | pBGS18- *MXAN0636* insertion, $Km^R$ | This study |
| pKA19 | pSW105-PpilA *agmE* (start-stop),Mx8 *attP*, $Km^R$ | This study |
| pKA20 | pSW105-PpilA *agmE*-GFP, Mx8 *attP*, $Km^R$ | This study |
| pKA21 | pBJ114- MXAN0636-mCherry, $Km^R$ | This study |
| pKA22 | pBJ114-mCherry | This study |
| pKA23 | pBJ114-mCherry with linker | This study |
| pKA24 | pBJ114- *MXAN3112* in frame deletion, $Km^R$ | This study |
| pKA25 | pBJ114-*MXAN3112*-mCherry, $Km^R$ | This study |
| pKA26 | pSWU30- Pnat $agmE^+$, Mx8 *attP* ,$Tc^R$ | This study |
| pKA28 | pSWU30- Pnat *agmE*-mCherry, Mx8 *attP* ,$Tc^R$ | This study |
| pKA30 | pMT935-Pnat *ftsZ*-mCherry, *carS* ,$Km^R$ | This study |
| pKA32 | pSWU30-Pnat *ftsZ*-mCherry, Mx8 *attP* ,$Tc^R$ | This study |
| pKA36 | pSWU30-Pnat $agmE^{D90A}$, Mx8 *attP* ,$Tc^R$ | This study |
| pKA37 | pSWU30-Pnat $agmE^{D175A}$, Mx8 *attP* ,$Tc^R$ | This study |
| pKA38 | pSWU30-Pnat $agmE^{K66Q}$, Mx8 *attP* ,$Tc^R$ | This study |
| pKA41 | pSW105- PpilA MXAN0636 (start-stop), Mx8 *attP* ,$Km^R$ | This study |

| | | |
|---|---|---|
| pKA42 | pSWU30-Pnat MXAN0636, Mx8 *attP* ,$Tc^R$ | This study |
| pKA43 | pSWU30- Pnat *agmE*$^{D90A}$-mCherry, Mx8 *attP* ,$Tc^R$ | This study |
| pKA44 | pBJ114-MXAN0634 in frame deletion | This study |
| pKA45 | pSW105- PpilA *agmE*-mCherry, Mx8 *attP* ,$Km^R$ | This study |
| pKA46 | pSWU30- Pnat mCherry-MXAN0636 Mx8 *attP* ,$Tc^R$ | This study |
| pKA47 | pSWU30- N-term mCherry with linker, Mx8 *attP* ,$Tc^R$ | This study |
| pKA48 | pSW105- ftsZ (start-stop) Mx8 *attP* ,$Km^R$ | This study |
| pKA49 | pBJ114- C-term mCherry with linker | This study |
| pKA51 | pSWU30- Pnat *ftsZ*-GFP, Mx8 *attP* ,$Tc^R$ | This study |
| pKA53 | pCT2- Pnat *agmE*-mCherry, *carS*, $Km^R$ | This study |
| pMM1 | pET45b+ - *ftsZ* with extra stop codon, $Amp^R$ | Marlen Mock (MPI-Marburg) |
| pMM2 | pET45b+ - *MXAN0636* with extra stop codon, $Amp^R$ | Marlen Mock (MPI-Marburg) |

### 5.4.2 Construction of plasmids

Purified *M. xanthus* genomic DNA was used as template to amplify chromosomal regions for cloning. Plasmid DNA was used as template to amplify XFP fusions.

**Plasmids pKA1, pKA24 (in frame deletions)**: Those plasmids are pBJ114 derivatives and were used for markerless in-frame deletion of specific genomic regions as described in Section 5.4.3**.** The corresponding *E. coli* clones were selected on LB plates containing kanamycin, X-Gal and IPTG. Isolated plasmids were sequenced to confirm the inserts were error-free and subsequently introduced into *M. xanthus* DK1622 to generate strains SA3108, SA3127 and SA3161

**Plasmids pKA2, pKA18 (insertion mutants):** Approximately 500bp internal fragments of the genes to be disrupted were PCR-amplified, purified and directly cloned into pBGS18. The corresponding *E. coli* colonies were selected on LB plates containing kanamycin, X-Gal and IPTG. Isolated plasmids were sequenced to confirm correctness of the insert and subsequently introduced into *M. xanthus* DK1622 to generate strains SA3109 and SA3111, by homologous recombination.

**Plasmids pKA26, pKA36, pKA37, pKA38 and pKA42 (complementation plasmids)**: Approximately 400bp upstream of the

gene to be complemented were PCR amplified. The putative promoter region and the gene were cloned into pSWU30. For plasmids pKA36, pKA37 and pKA38, an amino acid substitution was performed by PCR to generate different point mutations of *agmE*. The corresponding *E. coli* colonies were selected on LB plates containing tetracyclin. Plasmids were isolated and sequenced. Correct plasmid was afterward introduced into *M. xanthus* DK1622 to generate strains SA3120, SA3128, SA3129, SA3150, into SA3108 to generate strains SA3119, SA3130, SA3152, SA3153, SA3162 and finally into SA3111 to generate strain SA3137.

**Plasmids pKA19, pKA39 and pKA41 ("overexpression" plasmids in *M. xanthus*):** The complete *agmE, divIVA* and *MXAN0636* genes were PCR amplified and cloned directly into pSW105 containing *pilA* promoter. In *M. xanthus*, the *pilA* promoter is a strong promoter. Therefore by cloning the genes of interest after this promoter, we expect an overexpression, which was confirmed by immunoblot analyses in the case of *in vivo* overexpression of AgmE. The error-free plasmids were introduced into DK1622 to generate strains SA3125, SA3140, SA3141, also into SA3108 to generate strains SA3121, into SA3111 to generate strains SA3144 and into SA3127 to generate the strain SA3164.

**Plasmids pKA16, pKA22, pKA23, pKA49 (XFP fusion proteins)**: GFP and mCherry were PCR amplified from plasmids pFCrGFP and pMT935 respectively, with or without addition of linker sequence and cloned into pBJ114 for pKA16, pKA22 and pKA23 and into pSWU30 for pKA49. These plasmids were done to facilitate the fluorescence labeling of genes of interest.

**Plasmids pKA28, pKA43 and pKA53 (fluorescence labeling of AgmE):** The putative promoter region (400bp upstream of *agmE*) and *agmE* gene were amplified and cloned into pKA23 which contains a C-terminus mCherry with a linker. Then the fragment containing $P_{nat}$ *agmE*-mCherry was sub-cloned into pSWU30 generating plasmids pKA28 and pKA43 and into pCT2 plasmids generating plasmid pKA53. Plasmid pKA43 contains an amino acid substitution generating $AgmE^{D90A}$ point mutant. The error-free plasmids were introduced into DK1622 to generate strains SA3132, SA3154, SA3157 and into SA3108 to generate strains SA3131, SA3146 and SA3158.

**Plasmids pKA32 and pKA51 (fluorescence labeling of FtsZ)**: The putative promoter region (400bp upstream *ftsZ* gene) and *ftsZ* gene were amplified and cloned into pMT935 which contains a larger linker region and C-terminus mCherry. Then the fragment containing $P_{nat}$ *ftsZ*-mCherry was sub-cloned into pSWU30 plasmid generating plasmid pKA32. For plasmid pKA51, the putative promoter region and *ftsZ* gene were amplified and the linker sequence was added by the primer. This fragment was cloned into pSWU30 and the GFP was introduced by PCR amplification. The correct plasmids were introduced into DK1622 to generate strains SA3132, SA3157 and into SA3108 to generate strains SA3131 and SA3158.

### 5.4.3 Generation of *M. xanthus* in frame deletion mutants

In-frame deletions of specific genomic regions were generated as previously described (Shi *et al.*, 2008). In brief, approximately 500bp fragments directly up- and downstream of the target gene were amplified by PCR using primers designated as A, B, C and D. The primers A and D contain restriction enzymes for cloning into the plasmid pBJ114. The primers B and C were designed to possess compatible ends which allow fusing the 500bp fragments in a second PCR or having restriction sites for cloning. The fragments AB and CD were used to generate the full-length in-frame deletion fragment either by direct cloning or in a second PCR reaction with primers A and D and the two flanking PCR fragments as templates. Plasmids with error-free inserts were electroporated into *M. xanthus*. The plasmid pBJ114 cannot replicate in *M. xanthus* but provides for kanamycin resistance when integrated into the chromosome by homologous recombination. Therefore, *M. xanthus* transformants possess a plasmid insertion up- or downstream of the target gene. Insertions were mapped by PCR and both, up- and downstream insertion mutants were isolated, if possible.

To obtain markerless in frame deletion, a second homologous recombination has to take place to excise the plasmid. The plasmid pBJ114 also contains the counter selectable marker *galK* (*E. coli* galactokinase gene) which converts galactose into its phosphorylated form. Since *M. xanthus* cannot metabolize galactose phosphate, the compound accumulates to toxic levels when cells are grown on media containing galactose. Therefore, only cells

that have undergone a second recombination that results in excision of the plasmid are viable. After excision of the plasmid, only 50% of the mutants will have the in frame deletion, while the other 50% will have restore the original genomic situation (Figure 5-1).

The insertion mutants (upstream and downstream integration) were grown in CTT medium containing kanamycin to mid-log phase. Then, the cultures were diluted 1/100 into CTT medium without kanamycin and grown to an optical density of 0.5. 50, 100, 200 and 400µl of these cultures were added to 3ml CTT soft agar and plated on CTT agar containing 2.5% (w/v) galactose (Sigma, Taufkirchen). Emerging colonies were transferred to CTT plates containing galactose or kanamycin. Colonies growing on galactose but not on kanamycin were used to verify deletions by PCR.

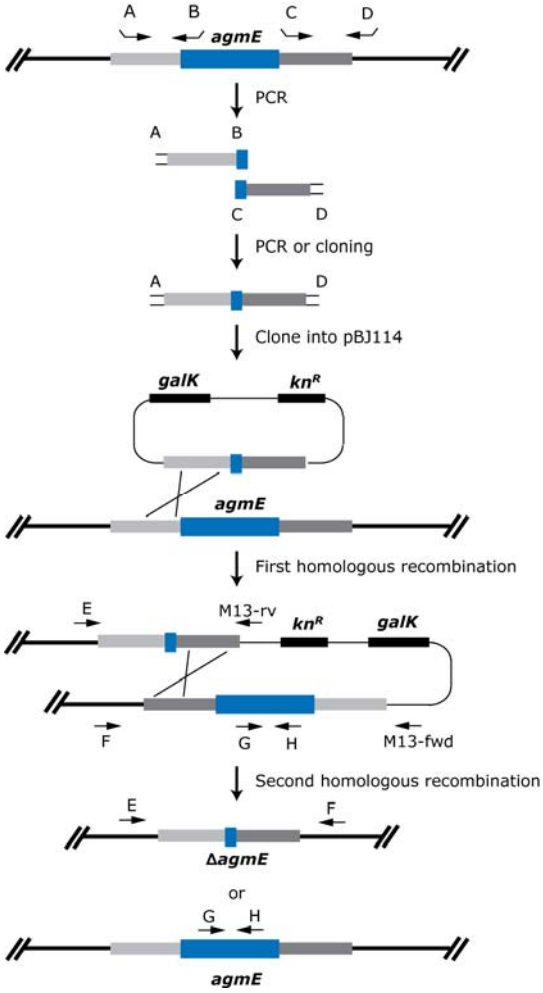


**Figure 5-1. Outline strategy for the generation of in-frame deletion mutants in *M. xanthus*.** The first homologous recombination leads to plasmid integration up- or downstream of the genomic region to be deleted. The second recombination event eliminates the vector with the target region (in-frame deletion) or only the vector (reconstitution) (Shi *et al.*, 2008).

### 5.4.4 Generation of *M. xanthus* insertion mutants

To generate insertion mutants in *M. xanthus*, a central part of the target gene (500bp) was amplified by PCR. The purified PCR product was cloned into the pBGS18 plasmid which provides kanamycin resistant. The plasmid pBGS18 cannot replicate in *M. xanthus*. Therefore, only insertion of the plasmid into the chromosome leads to resistant colonies and to disruption of the target gene (Figure 5-2). Insertion mutants were verified by PCR using oligonucleotides specific for the pBGS18 plasmid and a neighboring region up- or downstream of the target gene.

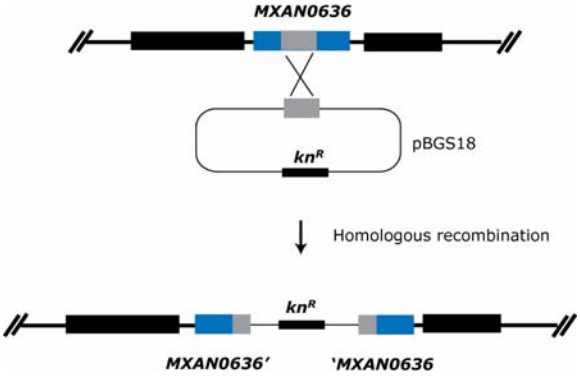


**Figure 5-2. Outline strategy for generation of insertion mutants in *M. xanthus*.** A central part (500bp) of the target gene was PCR amplified and cloned into pBGS18. Homologous recombination leads to the disruption of the target gene.

### 5.4.5 DNA preparation of *E. coli* and *M. xanthus*

Plasmid DNA from *E. coli* was isolated using the QIAprep Spin Miniprep-Kit (Qiagen). *M. xanthus* genomic DNA was prepared using the Master Pure DNA purification kit (Epicentre) according to the instructions of the manufacturer. Concentration and purity was determined with the Nanodrop ND-1000 spectrophotometer (Nanodrop, Wilmington). Crude genomic DNA preparations used to verify the presence of insertions by PCR were done by boiling cell samples for 10 min in 20µl of lysis buffer (10µl EB buffer (Qiagen) and 10µL of Lyse N GO (Pierce)) followed by cooling on ice and brief sedimentation of cell debris.

### 5.4.6 Polymerase Chain Reaction (PCR)

Amplification of specific DNA-fragments was carried out in 25µL reaction volume in FailSafe™ PCR PreMix Buffer J (Epicentre) with Platinum® *Pfx* DNA polymerase (Invitrogen). To check integration, colony PCR was performed using Eppendorf® MasterMix (Eppendorf) in a 20µL reaction volume.

**Table 5-20.** PCR reaction mix (25 µl) for cloning and PCR reaction mix (20µL) for check PCR are shown here.

| Component | Volume | Final concentration |
|---|---|---|
| **PCR for cloning** | | |
| Genomic DNA or plasmid DNA | 2 µL | 100ng |
| 50 µM Primer | 0.25 µL | 0.4 µM |
| 2X FailSafeTM PCR PreMix Buffer J | 12.5 µL | 1X |
| Platinum® Pfx DNA polymerase | 0.25 µL | 0.1 units |
| Sterile water | 9.75 µL | - |
| **Check PCR** | | |
| Crude genomic DNA | 2 µL | 100ng |
| 50 mM Primer | 0.2 µL | 0.4 µM |
| Eppendorf Mastermix | 10 µL | 1X |
| Sterile water | 7.6 µL | - |

The PCR programs used are shown in Table 5-21. The reaction conditions were modified based on predicted primer annealing temperatures, expected product sizes and polymerase used.

**Table 5-21.** PCR programs. Standard and touch down programs were used for amplifying PCR products for cloning and Pfx platinum® was used. The check PCR program was used to verify integration of plasmids and Eppendorf® Mastermix was used.

| Step | Temperature | Time | |
|---|---|---|---|
| **Standard PCR program** | | | |
| Initial denaturation | 95°C | 3 min | |
| Denaturation | 95°C | 30 s | x 25 |
| Primer annealing | 5°C below predicted melting temperature | 15 s | |
| Elongation | 68°C | 1 min per kb | |
| Final elongation | 68°C | 3 min | |
| Hold | 4°C | ∞ | |
| **Touch down PCR program** | | | |
| Initial denaturation | 95°C | 3 min | |
| Denaturation | 95°C | 30 s | x 9 |
| Primer annealing | 70°C | 30 s | |
| Elongation | 68°C | 1 min per kb | |
| Denaturation | 95°C | 30 s | x 9 |
| Primer annealing | 60°C | 30 s | |
| Elongation | 68°C | 1 min per kb | |
| Denaturation | 95°C | 30 s | x 20 |
| Primer annealing | 55°C | 30 s | |
| Elongation | 68°C | 1 min per kb | |
| Final elongation | 68°C | 3 min | |
| Hold | 4°C | ∞ | |

| **Check PCR program** | | | |
|---|---|---|---|
| Initial denaturation | 94°C | 3 min | |
| Denaturation | 94°C | 30 s | x 35 |
| Primer annealing | 51C | 30 s | |
| Elongation | 72°C | 1 min per kb | |
| Final elongation | 72°C | 3 min | |
| Hold | 4°C | ∞ | |

PCR products were purified with the QIAquick® PCR Purification Kit (Qiagen) or the DNA clean and concentrator™ Kit (Zymo Research) or extracted from agarose gels and purified with QIAquick® gel extraction Kit (Qiagen) or Gel recovery Kit (Zymo research).

### 5.4.7 Reverse transcription-PCR

Total RNA was isolated from cell pellets using the hot-phenol method (Overgaard *et al.*, 2006). Briefly, approximately 5 x $10^8$ *M. xanthus* cells were harvested to a tube containing 1/10 volume of ice-cold ethanol/phenol stop solution (5% saturated acid phenol pH <6.0 in 96% ethanol) and spin down (4700 rpm, 10 min, 4°C). The pellet was resuspended in 600µl ice cold solution 1 (0.3 M sucrose, 0.01 M NaAc, pH 4.5) and 300µL were transferrred into each 1.5mL tubes containing 300µL hot (65°C) solution 2 (2% SDS, 0.01 NaAC, pH 4.5). The cell lysis was performed twice with equal volume of hot phenot extraction (saturated acid phenol pH <6.0 at 65°C), once with phenol:chloroform extraction (saturated acid phenol pH <6.0: chloroform = 5:1), and once with equal volume of chloroform: isoamyl alcohol extraction (24:1). RNA was precipitated with 1/10 volume of 3M NaAC pH 4.5 and two volumes of 96% ethanol for 20min at -20°C. The RNA pellet was centrifuged 10000 *x* g at 4°C and washed twice with equal volum of ice cold 75% ethanol. The pellet was dried briefly at room temperature and resuspent in about 50µl RNase-free H2O. The RNA should be stored at -80°C for longer storage.

cDNA was synthesized using the cDNA archive kit (ABI) from 1µg of DNA-free total RNA. To map *agmE* locus, primers amplifying intergenic and internal regions are listed in Table 5-18.

### 5.4.8 Agarose gel electrophoresis

Nucleic acid fragments were separated by size with agarose gel electrophoresis at 120V in TAE buffer. Ethidiumbromide was added to agarose in a final concentration of 0.01% (v/v). 6x sample loading buffer (30% (v/v) glycerol, 50mM EDTA, 10mM Tris-HCl pH 7.5, 0.44µM bromphenolblue, 0.28µM xylencyanol, 8.8µM orange G) was combined with samples to 1x final concentration. After electrophoresis, agarose gels were imaged using a 2UV-Transilluminator (UVP-Bio-Doc-IT-System, UniEquip) at 365 nm wavelength and documented with an electronic P93E thermoprinter (Mitsubishi). DNA fragments were isolated from agarose gels by cutting out and purification with the QIAquick® Gel Extraction Kit (Qiagen) or Gel Recovery Kit (Zymo research).

### 5.4.9 Restriction and Ligation of DNA fragments

Restriction of DNA was carried out by incubation of 2.5- 5µg DNA with restriction endonucleases for 2 h according to specific requirements for the enzyme. Restricted DNA was purified with the QIAquick® PCR Purification Kit (Qiagen) or the DNA clean and concentrator™ Kit (Zymo Research).

Ligation reactions were performed with T4 DNA ligase. DNA fragments were ligated into vectors applying a 3 fold molar excess of insert-DNA. Usually, 10 fmol insert and 30 fmol vector DNA were ligated overnight at 18°C followed by heat inactivation of the enzyme at 65°C for 15min.

### 5.4.10 Transformation of electrocompetent *E. coli* cells

Over night cultures of *E. coli* strains were used to inoculate 1L LB-medium. Cells were grown at 37°C shaking at 240rpm to an $OD_{600}$ of 0.6 and harvested by centrifugation at 5,000 *x* g for 20 min, 4°C. The cell pellet was resuspended in 500ml ice cold sterile 10% (v/v) glycerol and centrifuged again. The washing steps were repeated with 100mL, 50mL and 10mL volumes. Finally, the cell pellet was resuspended in 2mL 10% sterile glycerol and 50 µl aliquots were shock frozen in liquid nitrogen and stored at -80°C for later use.

5µl heat inactivated ligation reaction were added to 50µl electrocompetent *E. coli* cells on ice. The suspension was transferred into an electroporation cuvette (Biorad) and pulsed with 1.8 kV, 25 µF and 200 Ω. 1mL LB medium

were added, the suspension transferred into a sterile plastic tube and incubated for 1h at 37°C shaking at 240 rpm. 50, 100 and 800µL aliquots were then plated on LB agar containing appropriate antibiotics. The plates were incubated at 37°C over night, colonies transferred onto fresh agar plates and screened for the presence of the plasmid containing the insert by restriction digestion.

### 5.4.11 Transformation of electrocompetent *M. xanthus* cells

*M. xanthus* strains were grown in 100 ml CTT medium to an $OD_{550}$ of 0.5 to 0.8 and harvested by centrifugation at 4000 *x* g for 10 min at RT. The cell pellet was resuspended in 50 ml sterile deionized water and centrifuged as above. This washing step was repeated three times. The pellet was then resuspended in 150 µl sterile water and the suspension divided into 50µl aliquots used directly for electroporation. 5µl plasmid DNA (corresponding to calculated 1µg DNA) were transferred to the suspension of electrocompetent cells. The suspension was transferred into a 0.1cm electroporation cuvette and pulsed with 650V, 25µF and 400Ω. 1ml CTT medium was added immediately, the culture transferred into a fresh plastic tube and incubated at 32°C and 240 rpm in the dark for 5h. Then, 50, 100, 200 and 600µl aliquots were added to 3ml soft agar, vortexed and used to overlay a CTT agar plate containing appropriate antibiotics. The plates were incubated at 32°C for 5 to 10 days and colonies transferred to fresh CTT agar plates containing appropriate antibiotics. The integration of the plasmid was verified by PCR.

### 5.4.12 DNA sequencing

DNA sequencing was performed applying the chain termination method after Sanger. Sequencing reactions were set up using the Big Dye® Terminator™ Cycle Sequencing Kit (Applied Biosystems, Darmstadt) according to the instructions of the manufacturer in a 20 µl reaction volume and incubated as shown in Table 5-22. Reaction products were purified either by DNA precipitation or with the BigDye® XTerminator™ Purification Kit (Applied Biosystems). For precipitation, 10µl 125mM EDTA, 9µl 3M sodium acetate, pH 4.6, 80µl HPLC-H2O and 400µl 96% ethanol were added to the reaction and incubated for 30 min at RT. DNA precipitates were pelleted by

centrifugation at 15,000 *x* g for 30 min at 20 °C. The supernatant was removed and the pellet washed twice with freshly prepared
70% ethanol followed by 5 min centrifugation at 15,000 *x* g each. Finally, the ethanol was removed and the pellet air dried. For sequencing, the pellet was dissolved in 20 µl formamide. DNA sequences were analyzed with the Vector NTI software suite 10.

**Table 5-22.** Incubation times and temperatures for DNA sequencing reactions

| Step | Temperature | Time | |
|---|---|---|---|
| Initial denaturation | 96°C | 1 min | |
| Denaturation | 96°C | 10 s | x 29 |
| Primer annealing and elongation | 60°C | 4 min | |
| Hold | 10°C | ∞ | |

## 5.5 Biochemical methods

### 5.5.1 Purification of *M. xanthus* AgmE

To purify the $His_6$-AgmE fusion protein, strain Rosetta (DE3)/pLysS (Invitrogen) was transformed with pKA3, and grown to $OD_{600}$ 0.5 in 1 L 2YT medium at 37°C. IPTG was added to final concentration of 0.5 mM and cultivation was continued for 2h. The cells were harvested by centrifugation for 10min at 10000 *x* g, washed in buffer B1 (50mM NaH2PO4, 300mM NaCl, 10mM imidazol adjusted to pH 8.0 with NaOH) and frozen in liquid nitrogen. The protein was purified according to the following protocol: 3.5g cells were resuspended in 20mL buffer B2 (buffer B1 + 1mM β-mercaptoethanol) containing 100µg/mL PMSF and 10 U/mL DNAse I and lyzed by three passages through French Press (10000 psi). After centrifugation of the suspension for 30 min at 10000 *x* g, the supernatant was loaded on a Ni-NTA agarose column (1.5mL column volume) (Qiagen), previously equilibrated with buffer B2. The column was washed with 25 column volumes of wash buffer (50mM $NaH_2PO_4$, 300mM NaCl, 20mM imidazol, 1mM β-mercaptoethanol, adjusted to pH 8.0 with NaOH). The protein was eluted with increasing amount of imidazol from 50mM to 500mM in elution buffer (50mM $NaH_2PO_4$, 300mM NaCl, 1mM β-mercaptoethanol, adjusted to pH 8.0 with NaOH). Fractions containing protein of interest were pooled and dialyzed against buffer A (50mM sodium phosphate, pH 7.0, 5mM $MgCl_2$, 0.1mM EDTA, 1mM β-mercaptoethanol). After removal of precipitates by centrifugation 20min at 30000 *x* g, the

supernatant was applied to a SP Sepharose Fast Flow column (GE Healthcare) equilibrated with buffer A. The column was washed with 50 mL of buffer A and the protein was eluted with 250 mL of NaCl linear gradient (50-500 mM NaCl in buffer A) at 2 mL/min. Fractions containing the protein were pooled, dialyzed for 20 hr against 2 l storage buffer 1 (50mM Hepes/NaOH, pH 7.2, 50mM NaCl, 5mM $MgCl_2$, 0.1mM EDTA, 10% glycerol, 1mM β-mercaptoethanol), aliquoted, snap frozen in liquid nitrogen, and stored at -80°C. The same procedure can be used for $AgmE^{D175A}$ and $AgmE^{K66Q}$. However, $AgmE^{D90A}$ is not soluble.

### 5.5.2 Purification of *M. xanthus* FtsZ

To purify the $His_6$-FtsZ fusion protein, strain Rosetta (DE3)/pLysS (Invitrogen) was transformed with pMM1, and grown to $OD_{600}$ 0.5 in 2 L 2YT medium at 37°C. IPTG was added to final concentration of 0.5mM and cultivation was continued for 2h. The cells were harvested by centrifugation for 10min at 10000 *x* g, washed in buffer B1 and frozen in liquid nitrogen. The protocol for FtsZ purification is as follows: 5g cells were resuspended in 20mL buffer B2 containing 100µg/mL PMSF and 10 U/mL DNAse I and lyzed by three passages through French Press (10000 psi). After centrifugation of the suspension for 30 min at 10000 *x* g, the supernatant was loaded on a Ni-NTA agarose column (1.5mL column volume) (Qiagen), previously equilibrated with buffer B2. The column was washed with 25 column volumes of wash buffer containing 40mM imidazol instead of 20mM. The protein was eluted with increasing amount of imidazol from 50mM to 500mM in elution buffer. Fractions containing protein of interest were pooled and dialyzed against storage buffer 2 (50 mM Hepes/NaOH, pH 7.2, 50mM KCl, 0.1mM EDTA, 10% glycerol, 1mM β-mercaptoethanol), aliquoted, snap frozen in liquid nitrogen, and stored at -80°C.

### 5.5.3 Purification of *M. xanthus* MXAN0636

To purify the $His_6$-MXAN0636 fusion protein, strain Rosetta (DE3)/pLysS (Invitrogen) was transformed with pMM2, and grown to $OD_{600}$ 0.5 in 100 ml 2YT medium at 37°C. IPTG was added to final concentration of 0.5mM and cultivation was continued for 2h. The cells were harvested by centrifugation for 10min at 10000 *x* g, washed in buffer B1 and frozen in liquid nitrogen.

MXAN0636 can only be purified using batch purification: 1g cells were resuspended in 20mL buffer B2 containing 100µg/mL PMSF and 10 U/mL DNAse I and lyzed by three passages through French Press (10000psi). After centrifugation of the suspension for 30 min at 10000 *x* g, the supernatant was mixed with 4mL of Ni-NTA agarose (Qiagen) in a falcon tube, previously equilibrated with buffer B2. The mixture was incubated for one hour in a rotating wheel at 4°C and washed 4 times with wash buffer (50mM $NaH_2PO_4$, 300mM NaCl, 20mM imidazol, 1mM β-mercaptoethanol, adjusted to pH 8.0 with NaOH) followed by centrifugation 5 min at 2000 *x* g. The protein was eluted with 250mM and 500mM of imidazol in elution buffer (50mM $NaH_2PO_4$, 300mM NaCl, 1mM β-mercaptoethanol, adjusted to pH 8.0 with NaOH). Fractions containing protein of interest were pooled and dialyzed against storage buffer 3 (50mM Hepes/NaOH, pH 7.2, 10% glycerol, 1mM β-mercaptoethanol), aliquoted, snap frozen in liquid nitrogen, and stored at -80°C

### 5.5.4 SDS Polyacrylamide Gel electrophoresis (SDS-PAGE)

SDS-PAGE (Laemmli, 1970) was performed to monitor heterologous protein expression, to separate and to purify proteins under denaturing conditions. To denature proteins, samples were combined with equal volumes of 2 x Laemmli sample buffer (LSB; 0.125 M Tris-HCl pH 6.8, 20% (v/v) glycerol, 4% (w/v) SDS, 10% (v/v) β-mercaptoethanol, 0.02% (w/v) bromophenol blue) and heated at 96°C for 5 min prior to loading the gel. PageRuler™ prestained protein ladder (Fermentas, St. Leon-Rot) was used to estimate the molecular weight of proteins. Electrophoresis was performed in Bio-Rad electrophoresis chambers (Bio-Rad, München) at 120 – 150 V in 1 x Trisglycine- SDS running buffer (25mM Tris, 190mM glycine, 0.1% (w/v) SDS). Proteins were visualized by staining in Coomassie brilliant blue R250.

### 5.5.5 Determination of protein concentrations

Protein concentrations were determined after Bradford (Bradford, 1976) using the Bio-Rad protein assay kit (Bio-Rad, München) according to the instructions of the manufacturer. Standard curves were obtained using dilutions of protein standard (bovine serum albumin). All sample protein concentrations were determined in duplicate with 10µl of a 1:10 dilution in

1ml reaction volume. Absorbance was measured at 595 nm with an Ultrospec 2100 pro spectrophotometer (Amersham Biosciences, Munich). Protein concentrations were calculated based on the slope value of the standard curve.

### 5.5.6 Immunoblot analyses

1mg of purified AgmE, FtsZ and MXAN0636 under native conditions was sent to Eurogentec (Seraing, Belgium) for antibody production.

Immunoblot analysis was performed using standard protocol (Sambrook, 2002). Same amount of total protein were loaded onto a SDS-PAGE and protein transfer was performed using Hoefer TE77 semi-dry blotting apparatus (Amersham Biosciences, Munich) with constant current of 0.8mA/cm$^2$. After transfer, nitrocellulose membranes were blocked using 1x PBS-T buffer (137 mM NaCl, 10 mM phosphate, 2.7 mM KCl, 0.1% (v/v) tween-20, pH 7.4) containing 5% (w/v) nonfat milk powder overnight at 4°C. Membranes were washed one time with 1x PBS-T buffer and subsequently incubated with the proper dilution of primary antibody (Table 5-23) in 0.5x PBS-T containing 2.5 % (w/v) nonfat milk powder for 2 hrs at RT. Membranes were then washed 5 times for 5 min with 1x PBS-T and then incubated with 1/15000 dilution of secondary anti-rabbit IgG horseradish peroxidase (HPR) coupled antibodies (Pierce, Bonn). After washing with 1x PBS-T, chemiluminescence substrate (Pierce) was added and signals were detected by exposure to CL-Xposure Film (Pierce).

**Table 5-23.** Dilution of primary antibodies used for immunoblot analyses

| **Antibody** | AgmE | FtsZ | mCherry | GFP |
|---|---|---|---|---|
| **Fold dilution** | 5000 | 5000 | 5000 | 250 |

### 5.5.7 Pelleting assay and electron microscopy

A clearing spin of the AgmE stock was performed at 20000 *x* g for 10 min immediately before the pelleting assay was carried out to remove any pre-aggregated molecules. AgmE (10µM) was mixed in a volume of 500µL with 20mM Tris-HCl (pH 7.5), 100mM KCl, 2mM $MgCl_2$, and 1mM DTT. 2mM of ADP or ATP were added when indicated. The reaction was incubated for 30 min at 32°C. For pelleting assay, the samples were subjected to ultracentrifugation 20000 *x* g for one hour and supernatant and pellet were separated. The same volume of supernatant and pellet were loaded on a

SDS-PAGE and proteins were visualized by staining in Coomassie brilliant blue. For electron microscopy, after incubation of the reactions, the sample was applied onto glow-discharged carbon-coated nickel grids for 1 min. The grids were blotted dry, washed with a drop on water and negatively stained with 1 % uranyle acetate.

For FtsZ pelleting assay, FtsZ (3μM) was incubated in the absence or presence of 2mM GTP for 30 min at RT in different buffers: Buffer P (50 mM Hepes/NaOH, pH 7.2, 50mM KCl, 10mM MgCl2, 1mM β-mercaptoethanol) and Buffer P1 (50mM MES, pH 6.5, 50mM KCl, 10mM MgCl2, 1mM β-mercaptoethanol). These buffers were supplemented with 10mM $CaCl_2$ or 0.1mM $CuSO_4$. The samples were then subjected to ultracentrifugation 200000 *x* g and the supernatant and pellet were separated and resolved in an SDS-PAGE.

### 5.5.8 ATPase assay

ATPase assay was carried out in different buffer conditions: Buffer 1 (30mM Tris-HCl pH 7.5, 200mM KCl, 10mM $MgCl_2$ and 1mM DTT) or Buffer P. Increasing concentrations (5μM, 10μM and 15μM) of AgmE were incubated with 0.5mM [α-$^{32}$P]ATP (110 Tbq mmol$^{-1}$, Amersham) for 10 min to 2 hours. The nucleotides were separated from the proteins using Microcon-Y10 ultrafiltration column (Millipore, Schwalbach). Labeled adenine nucleotides were separated by thin layer chromatography (TLC): 0.5μL of eluate were applied to a poly(ethyleneimine)-cellulose F TLC plate (Merck, Darmstadt) with 2.4M formic acid as the solvent system. Labeled nucleotides on the TLC plate were visualized and quantified by phosphoimaging and analyzed using ImageQuant software. As positive control for this assay and to mark the positions of [α-$^{32}$P]ADP and [α-$^{32}$P]ATP, the Apyrase ATPase (Sigma-Aldrich, Taufkirchen) was used.

### 5.5.9 DNA binding assay

The ability of AgmE to bind double stranded plasmid DNA (200fmoles of pMCS-2) was assayed in the absence of nucleotides and in the presence of ADP or ATP (2mM). Binding reactions were performed in 50mM Tris-HCl pH 8.5, 5mM MgSO4 with increasing amounts of AgmE 0-100 pmol. Reactions were incubated for 10 min at 25°C, mixed with gel loading buffer and run

on a 1 % agarose gel in 0.5 X TB + 1mM MgSO4 buffer and stained with ethidium bromide.

### 5.5.10 Pull down assay

AgmE and FtsZ were purified as described in section 5.5.1 and 5.5.2. Both proteins were dialyzed against buffer B1. 1mg of protein was loaded onto $Ni^{2+}$-NTA column (2mL, Qiagen). *M. xanthus* cell lysate were prepared as follow: 50mL of $OD_{550}$ 0.7 culture was resuspended in buffer B1 and protease inhibitor cocktails without EDTA was added (Roche). Cells were lysed by sonication (30% output control, 3 duty cycle, 2 times for 3 min) and centrifuged 4000 *x* g for 20 min. Lysate was added to the column and incubated for 20 min. Columns were washed for 20 column volumes and samples were eluted using buffer B1 with 500mM imidazol. Eluates were separated on a SDS-PAGE or directly separated using nano-HPLC and MS/MS for protein identification.

## 5.6 Fluorescence Microscopy

### 5.6.1 Preparation of sample for fluorescence microscopy

For all samples observed under the microscope, cell cultures were harvested at $OD_{550}$ between 0.3-0.6. For samples requiring DAPI staining, the procedure is a follow: 50µL of cell culture were incubated for 10 min in the presence of 1ng/mL DAPI in the dark with gently shaking. 5µL of suspension was spotted on a thin TPM- 1% agarose pad (Table 5-8).

For time-lapse microscopy, 5µL of cell suspension was spotted on a thin 0.25% CTT 1% agarose pad (Table 5-8) and pictures were taken every 5 min.

### 5.6.2 Analyses of fluorescence microscopy

Metamorph® 7.5 (Molecular Devices, Union City, CA) was used to analyze the fluorescence pictures. For the cell length measurement, the region measurement function was used. For the fluorescence intensity, the linescan function was used with the following parameters: maximum value, scan width 10. In average more than 100 cells were quantified.

## 5.7 Bioinformatics analyses

*M. xanthus* DNA- and protein sequences were obtained online from TIGR (http://www.tigr.org/cmr) and analyzed using the Blastn (against nonredundant database), Blastp and psiBlastp algorithms from NCBI or the SMART algorithm from EMBL (http://smart.embl-heidelberg.de/). The protein sequences for the generation of the alignments and phylogenetic trees (Figure 2-1) were obtained from NCBI (http://www.ncbi.nlm.nih.gov/). Selected sequences were aligned using ClustalW (v. 1.81,(Thompson *et al.*, 1994)). The alignment was manually curated using Bioedit (v. 7.0.5.3, T.A. Hall) and subsequently used to generate a bootstrapped (1000 iterations) Neighbor Joining tree. The tree was visualized and annotated using TreeDyn (v. 198.3, Chevenet, F., *et al.*).

# 6 References

**Aaron, M., *et al.*** (2007). The tubulin homologue FtsZ contributes to cell elongation by guiding cell wall precursor synthesis in Caulobacter crescentus. Mol Microbiol *64*, 938-952.

**Aarsman, M.E., *et al.*** (2005). Maturation of the Escherichia coli divisome occurs in two steps. Mol Microbiol *55*, 1631-1645.

**Addinall, S.G., *et al.*** (1996). FtsZ ring formation in fts mutants. J Bacteriol *178*, 3877-3884.

**Ades, S.E.** (2004). Proteolysis: Adaptor, adaptor, catch me a catch. Curr Biol *14*, R924-926.

**Adler, H.I., *et al.*** (1967). MINIATURE escherichia coli CELLS DEFICIENT IN DNA. Proc Natl Acad Sci U S A *57*, 321-326.

**Ausmees, N., and Jacobs-Wagner, C.** (2003). Spatial and temporal control of differentiation and cell cycle progression in Caulobacter crescentus. Annu Rev Microbiol *57*, 225-247.

**Barilla, D., *et al.*** (2005). Bacterial DNA segregation dynamics mediated by the polymerizing protein ParF. EMBO J *24*, 1453-1464.

**Bartosik, A.A., *et al.*** (2004). ParB of Pseudomonas aeruginosa: interactions with its partner ParA and its target parS and specific effects on bacterial growth. J Bacteriol *186*, 6983-6998.

**Beall, B., and Lutkenhaus, J.** (1992). Impaired cell division and sporulation of a Bacillus subtilis strain with the ftsA gene deleted. J Bacteriol *174*, 2398-2403.

**Bernhardt, T.G., and de Boer, P.A.** (2005). SlmA, a nucleoid-associated, FtsZ binding protein required for blocking septal ring assembly over Chromosomes in E. coli. Mol Cell *18*, 555-564.

**Beyer, A.** (1997). Sequence analysis of the AAA protein family. Protein Sci *6*, 2043-2058.

**Bi, E.F., and Lutkenhaus, J.** (1991). FtsZ ring structure associated with division in Escherichia coli. Nature *354*, 161-164.

**Blanche, F., *et al.*** (1991). Biosynthesis of vitamin B12: stepwise amidation of carboxyl groups b, d, e, and g of cobyrinic acid a,c-diamide is catalyzed by one enzyme in Pseudomonas denitrificans. J Bacteriol *173*, 6046-6051.

**Bork, P., *et al.*** (1992). An ATPase domain common to prokaryotic cell cycle proteins, sugar kinases, actin, and hsp70 heat shock proteins. Proc Natl Acad Sci U S A *89*, 7290-7294.

**Bradford, M.M.** (1976). A rapid and sensitive method for the quantitation of microgram quantities of protein utilizing the principle of protein-dye binding. Anal Biochem *72*, 248-254.

**Bramkamp, M., *et al.*** (2008). A novel component of the division-site selection system of Bacillus subtilis and a new mode of action for the division inhibitor MinCD. Mol Microbiol *70*, 1556-1569.

**Cha, J.H., and Stewart, G.C.** (1997). The divIVA minicell locus of Bacillus subtilis. J Bacteriol *179*, 1671-1683.

**Cordell, S.C., *et al.*** (2003). Crystal structure of the SOS cell division inhibitor SulA and in complex with FtsZ. Proc Natl Acad Sci U S A *100*, 7889-7894.

**Dai, K., and Lutkenhaus, J.** (1992). The proper ratio of FtsZ to FtsA is required for cell division to occur in Escherichia coli. J Bacteriol *174*, 6145-6151.

**Dajkovic, A., *et al.*** (2008). MinC spatially controls bacterial cytokinesis by antagonizing the scaffolding function of FtsZ. Curr Biol *18*, 235-244.

**Dajkovic, A., and Lutkenhaus, J.** (2006). Z ring as executor of bacterial cell division. J Mol Microbiol Biotechnol *11*, 140-151.

**Davis, M.A., *et al.*** (1992). Biochemical activities of the parA partition protein of the P1 plasmid. Mol Microbiol *6*, 1141-1147.

**de Boer, P.A., *et al.*** (1991). The MinD protein is a membrane ATPase required for the correct placement of the Escherichia coli division site. EMBO J *10*, 4371-4380.

**de Boer, P.A., *et al.*** (1992). Roles of MinC and MinD in the site-specific septation block mediated by the MinCDE system of Escherichia coli. J Bacteriol *174*, 63-70.

**de Boer, P.A.J., *et al.*** (1988). Isolation and Properties of Minb, a Complex Genetic-Locus Involved in Correct Placement of the Division Site in Escherichia-Coli. Journal of Bacteriology *170*, 2106-2112.

**de Pedro, M.A., *et al.*** (1997). Murein segregation in Escherichia coli. J Bacteriol *179*, 2823-2834.

**Den Blaauwen, T., *et al.*** (1999). Timing of FtsZ assembly in Escherichia coli. J Bacteriol *181*, 5167-5175.

**den Blaauwen, T., *et al.*** (2008). Morphogenesis of rod-shaped sacculi. FEMS Microbiol Rev *32*, 321-344.

**Derouaux, A., *et al.*** (2008). The monofunctional glycosyltransferase of Escherichia coli localizes to the cell division site and interacts with penicillin-binding protein 3, FtsW, and FtsN. J Bacteriol *190*, 1831-1834.

**Dworkin, M.** (1996). Recent advances in the social and developmental biology of the myxobacteria. Microbiol Rev *60*, 70-102.

**Easter, J., Jr., and Gober, J.W.** (2002). ParB-stimulated nucleotide exchange regulates a switch in functionally distinct ParA activities. Mol Cell *10*, 427-434.

**Ebersbach, G., *et al.*** (2008). Novel coiled-coil cell division factor ZapB stimulates Z ring assembly and cell division. Mol Microbiol *68*, 720-735.

**Ebersbach, G., and Gerdes, K.** (2004). Bacterial mitosis: partitioning protein ParA oscillates in spiral-shaped structures and positions plasmids at mid-cell. Mol Microbiol *52*, 385-398.

**Ebersbach, G., *et al.*** (2006). Regular cellular distribution of plasmids by oscillating and filament-forming ParA ATPase of plasmid pB171. Mol Microbiol *61*, 1428-1442.

**Edwards, D.H., and Errington, J.** (1997). The Bacillus subtilis DivIVA protein targets to the division septum and controls the site specificity of cell division. Mol Microbiol *24*, 905-915.

**Erickson, H.P.** (1997). FtsZ, a tubulin homologue in prokaryote cell division. Trends Cell Biol *7*, 362-367.

**Flynn, J.M., *et al.*** (2003). Proteomic discovery of cellular substrates of the ClpXP protease reveals five classes of ClpX-recognition signals. Mol Cell *11*, 671-683.

**Fogel, M.A., and Waldor, M.K.** (2006). A dynamic, mitotic-like mechanism for bacterial chromosome segregation. Genes Dev *20*, 3269-3282.

**Fu, X., *et al.*** (2001). The MinE ring required for proper placement of the division site is a mobile structure that changes its cellular location during the Escherichia coli division cycle. Proc Natl Acad Sci U S A *98*, 980-985.

**Garcia-Moreno, D., *et al.*** (2009). A vitamin B12-based system for conditional expression reveals dksA to be an essential gene in Myxococcus xanthus. J Bacteriol.

**Gerdes, K., *et al.*** (2000). Plasmid and chromosome partitioning: surprises from phylogeny. Mol Microbiol *37*, 455-466.

**Gerding, M.A., *et al.*** (2007). The trans-envelope Tol-Pal complex is part of the cell division machinery and required for proper outer-membrane invagination during cell constriction in E. coli. Mol Microbiol *63*, 1008-1025.

**Gitai, Z.** (2007). Diversification and specialization of the bacterial cytoskeleton. Curr Opin Cell Biol *19*, 5-12.

**Golovanov, A.P., *et al.*** (2003). ParG, a protein required for active partition of bacterial plasmids, has a dimeric ribbon-helix-helix structure. Mol Microbiol *50*, 1141-1153.

**Gregory, J.A., *et al.*** (2008). Bacillus subtilis MinC destabilizes FtsZ-rings at new cell poles and contributes to the timing of cell division. Genes Dev *22*, 3475-3488.

**Gueiros-Filho, F.J., and Losick, R.** (2002). A widely conserved bacterial cell division protein that promotes assembly of the tubulin-like protein FtsZ. Genes Dev *16*, 2544-2556.

**Haeusser, D.P., *et al.*** (2007). The division inhibitor EzrA contains a seven-residue patch required for maintaining the dynamic nature of the medial FtsZ ring. J Bacteriol *189*, 9001-9010.

**Haeusser, D.P., *et al.*** (2004). EzrA prevents aberrant cell division by modulating assembly of the cytoskeletal protein FtsZ. Mol Microbiol *52*, 801-814.

**Hagen, D.C., *et al.*** (1978). Synergism between morphogenetic mutants of Myxococcus xanthus. Dev Biol *64*, 284-296.

**Hale, C.A., and de Boer, P.A.** (1997). Direct binding of FtsZ to ZipA, an essential component of the septal ring structure that mediates cell division in E. coli. Cell *88*, 175-185.

**Hale, C.A., and de Boer, P.A.** (1999). Recruitment of ZipA to the septal ring of Escherichia coli is dependent on FtsZ and independent of FtsA. J Bacteriol *181*, 167-176.

**Hale, C.A., *et al.*** (2000). ZipA-induced bundling of FtsZ polymers mediated by an interaction between C-terminal domains. J Bacteriol *182*, 5153-5166.

**Harry, E., *et al.*** (2006). Bacterial cell division: the mechanism and its precison. Int Rev Cytol *253*, 27-94.

**Hayes, F., and Barilla, D.** (2006). The bacterial segrosome: a dynamic nucleoprotein machine for DNA trafficking and segregation. Nat Rev Microbiol *4*, 133-143.

**Hirano, T.** (1998). SMC protein complexes and higher-order chromosome dynamics. Curr Opin Cell Biol *10*, 317-322.

**Hirota, Y., *et al.*** (1968). Thermosensitive mutants of E. coli affected in the processes of DNA synthesis and cellular division. Cold Spring Harb Symp Quant Biol *33*, 677-693.

**Hodgkin, J., and Kaiser, D.** (1979). Genetics of Gliding Motility in Myxococcus-Xanthus (Myxobacterales) - 2 Gene Systems Control Movement. Molecular & General Genetics *171*, 177-191.

**Hu, Z., *et al.*** (2002). Dynamic assembly of MinD on phospholipid vesicles regulated by ATP and MinE. Proc Natl Acad Sci U S A *99*, 6761-6766.

**Hu, Z., and Lutkenhaus, J.** (2001). Topological regulation of cell division in E. coli. spatiotemporal oscillation of MinD requires stimulation of its ATPase by MinE and phospholipid. Mol Cell *7*, 1337-1343.

**Hu, Z., *et al.*** (1999). The MinC component of the division site selection system in Escherichia coli interacts with FtsZ to prevent polymerization. Proc Natl Acad Sci U S A *96*, 14819-14824.

**Inoue, I., *et al.*** (2009). New model for assembly dynamics of bacterial tubulin in relation to the stages of DNA replication. Genes Cells *14*, 435-444.

**Ishikawa, S., *et al.*** (2006). A new FtsZ-interacting protein, YlmF, complements the activity of FtsA during progression of cell division in Bacillus subtilis. Mol Microbiol *60*, 1364-1380.

**Jensen, R.B., and Shapiro, L.** (1999). The Caulobacter crescentus smc gene is required for cell cycle progression and chromosome segregation. Proc Natl Acad Sci U S A *96*, 10661-10666.

**Jensen, S.O., *et al.*** (2005). Cell division in Bacillus subtilis: FtsZ and FtsA association is Z-ring independent, and FtsA is required for efficient midcell Z-Ring assembly. J Bacteriol *187*, 6536-6544.

**Julien, B., *et al.*** (2000). Spatial control of cell differentiation in Myxococcus xanthus. Proc Natl Acad Sci U S A *97*, 9098-9103.

**Kaiser, D.** (1979). Social gliding is correlated with the presence of pili in Myxococcus xanthus. Proc Natl Acad Sci U S A *76*, 5952-5956.

**Kawai, Y., *et al.*** (2003). Identification of a protein, YneA, responsible for cell division suppression during the SOS response in Bacillus subtilis. Mol Microbiol *47*, 1113-1122.

**Kim, H.J., *et al.*** (2000). Partitioning of the linear chromosome during sporulation of Streptomyces coelicolor A3(2) involves an oriC-linked parAB locus. J Bacteriol *182*, 1313-1320.

**Koonin, E.V.** (1993). A superfamily of ATPases with diverse functions containing either classical or deviant ATP-binding motif. J Mol Biol *229*, 1165-1174.

**Kroos, L., and Kaiser, D.** (1987). Expression of many developmentally regulated genes in Myxococcus depends on a sequence of cell interactions. Genes Dev *1*, 840-854.

**Lackner, L.L., *et al.*** (2003). ATP-dependent interactions between Escherichia coli Min proteins and the phospholipid membrane in vitro. J Bacteriol *185*, 735-749.

**Laemmli, U.K.** (1970). Cleavage of structural proteins during the assembly of the head of bacteriophage T4. Nature *227*, 680-685.

**Larsen, R.A., *et al.*** (2007). Treadmilling of a prokaryotic tubulin-like protein, TubZ, required for plasmid stability in Bacillus thuringiensis. Genes Dev *21*, 1340-1352.

**Lasocki, K., *et al.*** (2007). Deletion of the parA (soj) homologue in Pseudomonas aeruginosa causes ParB instability and affects growth rate, chromosome segregation, and motility. J Bacteriol *189*, 5762-5772.

**Lee, P.S., and Grossman, A.D.** (2006). The chromosome partitioning proteins Soj (ParA) and Spo0J (ParB) contribute to accurate chromosome partitioning, separation of replicated sister origins, and regulation of replication initiation in Bacillus subtilis. Mol Microbiol *60*, 853-869.

**Leipe, D.D., *et al.*** (2002). Classification and evolution of P-loop GTPases and related ATPases. J Mol Biol *317*, 41-72.

**Leonard, T.A., *et al.*** (2005). Bacterial chromosome segregation: structure and DNA binding of the Soj dimer--a conserved biological switch. EMBO J *24*, 270-282.

**Leonardy, S., *et al.*** (2008). Reversing cells and oscillating motility proteins. Mol Biosyst *4*, 1009-1014.

**Leonardy, S., *et al.*** (2007). Coupling of protein localization and cell movements by a dynamically localized response regulator in Myxococcus xanthus. EMBO J *26*, 4433-4444.

**Levin, P.A., *et al.*** (1999). Identification and characterization of a negative regulator of FtsZ ring formation in Bacillus subtilis. Proc Natl Acad Sci U S A *96*, 9642-9647.

**Lewis, R.A., *et al.*** (2002). Chromosome loss from par mutants of Pseudomonas putida depends on growth medium and phase of growth. Microbiology *148*, 537-548.

**Libante, V., *et al.*** (2001). Role of the ATP-binding site of SopA protein in partition of the F plasmid. J Mol Biol *314*, 387-399.

**Lim, G.E., *et al.*** (2005). Bacterial DNA segregation by dynamic SopA polymers. Proc Natl Acad Sci U S A *102*, 17658-17663.

**Lin, D.C., and Grossman, A.D.** (1998). Identification and characterization of a bacterial chromosome partitioning site. Cell *92*, 675-685.

**Lowe, J., *et al.*** (2004). Molecules of the bacterial cytoskeleton. Annu Rev Biophys Biomol Struct *33*, 177-198.

**Lutkenhaus, J.** (2007). Assembly dynamics of the bacterial MinCDE system and spatial regulation of the Z ring. Annu Rev Biochem *76*, 539-562.

**Lutkenhaus, J., and Addinall, S.G.** (1997). Bacterial cell division and the Z ring. Annu Rev Biochem *66*, 93-116.

**Ma, L., *et al.*** (2004). Positioning of the MinE binding site on the MinD surface suggests a plausible mechanism for activation of the Escherichia coli MinD ATPase during division site selection. Mol Microbiol *54*, 99-108.

**Ma, X., *et al.*** (1996). Colocalization of cell division proteins FtsZ and FtsA to cytoskeletal structures in living Escherichia coli cells by using green fluorescent protein. Proc Natl Acad Sci U S A *93*, 12998-13003.

**Machon, C., *et al.*** (2007). Promiscuous stimulation of ParF protein polymerization by heterogeneous centromere binding factors. J Mol Biol *374*, 1-8.

**Margolin, W.** (2000). Themes and variations in prokaryotic cell division. FEMS Microbiol Rev *24*, 531-548.

**Margolin, W.** (2005). FtsZ and the division of prokaryotic cells and organelles. Nat Rev Mol Cell Biol *6*, 862-871.

**Marston, A.L., and Errington, J.** (1999). Selection of the midcell division site in Bacillus subtilis through MinD-dependent polar localization and activation of MinC. Mol Microbiol *33*, 84-96.

**Marston, A.L., *et al.*** (1998). Polar localization of the MinD protein of Bacillus subtilis and its role in selection of the mid-cell division site. Genes Dev *12*, 3419-3430.

**Mignot, T., *et al.*** (2005). Regulated pole-to-pole oscillations of a bacterial gliding motility protein. Science *310*, 855-857.

**Mignot, T., *et al.*** (2007a). Two localization motifs mediate polar residence of FrzS during cell movement and reversals of Myxococcus xanthus. Mol Microbiol *65*, 363-372.

**Mignot, T., *et al.*** (2007b). Evidence that focal adhesion complexes power bacterial gliding motility. Science *315*, 853-856.

**Migocki, M.D., *et al.*** (2002). The Min system is not required for precise placement of the midcell Z ring in Bacillus subtilis. EMBO Rep *3*, 1163-1167.

**Mohl, D.A., and Gober, J.W.** (1997). Cell cycle-dependent polar localization of chromosome partitioning proteins in Caulobacter crescentus. Cell *88*, 675-684.

**Mukherjee, A., *et al.*** (1998). Inhibition of FtsZ polymerization by SulA, an inhibitor of septation in Escherichia coli. Proc Natl Acad Sci U S A *95*, 2885-2890.

**Mukherjee, A., and Lutkenhaus, J.** (1999). Analysis of FtsZ assembly by light scattering and determination of the role of divalent metal cations. J Bacteriol *181*, 823-832.

**Mulder, E., and Woldringh, C.L.** (1989). Actively replicating nucleoids influence positioning of division sites in Escherichia coli filaments forming cells lacking DNA. J Bacteriol *171*, 4303-4314.

**Murray, H., and Errington, J.** (2008). Dynamic control of the DNA replication initiation protein DnaA by Soj/ParA. Cell *135*, 74-84.

**Oliva, M.A., *et al.*** (2004). Structural insights into FtsZ protofilament formation. Nat Struct Mol Biol *11*, 1243-1250.

**Osawa, M., *et al.*** (2008). Reconstitution of contractile FtsZ rings in liposomes. Science *320*, 792-794.

**Patrick, J.E., and Kearns, D.B.** (2008). MinJ (YvjD) is a topological determinant of cell division in Bacillus subtilis. Mol Microbiol *70*, 1166-1179.

**Peters, P.C., *et al.*** (2007). A new assembly pathway for the cytokinetic Z ring from a dynamic helical structure in vegetatively growing cells of Bacillus subtilis. Mol Microbiol *64*, 487-499.

**Pichoff, S., and Lutkenhaus, J.** (2002). Unique and overlapping roles for ZipA and FtsA in septal ring assembly in Escherichia coli. EMBO J *21*, 685-693.

**Pichoff, S., and Lutkenhaus, J.** (2005). Tethering the Z ring to the membrane through a conserved membrane targeting sequence in FtsA. Mol Microbiol *55*, 1722-1734.

**Pogliano, J., *et al.*** (1997). Inactivation of FtsI inhibits constriction of the FtsZ cytokinetic ring and delays the assembly of FtsZ rings at potential division sites. Proc Natl Acad Sci U S A *94*, 559-564.

**Pollard, T.D., and Borisy, G.G.** (2003). Cellular motility driven by assembly and disassembly of actin filaments. Cell *112*, 453-465.

**Raskin, D.M., and de Boer, P.A.** (1999). MinDE-dependent pole-to-pole oscillation of division inhibitor MinC in Escherichia coli. J Bacteriol *181*, 6419-6424.

**Reeve, J.N., *et al.*** (1973). Minicells of Bacillus subtilis. J Bacteriol *114*, 860-873.

**Rodriguez, A.M., and Spormann, A.M.** (1999). Genetic and molecular analysis of cglB, a gene essential for single-cell gliding in Myxococcus xanthus. J Bacteriol *181*, 4381-4390.

**Rosen, B.P.** (1990). The plasmid-encoded arsenical resistance pump: an anion-translocating ATPase. Res Microbiol *141*, 336-341.

**Rothfield, L., *et al.*** (2005). Spatial control of bacterial division-site placement. Nat Rev Microbiol *3*, 959-968.

**Rueda, S., *et al.*** (2003). Concentration and assembly of the division ring proteins FtsZ, FtsA, and ZipA during the Escherichia coli cell cycle. J Bacteriol *185*, 3344-3351.

**Sackett, M.J., *et al.*** (1998). Ordered expression of ftsQA and ftsZ during the Caulobacter crescentus cell cycle. Mol Microbiol *28*, 421-434.

**Sambrook, J.a.R., D.** (2002). Molecular Cloning: A Laboratory Manual (Cold Spring Harbor
Laboratory Press.).

**Schumacher, M.A.** (2008). Structural biology of plasmid partition: uncovering the molecular mechanisms of DNA segregation. Biochem J *412*, 1-18.

**Schumacher, M.A., *et al.*** (2007a). Segrosome structure revealed by a complex of ParR with centromere DNA. Nature *450*, 1268-1271.

**Schumacher, M.A., *et al.*** (2007b). Structure of a four-way bridged ParB-DNA complex provides insight into P1 segrosome assembly. J Biol Chem *282*, 10456-10464.

**Sharpe, M.E., and Errington, J.** (1996). The Bacillus subtilis soj-spo0J locus is required for a centromere-like function involved in prespore chromosome partitioning. Mol Microbiol *21*, 501-509.

**Shi, X., *et al.*** (2008). Bioinformatics and experimental analysis of proteins of two-component systems in Myxococcus xanthus. J Bacteriol *190*, 613-624.

**Shimkets, L.J.** (1990). Social and developmental biology of the myxobacteria. Microbiol Rev *54*, 473-501.

**Skerker, J.M., and Berg, H.C.** (2001). Direct observation of extension and retraction of type IV pili. Proc Natl Acad Sci U S A *98*, 6901-6904.

**Small, E., *et al.*** (2007). FtsZ polymer-bundling by the Escherichia coli ZapA orthologue, YgfE, involves a conformational change in bound GTP. J Mol Biol *369*, 210-221.

**Spratt, B.G., *et al.*** (1986). Kanamycin-resistant vectors that are analogues of plasmids pUC8, pUC9, pEMBL8 and pEMBL9. Gene *41*, 337-342.

**Stahlberg, H., *et al.*** (2004). Oligomeric structure of the Bacillus subtilis cell division protein DivIVA determined by transmission electron microscopy. Mol Microbiol *52*, 1281-1290.

**Stokes, N.R., *et al.*** (2005). Novel inhibitors of bacterial cytokinesis identified by a cell-based antibiotic screening assay. J Biol Chem *280*, 39709-39715.

**Sun, H., *et al.*** (1999). Effect of cellular filamentation on adventurous and social gliding motility of Myxococcus xanthus. Proc Natl Acad Sci U S A *96*, 15178-15183.

**Sun, H., *et al.*** (2000). Type IV pilus of Myxococcus xanthus is a motility apparatus controlled by the frz chemosensory system. Curr Biol *10*, 1143-1146.

**Sun, Q., and Margolin, W.** (1998). FtsZ dynamics during the division cycle of live Escherichia coli cells. J Bacteriol *180*, 2050-2056.

**Sun, Q., and Margolin, W.** (2001). Influence of the nucleoid on placement of FtsZ and MinE rings in Escherichia coli. J Bacteriol *183*, 1413-1422.

**Thanbichler, M., and Shapiro, L.** (2006). MipZ, a spatial regulator coordinating chromosome segregation with cell division in Caulobacter. Cell *126*, 147-162.

**Thanedar, S., and Margolin, W.** (2004). FtsZ exhibits rapid movement and oscillation waves in helix-like patterns in Escherichia coli. Curr Biol *14*, 1167-1173.

**Thompson, J.D., *et al.*** (1994). CLUSTAL W: improving the sensitivity of progressive multiple sequence alignment through sequence weighting, position-specific gap penalties and weight matrix choice. Nucleic Acids Res *22*, 4673-4680.

**Thompson, S.R., *et al.*** (2006). The positioning of cytoplasmic protein clusters in bacteria. Proc Natl Acad Sci U S A *103*, 8209-8214.

**Trusca, D., *et al.*** (1998). Bacterial SOS checkpoint protein SulA inhibits polymerization of purified FtsZ cell division protein. J Bacteriol *180*, 3946-3953.

**van den Ent, F., and Lowe, J.** (2000). Crystal structure of the cell division protein FtsA from Thermotoga maritima. EMBO J *19*, 5300-5307.

**Vaughan, S., *et al.*** (2004). Molecular evolution of FtsZ protein sequences encoded within the genomes of archaea, bacteria, and eukaryota. J Mol Evol *58*, 19-29.

**Watanabe, E., *et al.*** (1992). ATPase activity of SopA, a protein essential for active partitioning of F plasmid. Mol Gen Genet *234*, 346-352.

**Weart, R.B., *et al.*** (2005). The ClpX chaperone modulates assembly of the tubulin-like protein FtsZ. Mol Microbiol *57*, 238-249.

**Wolgemuth, C., *et al.*** (2002). How myxobacteria glide. Curr Biol *12*, 369-377.

**Wu, L.J., and Errington, J.** (2004). Coordination of cell division and chromosome segregation by a nucleoid occlusion protein in Bacillus subtilis. Cell *117*, 915-925.

**Wu, S.S., *et al.*** (1997). The Myxococcus xanthus pilT locus is required for social gliding motility although pili are still produced. Mol Microbiol *23*, 109-121.

**Yamaichi, Y., *et al.*** (2007). Distinct centromere-like parS sites on the two chromosomes of Vibrio spp. J Bacteriol *189*, 5314-5324.

**Youderian, P., *et al.*** (2003). Identification of genes required for adventurous gliding motility in Myxococcus xanthus with the transposable element mariner. Mol Microbiol *49*, 555-570.

**Yu, R., and Kaiser, D.** (2007). Gliding motility and polarized slime secretion. Mol Microbiol *63*, 454-467.

**Zhu, C., *et al.*** (2006). Spatiotemporal control of spindle midzone formation by PRC1 in human cells. Proc Natl Acad Sci U S A *103*, 6196-6201.

# Acknowledgements

I am deeply indebted to my supervisor Prof. Dr. MD. Lotte Søgaard-Andersen for her guidance, suggestions and encouragement during my research.

I wish to express my sincere gratitude and appreciation to my thesis committee members, Prof. Dr. MD Lotte Søgaard-Andersen, Prof. Dr. Martin Thanbichler, Prof. Dr. Uwe Maier, and PD Dr. Michael Feldbrügge for their invaluable time for ideas and comments.

Special thanks to Dr. Sigrun Wegener-Feldbrügge for fruitfull discussions and for making crucial comments on my thesis. I also would like to thank Dr. Stuart Huntley for help on the bioinformatics analysis and very helpful discussions.

My sincere thanks to Susan Schlimpert and members of Martin Thanbichler's lab for interesting discussions about cell division. I would like to thank my students who contributed on my work in particular Marlen Mock.

It is a pleasure to convey thanks to International Max Planck Research School for Environmental, Cellular and Molecular Microbiology and the Intra- and Intercellular transport and communication research school for providing financial aid. I am grateful to Susanne Rommel and Christian Bengelsdorff for taking care of all of the documents for my daily life. I would also like to thank Meike Ammon for helping me so much during my stay in Marburg.

I am obliged to all of the persons in Dept. of Ecophysiology, especially the persons in our lab including the previous lab members, who gave me much assistance and enjoyable time during my stay here.

In a special way, I would like to express my deepest gratitude to my parents and brother, for their encouragement and support throughout my life. Special thanks to Torben Söngen and my friends for giving me strength to achieve what I have today. In addition, I express my sincere thanks to all those who contributed to this thesis in one way or the other.

# Curriculum Vitae

**Personal data**

| | |
|---|---|
| Name | Kryssia Aguiluz Fabian |
| Date of birth | June 27th 1982 |
| Place of birth | San Salvador, El Salvador |

**Education**

| | |
|---|---|
| 2000-2003 | Bachelor in Cellular Biology & Physiology<br>Bachelor in Biology of Organisms<br>Université Joseph Fourier, Grenoble I, France |
| 2004 | Master of Cellular & Integrative Biology, 1st year<br>University of California, Irvine, USA<br>Laboratory of Virology, Irvine, California<br>Supervisor: Prof. Dr. E.K. Wagner<br>Master tesis: Generation of a recombinant virus with delayed expression of an immediate-early gene (ICP27) to study the effect on the levels of viral transcription and replication in Herpes Simplex 1 virus. |
| 2005 | Master of Cellular & Integrative Biology, 2nd year<br>Université Joseph Fourier, Grenoble I, France<br>Laboratory of Adaptation and Pathogenicity of Microorganisms, Grenoble<br>Supervisors: Dr. C. Lelong and Prof. Dr. J. Geiselmann<br>Master tesis: Study of the regulatory protein Crl in *E. coli* |
| 10/2005-02/2007 | Max-Planck-Institute for Terrestrial Microbiology, Germany.<br>Project: Study of the outer membrane proteome in *M. xanthus*.<br>Supervisor: PD. Dr. Reiner Hedderich |
| 03/2007-03/2009 | PhD (Dr. rer. nat.)<br>Philipps-Universität Marburg<br>Max-Planck-Institute for Terrestrial Microbiology, Germany<br>Supervisor: Prof. Dr. MD. Lotte Søgaard-Andersen<br>PhD thesis: The ParA-like protein AgmE positively regulates cell division in *M.xanthus*. |

**List of publications**

Kahnt, J., Aguiluz, K., Koch, J., Hoppet, M. and Hedderich, R. Proteomic Profiling of the *Myxococcus xanthus* outer membrane and native outer membrane vesicles. *In preparation*

Lelong C, Aguiluz K, Luche S, Kuhn L, Garin J, Rabilloud T, Geiselmann J. The Crl-RpoS regulon. Mol Cell Proteomics. 2007 Apr;6(4):648-59

# Erklärung

Ich erkläre, dass ich meine Dissertation
"The ParA-like protein AgmE positively regulates cell division in *Myxococcus xanthus"*

selbstständig, ohne unerlaubte Hilfe angefertigt und mich dabei keiner anderen als der von mir ausdrücklich bezeichneten Quellen und Hilfen bedient habe.
Die Dissertation wurde in der jetzigen oder einer ähnlichen Form noch keiner anderen Hochschule eingereicht und hat noch keinen sonstigen Prüfungszwecken gedient.

Marburg, _____

Kryssia Aguiluz Fabian